QUASI-UNSTEADY FLOW IN A RADIAL VANELESS DIFFUSER

by

WILLEM JANSEN

Diploma, H.T.S., Arnhem
1954

Technische Hogeschool, Delft
1957

Submitted in Partial Fulfillment of the Requirements
for the Degree of Doctor of Science in Mechanical Engineering

at the

Massachusetts Institute of Technology

February 1961

Signature of the author.....
Dept. of Mechanical Engineering
December 1960

Certified by.....
Thesis Supervisor

Accepted by.....
Chairman, Departmental Committee on Graduate Students

ACKNOWLEDGEMENTS

This research project has been conducted as a part of the activities of the Gas Turbine Laboratory under the sponsorship of General Electric Company, Westinghouse Electric Corporation and Allison Division of General Motors Corporation.

Professor Y. Senoo extended his help during the initial phase of this work. Professor E. S. Taylor made valuable contributions during the discussions. Professors E. L. Mollö-Christensen and A. J. Erickson made suggestions from which this work profited. The author wishes to express his gratitude for the help he received.

ABSTRACT

The quasi-steady flow in the radial vaneless diffuser is divided into two parts. First the problem of the behavior of the wakes caused by the impellor blades in the diffuser and secondly the problem of self-excited waves. For the problem of the wakes a model was adopted which enabled one to treat the flow as a steady flow. By introducing some necessary changes in the existing theory it was found that an adequate prediction of the wake flow could be made. The wake seemed to disappear in similar fashion as the wakes behind obstructive bodies; i.e. the velocity difference smoothes out as the distance from the origin increases.

In the case of the self-excited wave, a theoretical analysis was made to describe the phenomenon of the periodic oscillations superposed on the steady free vortex flow. The analytical part is subdivided into two parts, one for the case where μ is small and one for the case where μ is big. (μ is the tangent of the angle which the steady flow makes with the circumferential direction.) Agreement was very good in the former case for $\mu = 0$, for both wave speed and perturbed velocity distributions versus radius. The analysis for big μ gave good agreement for the velocity distribution for $\mu > 0.4$ The wave speed from the experiments appears to fall between those predicted by the theory of big μ and small μ . A stability criterion indicated that pulsating flow can occur if and only if the value of μ lies between $-.2$ and 0.

TABLE OF CONTENTS

BIBLIOGRAPHY

1. Towsend, A.A. "The Structure of Turbulent Shear Flow" Cambridge University Press, 1956.

2. Isom, M.P. "The Three-Dimensional Boundary Layer in a Vaneless Diffuser" S.M. Thesis, Electrical Engineering Department, 1956 M.I.T.

3. Dean, R.C. and Senoo, Y. "Rotating Wakes in a Radial Vaneless Diffuser" ASME Preprint 59-A-104

4. Gardow, E. B. "The Three-Dimensional Turbulent Boundary Layer in a Free Vortex Diffuser" M.I.T. Gas Turbine Laboratory Report No. 42, January 1958.

5. Jansen, W. "Incompressible Fluid Flow in a Radial Vaneless Diffuser" M.I.T. Gas Turbine Laboratory Report 52, May 1959.

6. Lin, C.C. "Theory of Hydrodynamic Stability", University Press, Cambridge 1955.

7. Schlichting, H. "Boundary Layer Theory", McGraw-Hill Book Co., New York 1955.

8. Hinze, J.O. "Turbulence", McGraw-Hill Book Co., New York, 1959.

9. Jansen, W. "Compressible Fluid Flow in a Radial Vaneless Diffuser" M.I.T. Gas Turbine Laboratory Report 58.

10. Jacob, M. "Heat Transfer", Vol. I, John Wiley and Son, 1956.

11. Lin, C.C., editor "Turbulent Flows and Heat Transfer", Princeton University Press 1959.

12. Taylor, A.I., "Stability of a Viscous Liquid Contained between Two Rotating Cylinders" Phil. Transactions A223 pg 289-393.

13. Maroti, L.A. ea "Flow Phenomena of Partially Enclosed Disks: ASME Preprint 59-A-49.

14. Lamb, Sir H. "Hydrodynamics" Dover Publication

15. Rayleigh, Lord "On the Stability of the Laminar Motion of an Inviscid Fluid" Scientific Papers, 6, pg. 197-204, Cambridge University Press.

16. Tolmien, W. NACA Tech Memo, 792, 1936.

17. Dunn, D.W. "On the Stability of the Boundary Layer in a Compressible Fluid", Ph.D. thesis, M.I.T. 1953.

18. Stuart, J. T. "On the Stability of Three-Dimensional Boundary Layers with Application to the Flow due to a Rotating Disk", Part II, Proceedings of a Symposium held at the National Physical Laboratory, April 1955.

19. Bateman, H. "Partial Differential Equations of Mathematical Physics", Dover Publications, 1944.

1. INTRODUCTION TO PART I

The flow of wakes (i.e. the smoothing out of two parallel streams with different velocities) has been investigated very thoroughly in the past. At present, investigators use the wake flow to obtain a more detailed picture of the mixing and transport phenomena in turbulent flows.

In contrast to the wealth of experiments available in the literature no rigorous analytical solution is available to determine the entire flow field. However, with the help of some empirical constants, which had to be estimated from experiments, the analytical solution of the problem becomes quite satisfactory.

In the case where there are no pressure gradients present the wake problem is straightforward and no difficulties arise.

Townsend (1) in the introduction of the chapter on turbulent wakes, writes that no new features seem to arise when the freestream velocity changes with distance. However, experiments conducted in the Gas Turbine Laboratory (2) in a vaneless radial diffuser showed that the wakes from stationary vanes increased in width markedly and that a large part of the diffuser was occupied by a region of stationary air. See sketch 1.

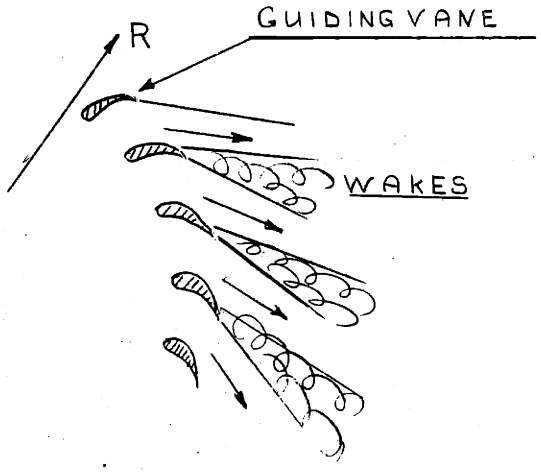

SCETCH 1

In the case of the wake flow for constant free stream velocity, the shear forces between wake and free stream are sufficient to flatten out the wake velocity profile. In the case of decelerating free stream velocity, this shear force apparently was not sufficiently large compared to the force due to the pressure gradient. The previous statements offer a general picture, but actually the complete picture of the problem is far more complex.

One may go one step farther and ask what will happen if the wake is rotating and has some prescribed velocity entering the diffuser. This is, for example, the case when one has a centrifugal impellor and a diffuser, working together as a pump where the impellor is known to discharge a non-uniform flow (see sketch 2). The flow is often separated from the suction side of the blade, and a region of dead air is formed. This region will extend into the vaneless diffuser, but will have an absolute velocity equal to the circumferential velocity of the impellor. This problem finds its importance in the design of a radial vaneless diffuser. The pressure losses are often quite severe at the entrance of the diffuser, and it is believed that the mixing out of the impellor wakes is the reason for this.

It is this problem which will be analysed in the following chapters. Special attention is focused on how the absolute velocity of the wake and the wake width changes with radius. Analysis of the data and a comparison with the existing theory (ref. 3) show that,

for this case and in general, a more complex analysis is necessary. This analysis is a refinement of that of ref. (3).

2. EXPERIMENTAL WORK

2-1 APPARATUS

The experiments were performed on the vaneless diffuser about which some brief details follow. The complete description of the apparatus may be found in Gas Turbine Laboratory report no. 42.

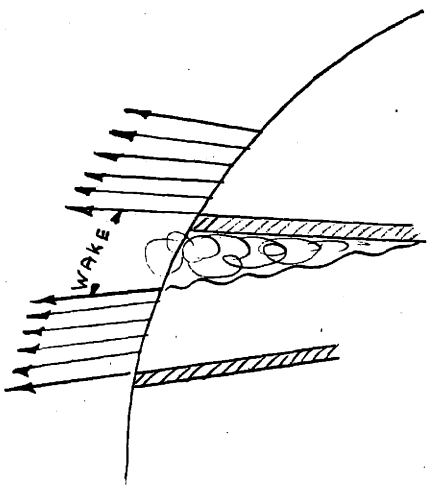

SKETCH 2

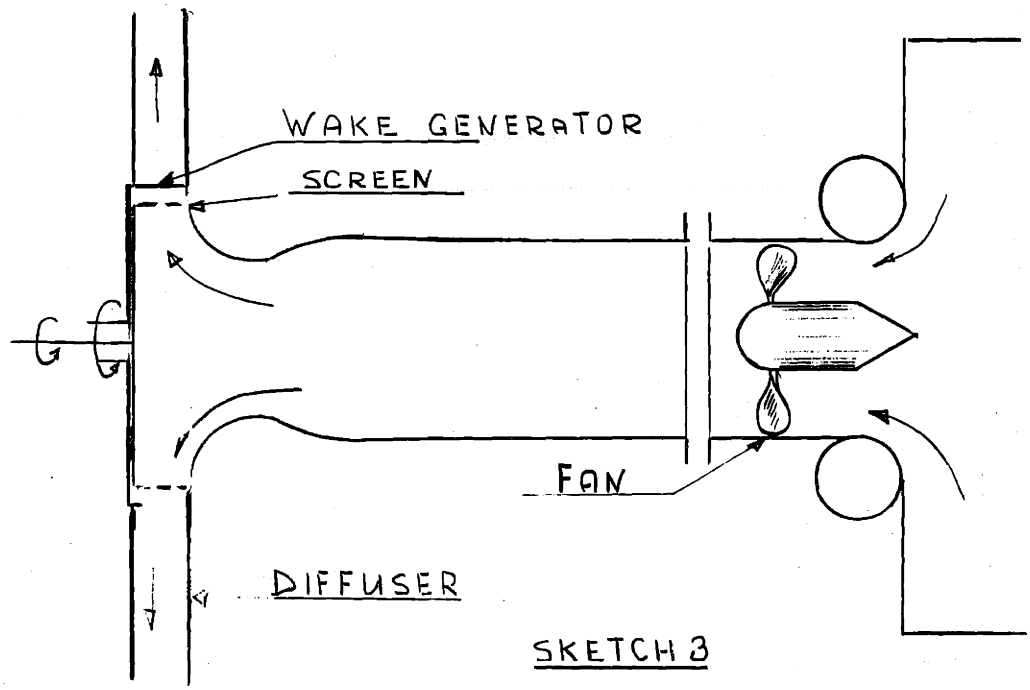

SKETCH 3

The air enters at the right through a cloth filter, passes through a fan and enters the radial diffuser. At the center of the diffuser wall on the left there are two concentric shafts, one which rotates the screen, creating a swirling flow, while the other rotates a blade three inches long, covering 3% of the circumference. The blade, which caused the wake, can be rotated at any velocity, independently of the screen (sketch 4).

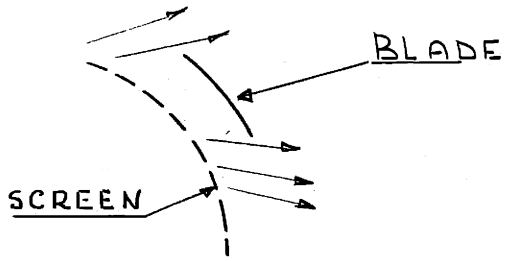

SKETCH 4

The diffuser starts at the screen, but R = 1 is the radius where the blade rotates. For large differences between the wake and free stream velocities it was found that the flow was distorted quite severely, i.e. on the front edge of the wake blade there was a severe increase in velocity coming from behind the blade (sketch 5).

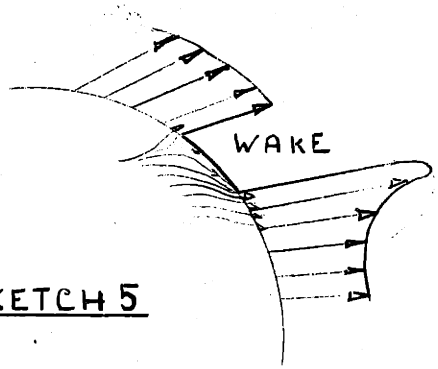

SKETCH 5

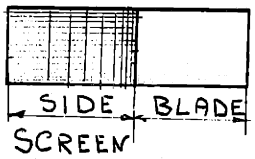

SKETCH 6

This was corrected by using a modified blade which had on one edge of the blade a high pressure loss screen (sketch 6). The density of this screen was decreased outwardly by pulling out some wires. This screen material was inserted in a wire frame to keep it in place.

By using this modified blade a far better flow field was obtained, one where the free-stream flow was more or less uniform

up to the edges of the wake generator. Fig. 1 shows pictures taken by a polaroid camera of a trace on the oscilloscope. In all the pictures the velocity increases upwards. Picture A was taken when a blade without a side screen was used. The free-stream flow was about 75 ft/sec. The maximum velocity was around 95 ft/sec, while the wake velocity was approximately 30 ft/sec.

Picture B was taken with the combined blade and side screen. The peak in velocity is largely eliminated. The free stream and wake velocities have the same values as before. The apparent difference is caused by a faster sweep in picture B, stretching the time scale.

In picture C the wake velocity is increased to around 88 ft/sec with the use of the blade without side screen.

As was previously stated, it was only for low wake velocities that such a distorted flow pattern was found, and a side screen had to be used. As the wake velocity is increased the angle of attack of the wake generator becomes larger with the result that there is less tendency for the flow to escape to the sides.

2.2 MEASURING TECHNIQUES

Two kinds of hot-wire probes were used. To measure the velocities, independently of angle of attack, the hot wire was placed perpendicular to the diffuser walls. To find the angle of flow a hot-wire parallel to the wall was used. The latter was oriented to give a minimum response and thus provided a reasonably accurate method of determining the angle of flow.

Time varying pressure measurements were obtained by placing a hot wire right behind the static pressure tap.

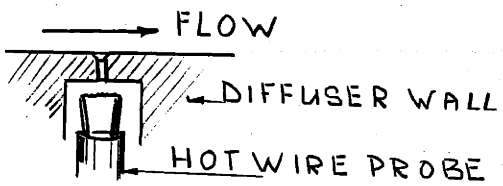

The combination pressure tap-hot wire was calibrated statically and appeared to yield good results. The amplitude of the response decreases rapidly for equal pressure differences as the pressure increases. This is a result of the fact that the hot-wire response becomes less sensitive, when the velocity (in this case the difference between diffuser and outside pressure) increases. Figure 4 gives some traces of the dynamic pressures.

The output of the hot wire was recorded either by a cathode ray oscilloscope and camera or by means of a Sanborn recorder. Most of the velocity measurements were recorded with the last method. This gave a trace of the hot-wire response at one place in the diffuser. For the free-stream flow this trace was always at one single value but the wake trace seemed to vary from one wake to another. This unsteadiness increased with radius. At a radius R = 1.03 the response is almost steady for the wake velocity, while at R = 1.4 a velocity difference of 20 ft/sec was recorded at different instants of time.

Problems related to this unsteadiness will be studied in a later chapter; here we will describe only the results of the experiments. Fig. 2 shows two traces of the hot-wire responses. The velocity is traced as the ordinate, with time as the abscissa.

Trace a is at R = 1.03, while trace b is at R = 1.26, where the wake velocities are accentuated. The unsteadiness in wake velocity may be observed very clearly.

Fig. 3 follows a slow rotating wake as it passes through the diffuser. At the first few stations there is still a high velocity peak in the trace because no side screen was used on the rotating blade.

In Fig. 3, only the velocity differences are significant and it may be seen that the wake velocity increases and that the free stream velocity decreases. In fact, at R = 1.59 and R = 1.75 the absolute value of the wake velocity becomes greater than the absolute value of the free stream velocity. At a certain stage the increase of the wake velocity levels off and then starts to decrease. When that occurs (in Fig. 3 at R = 1.75) the wake velocity becomes unsteady again; i.e. the wake velocity is not single valued. From then on an increasing unsteadiness was recorded in the wake velocity. At larger stations (R = 2) the wake and free stream trace becomes blurred and no definite conclusion can be drawn.

This unsteadiness both in Fig. 2 and Fig. 3 is not arbitrarily drawn. Trace b in Fig. 2 shows clearly that the wake velocity has a wavy pattern with respect to time. This kind of pattern was observed earlier in a radial vaneless diffuser when stall occurred (5). The total flow field in the diffuser became oscillatory when the angle of flow was increased beyond 76°.

As is indicated here, the unsteadiness in wake velocity occurs mainly when the wake velocity decreases sharply, both immediately in fig. 2 and after R = 1.75 in Fig. 3. This recalls a statement of Rayleigh in 1880 which maintains that a revolving fluid motion is unstable when $(V_\theta R)_{R_1} > (V_\theta R)_{R_2}$ where $R_1 < R_2$ and V_θ the tangential velocity. (See also 6.)* We have this same case in the wake flow region; however we will not pursue this point here. In addition it should be said that no artificial measure could be thought of to improve the situation. In the future when the date are exhibited the wake velocities will always be presented within a certain range, indicating that the wake velocities have different values at different instants of time.

3. ANALYSIS

3.1 DESCRIPTION OF MODEL

In treating this problem analytically the main ideas stem from reference (3); however some of the assumptions made there could not be maintained in several cases.

The real flow field is approximated by the following model. The flow is assumed to consist of two parts of essentially one-dimensional flow. The two parts are the free stream and the wake flow. The free stream part is that which has the larger radial velocity component and usually occupies the larger portion of the circumference.

The boundary between wake and free stream is assumed to

---

* The present studies found that the diffuser stalled at a smaller angle (70° instead of 75°) when a rotating wake was present.

be discontinuous (see sketch). The form of the real wake velocity

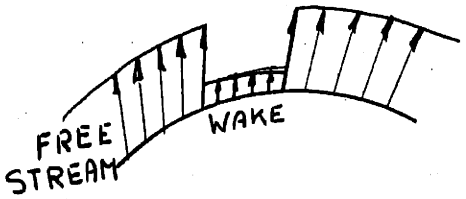

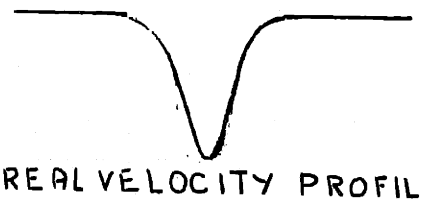

profile is a smooth curve (see sketch). An effective width ϵ is assumed to be half the real wake width. (The real wake width is the distance between the points where a velocity defect is first observed.) This definition of wake width differs with the usual definition, where the edge of the wake really is a boundary across which no mass is transported and where the velocity changes continuously due to the turbulent mixing.

The wake velocity is assumed to be the average of total real wake fluid momentum flux divided by the wake velocity. The wake velocity then is approximately the sum/difference of the minimum/maximum total velocity and 1/4 of the deficit velocity (see sketch). (These alternatives are for the case when the wake velocity is greater than the free stream velocity.)

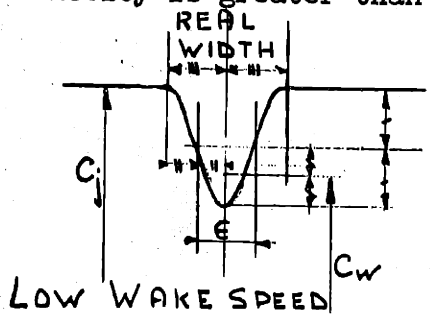

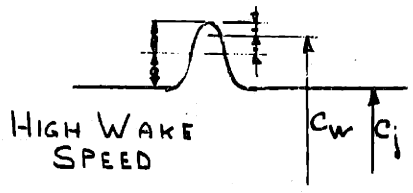

The flow consisting of a free stream and a rotating wake is unsteady. However, the flow is steady in a coordinate system rotating with the

angular velocity of the impeller and the stream flow velocity is W_j and the wake velocity W_w. (See sketch 7.) In this theoretical model the flow is one-dimensional, which means that for example the relative angle β does not change with Θ, the circumferential direction.

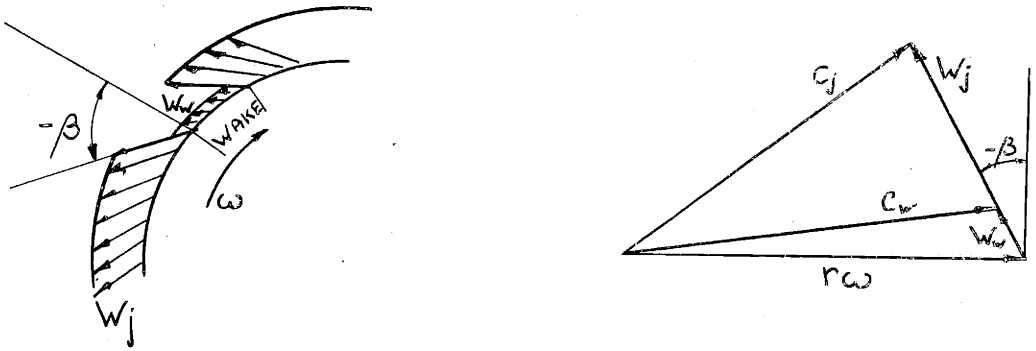

SKETCH 7

The forces involved are the walk skin friction forces, the turbulent shear force between wake and free-stream interface and a pressure force on the boundary between free stream and wake. Work done by this pressure force is the cause of the difference in behavior of rotating and stationary wakes.

This pressure force is created by a pressure difference between the leading and trailing boundary of the wake and hence rotates at impeller speed. This pressure force then causes a reversible work transport from free stream to wake flow or from wake to free-stream flow, depending on the situation (sketch 9).

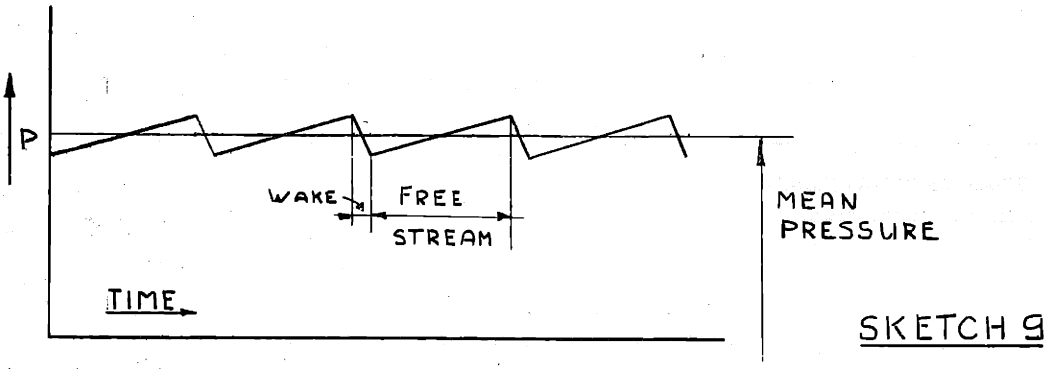

SKETCH 9

Appendix I gives some more details about the exact character of this pressure force.

The term static pressure at a given radius refers to the mean pressure (sketch 9).

Fig. 4 shows some time varying pressure measurements indicating qualitatively the existence of these forces. The shape of the leading and trailing boundaries of the wake are not the same. However, in the analysis we will neglect this and consider β to be single valued at a certain radius. The relative angle β then is the same in both wake and free stream flow as the streamline on the boundary belongs to the free stream as well as to the wake.

Even though the analysis is one dimensional the equations become quite involved. Certain two-dimensional effects are included in the theory, where it seemed necessary, but on the whole the algebra is kept as simple as possible.

For this reason, the shear force, the wall friction force, and the mass transfer from free stream to wake flow are expressed in the simplest form possible. The forces are expressed per unit area.

The wall friction force:

for free stream $F_j = c_f \frac{\rho}{g_o} \frac{C_j^2}{2}$ for wake $F_w = c_f \frac{\rho}{g_o} \frac{C_w^2}{2}$

The shear force between free stream and wake $S = \mu \zeta \frac{\rho}{g_o} \frac{(W_j - W_w)^2}{2}$

where μ is a multiplier, as explained in chapter 5.

The mass transfer between free stream and wake

$$V_\perp = \epsilon_\Gamma \frac{\partial W}{\partial y} = \Gamma (W_j - W_w)$$

Some details of the coefficients ζ and Γ will follow in a later chapter. The coefficient c_f is assumed to be .005.

It is not that the author lacks appreciation of the work done in free turbulent shear flow and skin friction experiments, but the extreme complexity of the modern description of these two topics, together with the further complications encountered in the present problem results in a massive obstruction to solving the problem. Simplification seems essential.

3.2 FLOW EQUATIONS

The model of the flow as described in the former chapter allows us to set up the equations. The free stream occupies the greater part of the diffuser and for this part three equations will be used.

1. Equation of motion in radial direction
2. Equation of motion in tangential direction

3. Equation of continuity

The wake is treated as a separate flow with the following conditions:

a. a pressure force and a shear force do work on it

b. wall friction is included

c. a net inflow of mass occurs due to the turbulent transport in a case of two streams with different velocities. (This is consistent with the definition of the wake width, as it was not assumed that the wake edge was defined by a streamline, across which no mass is transported.)

For the wake then one may use similar equations as for the free stream.

We have a total of six equations. The total number of unknowns is also six. The following quantities are treated as unknowns: $\epsilon, \beta, p, q, W_j, W_w$ where ϵ is the ratio of wake width and sum of wake and free-stream width; β the relative flow angle; p the pressure; q the pressure difference on trailing and leading end of wake zone. W_w the relative wake velocity and W_j the relative free-stream velocity.

I <u>The continuity equations</u> are as follows:

for free stream

$$2\pi r(1-\epsilon) b W_j \cos\beta = 2\pi r_i b_i W_{ji}(1+\epsilon_i)\cos\beta_i - \int_{r_i}^{r} f\,dr \qquad (1)$$

and for wake

$$2\pi r \epsilon W_w b \cos\beta = 2\pi r_i b_i W_{wi} \epsilon_i \cos\beta_i + \int_{r_i}^{r} f\,dr \qquad (2)$$

The term $\int_{r_i}^{r} f\,dr$ is the total volume rate of flow passing the boundary between wake and free stream where

$$f = V_\perp \frac{b}{\cos\beta} = \Gamma \frac{W_j - W_w}{\cos\beta} b$$

Γ will be estimated with information from the literature.

II Angular Momentum

For the free stream

$$2\pi r b (1-\epsilon) W_j \cos\beta \frac{d}{dr}\left(r^2\omega + r W_j \sin\beta\right) =$$

$$= -c_f 2\pi r^2 (1-\epsilon) C_j \left(r\omega + W_j \sin\beta\right) - \xi \mu b r \left(W_j - W_w\right)^2 \operatorname{tg}\beta - \frac{b r q_r}{\rho} \qquad (3)$$

The details of the derivations of these forms may be found in Appendix I. The momentum exchange associated with the mass transfer from free stream to the wake is not included separately, but this is considered as part of the shear force and has the same effect. The shear force indeed may be expressed as a Rayleigh stress, $\overline{u'v'} = \frac{\tau}{\rho}$. The form $\overline{u'v'}$ is the momentum flux per unit mass of the fluid particles crossing the borderline.

The wake flow is similarly

$$2\pi b \epsilon W_w \cos\beta \frac{d}{dr}\left(r^2\omega + r W_w \sin\beta\right) =$$

$$= -c_f 2\pi r^2 \epsilon C_w \left(r\omega + W_w \sin\beta\right) + \xi \mu b r \left(W_j - W_w\right)^2 \operatorname{tg}\beta + \frac{b r q_r}{\rho} \qquad (4)$$

III Momentum, Radial Direction

For the free stream part:

$$2\pi r(1-\epsilon)\left\{W_j\cos\beta\frac{d}{dr}(W_j\cos\beta)+\frac{1}{\rho}\frac{dp}{dr}-\frac{(W_j\sin\beta+r\omega)^2}{r}\right. \tag{5}$$

$$\left.+c_f C_j\frac{W_j\cos\beta}{b}\right\}+\mu\xi\left(W_j-W_w\right)^2-\frac{q}{\rho}\operatorname{tg}\beta=0$$

for the wake flow

$$2\pi r\epsilon\left\{W_w\cos\beta\frac{d}{dr}W_w\cos\beta+\frac{1}{\rho}\frac{dp}{dr}-\frac{(W_w\sin\beta+r\omega)^2}{r}\right. \tag{6}$$

$$\left.+\frac{c_f C_w W_w\cos\beta}{b}\right\}-\mu\xi\left(W_j-W_w\right)^2+\frac{q}{\rho}\operatorname{tg}\beta=0$$

The two equations above also result when the energy equation neglecting thermodynamic effects is employed for both wake and free-stream flow separately.

These six equations are simultaneous differential equations with non-linear terms and no solution in closed form has been found. All the calculations had to be performed numerically.

The following formulas give $\frac{dW_j}{dr}$ and $\frac{dW_w}{dr}$ as the only differentials besides $\frac{d\epsilon}{dr}$ which is very small for large radii.

For numerical procedures these two equations seem to be the easiest to manage

$$(1-\epsilon)W_j^2+W_j r\dot{W}_j-\dot{\epsilon}\cos^2\beta\, r\left(W_j^2-W_w^2\right)+\frac{f}{2\pi b}\cos\beta\left(W_j-W_w\right)+$$

$$+W_w^2\epsilon+2r\omega\sin\beta\left[W_j(1-\epsilon)+W_w\epsilon\right]+\frac{\mu\xi\left(W_j-W_w\right)^2+}{2\pi(1-\epsilon)\cos^2\beta}$$

$$+\frac{c_f r}{b\cos\beta}\left[\left(r\omega\sin\beta+W_j\sin^2\beta\right)C_w+\epsilon\cos^2\beta\left(W_jC_j-W_wC_w\right)\right]=0 \tag{7}$$

$$(1-\epsilon)W_j^2 + W_w r\overset{\circ}{W}_w - \overset{\circ}{\epsilon}\cos^2\beta\, r(W_j^2 - W_w^2) + \frac{f\cos\beta}{2\pi b}(W_j - W_w) + W_w^2\epsilon +$$
$$+ 2r\omega\sin\beta\,[W_j(1-\epsilon) + W_w\epsilon] - \frac{\mu\zeta(W_j - W)^2}{2\pi r\epsilon\cos^2\beta} +$$
$$+ \frac{c_f r}{b\cos\beta}\left[(W_w\sin^2\beta + r\omega\sin\beta)c_w - (1-\epsilon)\cos^2\beta(W_j c_j - W_w c_w)\right] = 0 \qquad (8)$$

One is now able to solve for the unknowns $W_j, W_w, \epsilon, \beta$ with the equations 1, 2, 7 and 8, and for p with 9, provided one has information about the coefficients c_f ζ AND Γ .

The next chapter will go somewhat deeper into that problem. $\frac{1}{\rho}\frac{dp}{dr} = r\omega^2 - \frac{1}{2}\frac{dW_j^2}{dr} - \frac{c_f c_j}{b\cos\beta}(r\omega\sin\beta + W_j) - \frac{\mu\zeta(W_j - W_w)}{2\pi r(1-\epsilon)\cos^2\beta}$ (9)

By subtracting equation (3) from (5) one obtains an expression to calculate the pressure distribution.

4. ESTIMATE OF SKIN FRICTION

To estimate the skin friction many expressions are available in the literature, taking into account the boundary layer thickness and the shape factor. The most accurate form known to the author is the one derived by Ludwig and Tillman, which is written in the following form:

$$c_f = 0.246\left[\exp(-1.561\,H)\right]\mathrm{Rey}_\vartheta^{-0.268}$$

where H is the shape factor and Rey_ϑ is the Reynolds number with respect to the momentum thickness.

A simpler form is the skin friction coefficient used for flat plates, which is only a function of Reynolds number

$$c_f = 0.045\sqrt[4]{\frac{2}{\mathrm{Rey}_\delta}}$$

With the diffuser geometry which was used here $r_i/b \cong 8$ the skin friction does not have much effect. It was decided to use a constant skin friction coefficient $C_f = 0.005$

5. SHEAR FORCE ON WAKE BOUNDARIES

With the diffuser geometry which was used, it appeared that the turbulent shear force on the forder of wake and free stream was very important.

Fig. 17 shows the variation of the free stream velocity wake velocity and wake width between the two diffuser walls. The traverse was made for a radius $R = 2.17$ One may observe that the wake velocity profile and free stream velocity profile are identical in form. The wake width increases slightly at the side walls, due to the low energy flow at the proximity of the diffuser walls. The wake width curve is plotted with maximum and minimum values. Fig. 18 shows a similar plot, but now the wake speed at the entrance of the diffuser is much less than that of fig. 17 (3 to 1 respectively). The wake velocities are not plotted in fig. 18, because at this radius ($R = 2.17$) the response was very unsteady with time (see also fig. 3). Again it is seen that the wake width increases slightly at the side walls.

Although the wake width approximates the two-dimensional model quite well, it was found that the analysis needed amendment to include the effect of the curved velocity profile.

By using just one constant value for ζ it seemed that the theoretical predictions did not agree too well with the

experimental data. Especially values for wake width were very much influenced by ζ . To determine the change in ζ with radius, several sets of data were taken and from these data the variation of ϵ with radius was established. The six unknowns reduce to five, but if one introduces ζ as an unknown one may solve for ζ . Of special interest were sets of experiments where ϵ remained constant.

Fig. 5 shows the results of those calculations. The multiplier μ with which one should multiply the initial value of ζ is plotted in y-direction. This initial value for ζ varies with high and low wake speed. For high wake speed 100 ft/sec it amounts to 0.094 while for low wake speed values between 0.13 and 0.18 are found.

These values for ζ are very close to values found for wake flow with zero pressure gradient. Schlichting in his experiments found the lower value of $\zeta = 0.094$ (ref. 7).

The explanation of the existence of such a multiplier for the shear force coefficient is anything but easy. Although it cannot be proven, it is thought that the boundary layer is mainly responsible for this effect.

The following formulations consider essentially the effect of the diffuser wall boundary on the idealized one-dimensional fluid model. In the following section, the expression "wake velocity profile" is then the velocity profile, which extends

between the diffuser walls (z-direction). The wake velocity profile in circumferential direction was already defined as a straight line in chapter 3-2.

At the entrance of the diffuser, the flow has a flat velocity profile, but as is known from previous experiments a boundary layer will build up along both side walls (ref. 5, and figs. 17 and 18). This then causes the flow in the neighborhood of the wall to slow down with respect to the stream in the middle of the passage. Consequently, the border line between wake and free stream near the wall will not be in the same geometrical place as the border line in mid stream.

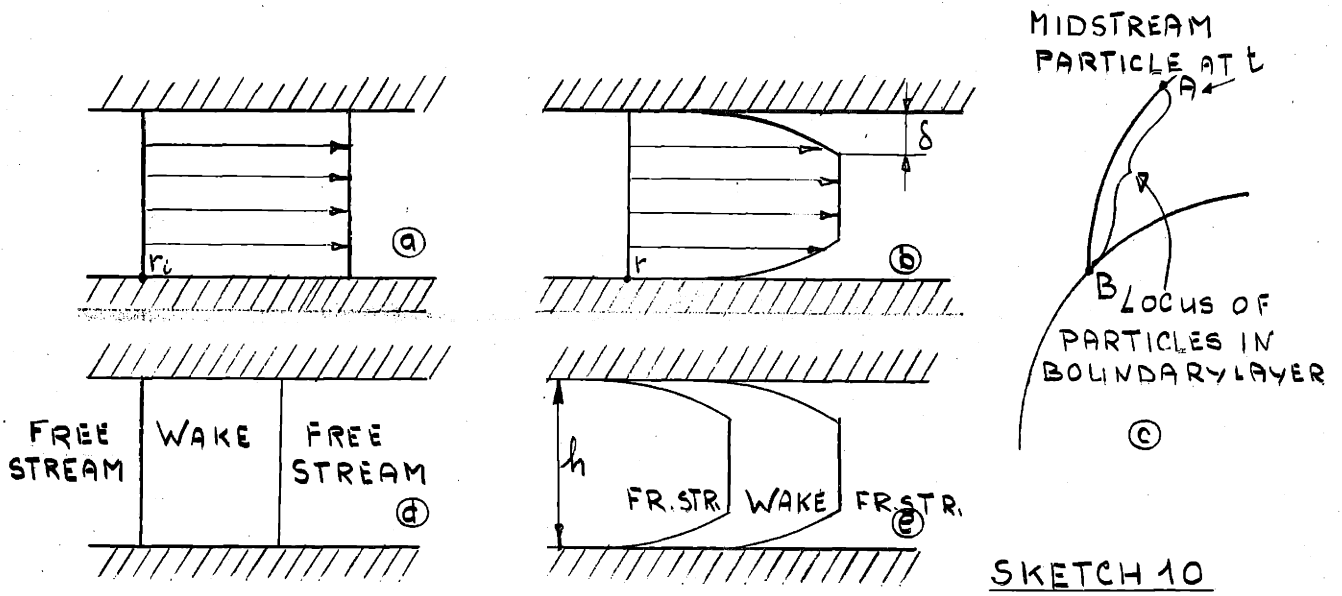

SKETCH 10

Sketch 10 gives an illustration of this. Sketch 10a shows the velocity profile entering the diffuser; 10b, the velocity profile somewhere in the diffuser; 10c, the position of the fluid

particles starting at B at time t_0 after time t. The fluid particle against the wall does not move (no slip condition) and the midstream particles are at A; the particles in the boundary layer are between A and B. In d and e one looks in the direction along the spiral path of the free stream particles. In d the wake boundaries are straight when the wake is at $r = r_i$, but in e, where the wake is pictured somewhere in the diffuser, its boundaries have the form indicated in the sketch. This means that the surface on which S acts is increased by the extended boundary. The boundary is straight for a distance $h - 2\delta$, but is curved approximately in the form of a tenth power, $s = c(\delta^{1/10})$ and runs between r and r_i. This discussion is very much idealized, especially in the fact that the wake boundary should extend all the way down to the initial radius. It would be far more realistic to assume that the shear force acts only on a part of this curved surface. It was assumed then that only the part between the edge of the laminar sublayer of the turbulent boundary layer and the free stream flow plays a role in the increased friction coefficient.

The laminar sublayer extends up to the place where the Reynolds number with respect to the friction velocity u^* equals 50

$$\frac{\delta u^*}{\nu} = 50$$

Appendix II presents the calculation of the increased surface of the wake; consequently this increased surface area may be denoted as the multiplier in the shear force equation.

The dotted line in fig. 5 shows the result for $Rey_{u^*} = 50$ as a cut-off. From this figure it would appear that the multiplier found in the experiments is caused by the effect of the boundary layer.

Note also however that at a certain point the multiplier found in experiments levels off, while the multiplier found from the extended surface theory goes on increasing. This takes place at a radius ratio of 1.5, which radius is often an upper limit in practical diffuser design.

It may be remarked that the effect of three dimensionality is ignored in computing the dotted line in fig. 5.

6. MASS TRANSPORT ACROSS THE BOUNDARIES

The transport of any transferable quantity by random motions is diffusive in nature (8). The random motion may be molecular agitation which in a macroscopic sense, for example, causes the viscosity and smoothing out of velocity differences or molecular diffusion such as in the drying of a wet piece of wood. In other words the differences in a concentration of transferable quantities cause diffusion of these quantities until equilibrium is reached. The random motion is very often turbulence. The transport processes formed a central subject in the early study of turbulent flow. The theories which were introduced were the so-called "mixing length" theories. These theories do not necessarily describe the phenomenon, but are born out of an attempt

to make a model which could more nearly "explain" the phenomenon. For engineering purposes these theories are extremely valuable and they will be used here frequently.

First the problem of the wake without a pressure gradient is considered. In sketch 11-a the wake flow is drawn at x_o . Sketch 11-b is the same picture at some distance $x + x_o$. It is found that the center line velocity of the wake increases, which indicates a cross flow towards the center line (continuity). This cross flow occurs as a result of the diffusion, which forces the center line velocity to approach the free stream velocity.

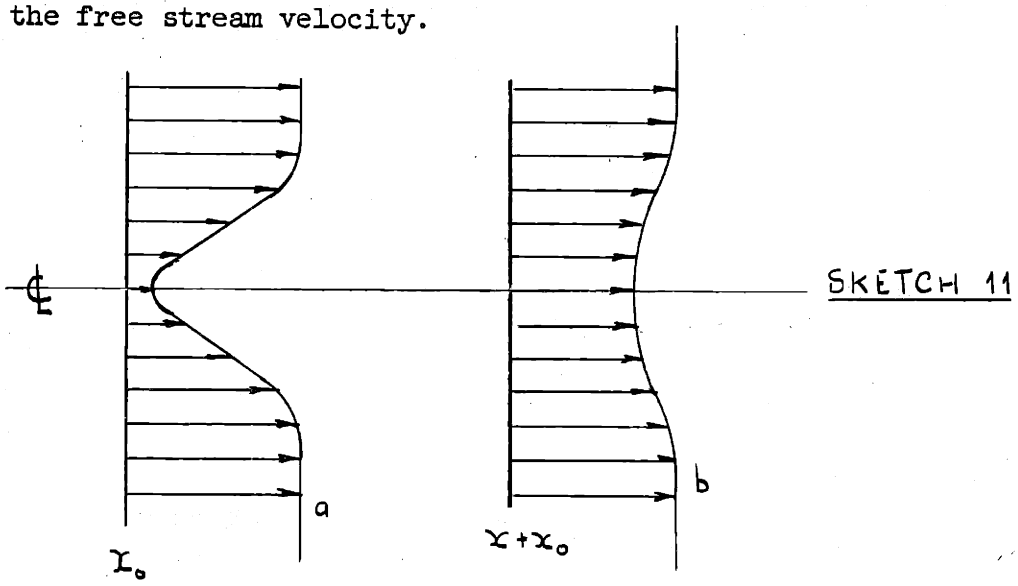

SKETCH 11

One is inclined to use a similar approach to the problems occurring in rotating wakes.

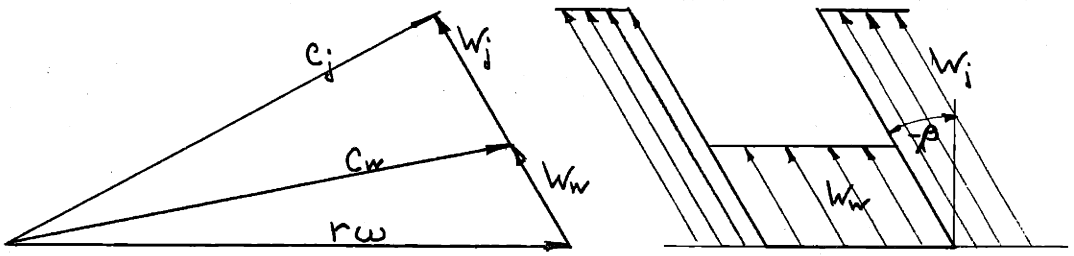

SKETCH 12

A simple way to handle this problem would be to assume that the cross-flow velocity with Γ constant for all cases. This cross flow coming into the wake then increases the velocity W_w. However the circumferential velocity $r\omega$ increases too, which means that when Γ equals a certain assigned value C_w will never come equal to C_j (sketch 13) for high $r\omega$; the velocity differences between free stream and wake will increase instead of decrease.

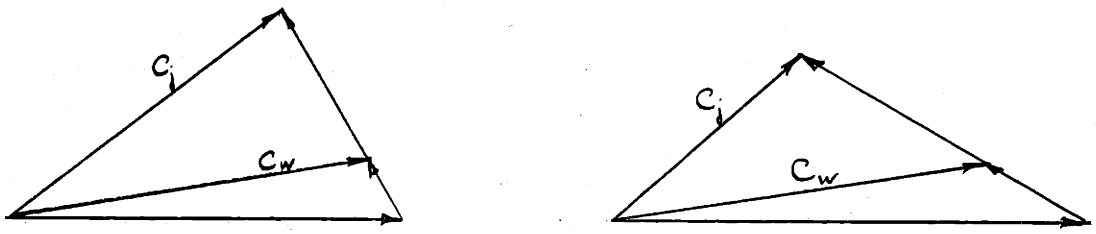

SKETCH 13

On the other hand, for low rotating wake speed, having almost no cross flow, the absolute velocities will approach each other (sketch 14).

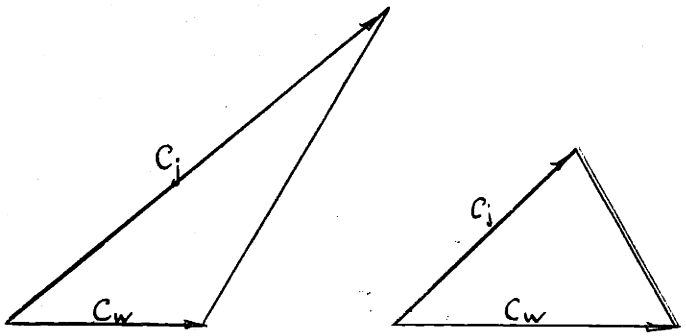

SKETCH 14

This qualitative picture already suggests that the cross flow is highly dependent on the flow pattern (r_ω and β).

As a matter of curiosity it may be recalled that the transport of heat by turbulence behaves in a similar way. It is possible that with a temperature difference, a net heat flow occurs from the low temperature region to the high temperature region. An example is a stable stratified atmosphere where the air particles moved up and down from one layer to another and are compressed or expanded adiabatically (8). The temperature rise or fall due to adiabatic compression or expansion causes an air particle to have a higher temperature than its surroundings when moving down and a lower temperature when moving up. Hence this unexpected heat transfer is directed up the temperature gradient. In the case which is dealt with here, a numerical example shows that for certain low wake speed we may expect a small cross flow from the wake to the free stream.

As has been said before, we will not seek to find some elaborate expression for the cross flow $V_\perp$, but try to keep

it in the form

$$V_\perp = \Gamma\left(W_j - W_w\right)$$

We now assume $\Gamma = \Gamma\left(W_j, W_w, r\omega, \beta\right)$ and we will try to find this function of Γ .

If we consider the wake and take a control volume with the velocities and geometry as indicated in sketch 15, we may write the equation governing the mass transport.

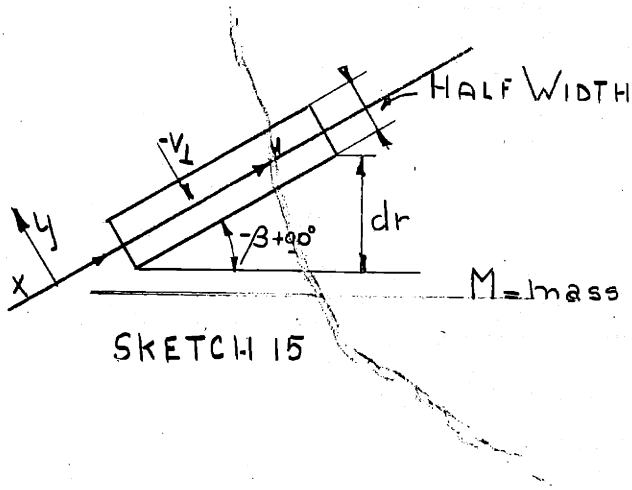

SKETCH 15

$$\frac{DM}{Dt} = \epsilon_M \frac{\partial^2 M}{\partial y^2} - F_i$$

where $\frac{D}{Dt}$ is the substantial derivative and F_i is some driving force which can be a pressure gradient. For steady flow this amounts to

$$u\frac{\partial u}{\partial x} + V_\perp \frac{\partial u}{\partial y} = \epsilon_m \frac{\partial^2 u}{\partial y^2} - \frac{1}{\rho}\frac{\partial p}{\partial x} \qquad (18)$$

Now $\epsilon_m = l^2 \frac{\partial u}{\partial y}$ so the first term on the right-hand side becomes $l^2 \frac{\partial^2 u}{\partial y^2} \frac{\partial u}{\partial y}$ Von Karman showed that the form $\frac{l \partial^2 u/\partial y^2}{\partial u/\partial y}$ equals a constant which is universal and which numerical value is equal to 0.38.

Neglecting the smaller term, the value for $\frac{1}{\rho} \frac{\partial p}{\partial x}$ follows from equation 9

$$\frac{1}{\rho} \frac{\partial p}{\partial x} = \frac{1}{\rho} \frac{\partial p}{\partial r} = r\omega^2 - W_j \frac{dW_j}{dr}$$

Formula (18) then becomes

$$V_1 = 0.38\, l \frac{\partial W}{\partial y} - \frac{r\omega^2 + \frac{W_j}{2} \partial W_j/\partial r - \frac{W_w}{2} \partial W_w/\partial r}{\partial W/\partial y}$$

where we assumed $u \frac{\partial u}{\partial x}$ to be average value of free stream and wake flow

$$u \frac{\partial u}{\partial x} = W \frac{\partial W}{\partial r} = \frac{W_j}{2} \frac{\partial W_j}{\partial r} + \frac{W_w}{2} \frac{\partial W_w}{\partial r}$$

Additionally it was assumed that

$$l \frac{\partial}{\partial y} = 0.18\, \Delta \qquad \text{SEE (REF. 7)}$$

$$V_1 = 0.18 \times 0.38 \left(W_j - W_w\right) - \frac{r\omega^2 + W_j/2\, \partial W_j/\partial r - W_w/2\, \partial W_w/\partial r}{\partial W/\partial r}$$

The function Γ then becomes approximately

$$\Gamma = 0.0685 - \frac{r\omega^2}{\partial W_j/\partial y \left[W_j - W_w\right]}$$

From (20) it may be seen that for very small wake velocities the cross flow becomes positive, which indicates that then the flow should go from wake to free stream.

This was never observed in the experiments because at very low wake speeds the wake grew tremendously and the effects such as mass transport became negligible.

The values for Γ found by this method were as follows:

$C_{ji} = 80\ ft/_{SEC}$ $\quad \alpha = 60°$ $\quad r\omega_i = 30\ ft/_{SEC}$ $\quad \Gamma = 0$

$C_{ji} = 80\ ft/_{SEC}$ $\quad \alpha = 60°$ $\quad r\omega_i = 90\ ft/_{SEC}$ $\quad \Gamma = -.26$

$C_{ji} = 80\ ft/_{SEC}$ $\quad \alpha = 60°$ $\quad r\omega_i = 110\ ft/_{S}$ $\quad \Gamma = -.36$

For ordinary wake flow with no pressure gradient the value of Γ would be 0.18.

In the calculation Γ is kept constant with radius throughout. This is not consistent with the equations derived here. However as this derivation is only an approximation for $V_\perp$ it is thought not worth while to introduce a fine adjustment on a crude step. Moreover if one were to plot $V_\perp$ versus R, the value of $V_\perp$ would increase first to a minimum and then increase even above the initial value. Hence a constant value of Γ would represent a fair average.

According to the similarity of the mass momentum and heat transfer process it might be expected that the coefficients

of diffusivity for these three cases are equal or about equal. However one finds a variety of answers in the literature (11), (pages 420-430).

For a two-dimensional wake one finds $\frac{\epsilon_r}{\epsilon_m} = 1.85$ while for concentric streams $\frac{\epsilon_r}{\epsilon_m} = 1.2 \sim 2.0$. In most cases it was found that the ratio of $\epsilon_m / \epsilon_T = 1$. See also (9). It might be worth while to see what the ratio of these two eddy diffusivities are in the case we are considering. If all the momentum associated with the cross flow were used to create the turbulent shear force then one would find with $\Gamma = -0.18$; $\frac{\rho}{g_0} V_\perp \times b \times \frac{dr}{\cos\beta} \times (W_j - W_w) =$

$= 0.18 (W_j - W_w)^2 b \frac{dr}{\cos\beta} \frac{\rho}{g_0} = \frac{\zeta}{2} \frac{\rho}{g_0} (W_j - W_w)^2 \frac{dr}{\cos\beta} b.$ OR $\zeta = 0.36$

In our calculation for $\Gamma = 0.18$ we had to use ζ equal to 0.094 . Taking into account the multiplier $\mu = 1$ then at $R = 1$; $\epsilon_r / \epsilon_m = 3.82$. At a larger radius of $R = 1.5$ where a multiplier $\mu = 3$ should be used, $\epsilon_r / \epsilon_m = 3.6 / 3 \times .094 = 1.23$ The average value then is in the same order of magnitude as the values quoted in the literature.

This comparison does not hold true for very slow rotating or very fast rotating wakes, as then $V_\perp$ changes too much.

7. PRESENTATION OF THE EXPERIMENTAL RESULT

Various experiments have been conducted measuring wake velocities, free stream velocities, wake widths, dynamic pressures, static pressures and angles of flow for changing wake rotation speeds. The angle of flow measurements were conducted to obtain

the angles of the velocity triangles and will not be shown here, but they are used in the calculations. Of the static pressure measurements only some examples will be given, as these seem all to follow the same trends. Fig. 6 gives the wake boundaries for the observer rotating with the wake. The dotted line gives the shape of the wake as it would be when Senoo's theory was adopted. Almost at a radius ratio R = 1.01 the wake would have disappeared and no trace would have been found.

In our experiments however this was not observed. The wake could be followed up to radii of 2. and it seemed that the wake mixes out as is usually the case in ordinary wake flow.

However even the theory employed here shows a sharp decrease in width due to the effect, which causes the wake in Senoo's case to collapse. The inflow effect becomes stronger as the radius increases.

Note that for higher wake speeds the sharp decrease in wake width is more severe than for slower rotation wakes. As a matter of curiosity it is found that for wake speeds being about one third of the total free-stream velocity the wake width stays constant for considerable time. One must remember that then the cross flow is nil.

Fig. 7 shows the result of the calculations and these are compared with the experimental values. The velocity triangles show the flow configuration. With the analysis of ref. (3) the wake would have disappeared at R = 1.017 and wake speed would

remain $r\omega$. The present theory is represented by the drawn line C and this just falls in the range of values for C found by experiment.

The free stream flow is, as known from (5), not one-dimensional due to the boundary layer formation, hence the deviation at large radii. The velocity triangles also show how the velocities smooth out. At $R=1$, C_w and C_j differ 29° in direction of flow and are about equal. As the cross flow creates a mass flow outwards W_w starts to grow so that the angle between C_j and C_w decreases; W_w increases more than W_j with the result that $|C_w| \to |C_j|$ and the angle between C_j and C_w decreases with radius. They will be equal at infinity due to the asymptotic character of the solution.

Fig. 8 shows the behavior of W_j and W_w with radius. It may be observed that $\partial W_w/\partial r\big|_{R=1} = 0$. The wake width ϵ is also shown. The figures 1-3 show that the exact determination of the wake width is extremely difficult. In fig. 8 the small triangles are the average values found by experiments. Of the comparison of the wake width with them it can only be said that there is a tendency to agreement.

Fig. 9 is again for high wake velocity, the initial velocity difference between free stream and wake is around 85% of the total. Again the velocity triangles show how the flow behaves and smooths out.

The theoretical curve for the wake velocity seems to fit the range of experimental values very well. The calculations have been performed with $\zeta = .075$ and $\zeta = .094$ The difference shows only in the entrance of the diffuser. No preference is suggested for using either one of the values of ζ . Fig. 10 for the same flow conditions shows the relative velocities w_j and w_w . Again it can be seen how they approach each other asymptotically. The wake width is drawn and some values from experiment are drawn in also. As was said before, there is only the tendency to agree. However, if one looks for improvements over existing theories, note that Senoo's theory indicates that the wake disappears at R = 1.008. This however is not observed.

Fig. 11 is one of the experiments where ϵ was constant; the wake velocity is just equal to $r\omega(\Gamma=0)$. The free stream velocities at larger radii are in disagreement due to the boundary layer formation. The boundary layer will displace the flow toward the middle of the passage where the measurements were taken. In connection with this it should be observed that at larger radii the wake velocities predicted by the present theory are on the low side, exactly at those instances where the free stream velocities are higher than the theory predicts. With this in mind one can see that at larger radii the boundary layer formation has an effect on the free stream flow as well as on the wake flow.

The theoretical analysis of such an effect is extremely complex if not impossible, especially considering the already involved set of equations needed to solve the present model.

Fig. 12 shows again the absolute wake and free stream velocities. The three velocity triangles illustrate how the wake velocity approaches the free stream velocity. At R = 1.00 the wake velocity is in the tangential direction, but at larger radii the through flow in the wake increases and the wake velocity decreases and bends towards the free stream velocity.

An effort was made to observe the angle which the wake velocity makes with the circumferential direction, but due to the severe fluctuations of the wake velocity itself, it was impossible to determine one definite angle. The value for Γ was estimated by the functional relation for Γ found earlier (20).

Fig. 13 shows the relative velocities for wake and free-stream W_w and W_j approach each other asymptotically. Also the wake width is shown for the same conditions. In this case for the highest circumferential wake velocity Senoo's theory would predict the wake to disappear at R = 1.0045.

Fig. 14 is again a plot of a slow moving wake. The wake width stayed more or less constant, the inflow was zero, so $W_w = 0$ and does not change with radius. W_j goes through a minimum at a radius beyond our range. The theoretical values seem to check the experimental values quite well for absolute free-stream and wake velocities and wake widths.

In Fig. 15 the result is plotted allowing for cross flow. The value of Γ was taken from (7) and the results are that the wake velocity stays rather well in the range of the experimental values. However, both free stream velocity and wake width deviate considerably from the data found in the test. ϵ = 50% of the circumference at R = 1.4, while the experiments show that ϵ = 4% which indicates the need of a value of Γ chosen in fig. 14 and derived from equation (20). At the same time for high wake flows Γ = 0 gives us about the same results as obtained by Senoo (3).

Finally, in fig. 16, a comparison of the pressure is given for the case discussed in fig. 14. The uncertainties of the pressure measurements are probably the reason for the deviations of the experimentally found pressures. One must keep in mind that the static pressure which one measures is an average over the pressure fluctuations (fig. 4). The process of averaging is done by using a long lead, but nevertheless some errors are expected to occur. In addition, no dependency of the three-dimensional boundary layer is assumed for the theoretical pressure estimation. Ref. 5 showed the influence of boundary layer effects on the pressure rise in a vaneless diffuser.

8. INFLUENCE OF COMPRESSIBILITY

In the case of the turbulent compressible wake flow the problem of changing density in both wake and free stream flow arises; the number of equations governing the flow is

expanded by the introduction of another unknown. One could treat this problem in two different manners. One way is to transform the coordinates in such a fashion that an equivalent incompressible case is obtained as has been done for the axi-symmetric flow in a radial diffuser (9). This method, which is like the Gothert rule, including two-dimensional effects and viscosity, will not ease the problem because of the fact that the solution of the energy equation for adiabatic flow (WITH $P_R = 1$

$$c_p T_w + \tfrac{1}{2} C_w^2 = c_p T_{ow} \quad \text{AND} \quad c_p T_j + \tfrac{1}{2} C_j^2 = c_p T_{oj}$$

for wake and free stream respectively is not true any more.

In the previous chapters we have seen that there is mass transport across the wake boundaries. In the compressible flow we will show that there is heat transfer across the wake boundaries. If the wake and free stream temperature are the same then no heat transfer will occur. However in general the temperature of both free stream and wake will differ when the flow proceeds outwards. Even when the temperature of free stream fluid and wake fluid right at the entrance of the vaneless diffuser are the same; still they will differ at some larger radius.

The fact which causes this is the different change of absolute velocity in free stream and wake.

Let us assume that at $R = 1$, $\overline{T}_j = \overline{T}_w$ then

$$c_p \overline{T}_j + \tfrac{1}{2} C_j^2 = c_p T_{oj} \qquad c_p \overline{T}_w + \tfrac{1}{2} C_w^2 = c_p \overline{T}_{ow}$$

For this instance we will assume no heat transfer across the free stream border. Then for adiabatic flow $T_{oj} = CONST$ and $T_{ow} = CONST.$

As we have seen in the previous chapter C_j and C_w do not change at the same rate with respect to the radius. For slow rotating wakes C_w increases and C_j decreases; for high rotating wakes C_w decreases faster than C_j . This indicates then that while the stagnation temperatures stay constant at any radius, T_j and T_w will differ.

In general, when there is a quantitative difference of a property between two substances, then the tendency is there to restore the equilibrium to one single value of that property which is in this case the temperature. The pressure on both sides of the boundary is the same, so that we do not have to worry about an increase or even negative heat transfer. To restore the equilibrium, heat transfer will occur across the boundary of the free stream and wake region. Note here that temperature, like density and pressure but unlike velocities, is an invariant of the transformation of the coordinate system.

The heat transferred will amount to

$$\frac{Q}{A} = -\epsilon_h c_p \frac{\partial T}{\partial y}$$

For slow rotating wakes heat leaves the free stream and for fast rotating wakes heat will be supplied by the wakes to the free stream.

However if heat is transferred from one region to the other, then the enthalpy of the regions changes to

The enthalpy of the free stream region is

$$m c_p T_o = \rho (1-\epsilon) W_j \cos\beta \, 2\pi r b c_p T_{oj} \qquad \text{1a}$$

and for the wake flow region

$$\epsilon \rho W_w \cos\beta \, 2\pi r b c_p T_{ow}$$

The energy equation for the free stream flow region is modified due to the fact that there is a heat out-in flow and mass out-in flow.

$$2\pi \rho_i (1-\epsilon_i) W_{ji} \cos\beta_i r_i b_i c_p T_{oji} =$$

$$= \left[2\pi (1-\epsilon) W_j \cos\beta \, r b \rho - \int_{r_i}^{r} f \rho \, dr\right] c_p T_{oj} - \int_{r_i}^{r} Q \, dr \qquad (2)$$

neglecting the secondary terms due to the temperature difference of the mass flowing across the jet-wake borderline.

For the wake flow this becomes

$$2\pi \rho_i r_i \epsilon_i W_{wi} \cos\beta_i b_i c_p T_{owi} = \left[2\pi \epsilon W_w \cos\beta \, r b \rho + \int_{r_i}^{r} f \rho \, dr\right] c_p T_{ow} + \int_{r_i}^{r} Q \, dr. \qquad (3)$$

The equations 2 and 3 give the additional information to estimate the density variation due to the compressibility effect. Note that in both equations 2 and 3 the unknown density appears however, this may be converted to the temperature.

$$\rho = P/\bar{R}T = \frac{p}{\bar{R}\left(T_o - \frac{1}{2} C^2/c_p\right)}$$

For general information it may be argued that the heat transfer between free stream and wake flow is negligible, but if one wants

to pursue the real behavior of the detailed flow it is a necessity to make this correction for heat transfer.

In effect, if one is to predict the wake width and velocity, then omission of the heat transfer effect, especially for low wake speeds, may lead to misleading conclusions. The following example stresses the previous point with quanititative proof. In the case of impeller exit data like

$$M C_j = 1.3 \qquad M C_w = .5 \qquad T_i = 525^\circ F$$

$$M W_j = .98 \qquad M W_w = 0$$

$$\alpha = 25^\circ \qquad \beta = 30.5^\circ$$

At R = 1.5 with the help of the gas table, the velocities change to $M C_j = 0.75$ $M C_w = 0.74$

$$T_{oj_i} = \frac{525}{\left(1 - \frac{\gamma-1}{2} M_j^2\right)} = 795^\circ, \quad T_{ow_i} = \frac{525}{1 - .2 \times .25} = 554^\circ$$

At $R = 1.5$: $T_{oj} = T_{oj_i}$, $T_j = 705^\circ$; $T_{ow} = T_{ow_i}$, $T_w = 465$.

This example shows that at R = 1.5 there would be a temperature difference of 250°F, which is very improbable.

We also see that for slow rotating wakes the density ρ decreases, which means that ϵ increases. (W is mainly determined by the pressure distribution) This shows then that in the case of slow wake speed there is the tendency for the distortion of the flow field to become bigger, while in the case of the high speed wake the distortion will be smaller, everything relative to the equivalent incompressible case.

The literature gives some values for ϵ_h, Jacob, etc.(10). With the help of these empirical values we may proceed and solve the problem of compressible wake flow.

In conclusion, we will repeat the main steps taken in the approach of the solution of the compressible flow problem.

1) Determine temperature of wake and free stream flow at the entrance, say, $T_W = T_j$ (given from exit data of impeller).

2) Determine stagnation temperature and enthalpy of flow (formula 1a)

3) By taking successive steps the stagnation temperature can be estimated by calculating the heat transfer between free stream and wake flow. (2) AND (3).

4) Knowing the stagnation temperature and velocity, the temperature and density are known from the perfect gas law

$$\rho \bar{R} T = p$$

It is clear that this is a process of iteration and step by step integration and that the above procedure is necessary to find p, which then can be used in solving the equations of flow discussed in former chapters.

The following example shows what the influence of the heat transfer is in smoothing out the temperature differences.

The heat transfer is given by an orthodox form still in use, not because of its great accuracy, but rather because of its lone representation of the phenomenon.

$$\frac{Q}{A} = -\epsilon_h c_p \frac{\partial T}{\partial y}$$

Now $P_{rt} = \frac{\epsilon_m}{\epsilon_h} c_p$ where ϵ_m is defined by the equation $\tau \equiv -\epsilon_m \frac{\partial u}{\partial y}$. The turbulent Prandtl number is the ratio of turbulent shear stress to the turbulent heat transfer. This ratio has a value of about 0.86 for air.

$$\frac{Q}{A} = -\frac{\rho c_p^2 \epsilon_m}{.86} \frac{\partial T}{\partial y} = -\rho c_p^2 l^2 \frac{\partial u}{\partial y} \frac{\partial T}{\partial y}$$

From Schlichting (7) the value of $l \frac{\partial}{\partial y}$ is around 0.18. Hence

$$\frac{Q}{A} \approx -\frac{\rho c_p^2}{.86} (.18)^2 (W_j - W_w)(T_j - T_w)$$

If we assume for $W_j - W_w$ an average value of 500 ft/sec and $T_j - T_w$ = 250°F as was seen in the previous estimate, then it follows with b = 1.7 inch and r_i = 1.11 ft.

$$\frac{Q}{A} = 0.5 \text{ BTU}\Big|_{\text{SEC.ft}^2} \quad ; \quad Q = \int_{r_i}^{r} \frac{b\,dr}{\cos\beta} \times .5 \text{ BTU}\Big|_{\text{SEC.}}$$

or with r = 1.5

$$Q = 0.08 \text{ BTU}|_{\text{SEC}}$$

The heat content is the wake flow, given by lb. With $\epsilon = .03$; $W_w = 100$ ft/sec; $T_o = 554$, the total enthalpy

$$\bar{h} = 0.43 \text{ BTU}|_{\text{SEC}}$$

now at R = 1.5 this enthalpy is changed to $\bar{h} = 0.43 + 0.08 = 0.51$ Hence the final stagnation temperature becomes $51/43 \times 554 = 648^\circ F$ which is around 100° higher. With these simple numbers, one may not believe in the exactitude of the final answer, which may be off by 40%. However, the general order of magnitude is believed to be correct. Therefore this example illustrates the necessity of including heat transfer by analyzing wake flow in compressible flow.

Appendix I

THE PRESSURE FORCE q_t

Perhaps the explanation of a pressure force in tangential direction with the help of the velocity triangles is the most enlightening. In sketch "a" the velocity triangle at $r = r_i$

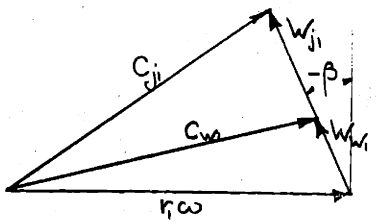

SKETCH a

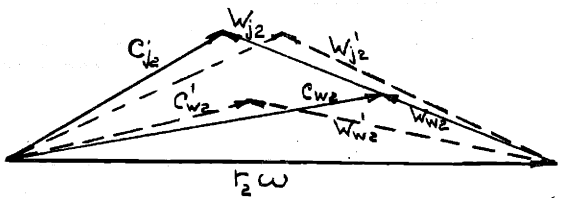

SKETCH b

The dotted line in sketch "b" shows the velocity triangle of wake and free stream. These were treated separately. However, we have assumed that the free stream and the wake have common borders in the rotating coordinate system. This means that the velocity vectors W must fall on one line. If we consider the through flow to be equal in the two cases, then $C'_{j2} < C_{j2}$ and $C_{w_2} > C'_{w_2}$ which means that the wake speed increases and the free stream speed decreases. This happens as a result of the work exchange of the free stream and the wake flow by means of the rotating pressure force q_t.

DERIVATIONS OF EQUATIONS OF FLOW

ANGULAR MOMENTUM:

1) For free stream

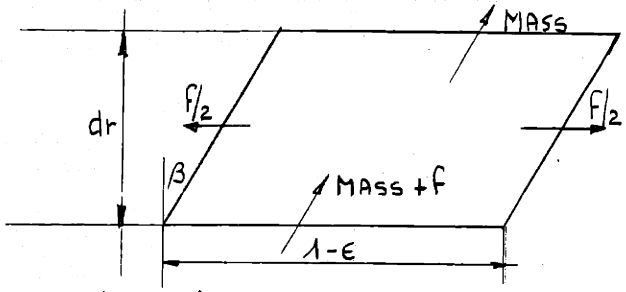

$$-\left(2\pi r b(1-\epsilon)W_j\cos\beta + f\right)\left(W_j r\sin\beta + r^2\omega\right) + f\left(r^2\omega + rW_j\sin\beta\right) +$$

$$+2\pi r b(1-\epsilon)W_j\cos\beta\left(r^2\omega + rW_j\sin\beta + \frac{d}{dr}\left(r^2\omega + rW_j\sin\beta\right)dr\right) =$$

$$= 2\pi r b(1-\epsilon)W_j\cos\beta\,\frac{d}{dr}\left(r^2\omega + rW_j\sin\beta\right)dr$$

2) For wake flow

$$-\left(2\pi r b\epsilon W_w\cos\beta - f\right)\left(W_w r\sin\beta + r^2\omega\right) - f\left(r^2\omega + rW_w\sin\beta\right)$$

$$+2\pi r b\epsilon W_w\cos\beta\left(r^2\omega + rW_j\sin\beta + \frac{d}{dr}\left(r^2\omega + rW_j\sin\beta\right)dr\right) =$$

$$= 2\pi r b\epsilon W_w\cos\beta\,\frac{d}{dr}\left(r^2\omega + rW_j\sin\beta\right)dr$$

b. Including other forces

1) Free stream

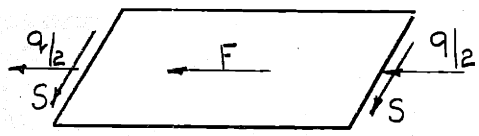

$$2\pi r\, b\,(1-\epsilon) W_j \cos\beta \frac{d}{dr}\left(r^2\omega + r W_j \sin\beta\right) +$$

$$+ c_f\, 2\pi r^2 (1-\epsilon) C_j \left(r\omega + W_j \sin\beta\right) +$$

$$+ \xi \mu b r \left(W_j - W_w\right)^2 \operatorname{tg}\beta + \frac{b r q_r}{\rho} = 0 \qquad (3)$$

The forms for the other equations are to be found in chapter 4 and are derived in the same way as the equation just cited.

DERIVATION OF THE EQUATIONS (7) and (8)

Combining equations (3) and (4) and multiplying by $\sin\beta$ one gets

$$W_j (1-\epsilon)\sin^2\beta + W_j^2 (1-\epsilon) r \cos\beta \sin\beta \dot{\beta} + W_j (1-\epsilon)\sin^2\beta\, r \overset{\circ}{W}_j +$$

$$+ W_w^2\, \epsilon \sin\beta \cos\beta\, r\dot{\beta} + W_w^2\, \epsilon \sin^2\beta + W_w\, \epsilon\, r \sin^2\beta \overset{\circ}{W}_w$$

$$+ 2 W_j (1-\epsilon) r\omega \sin\beta + 2 W_w\, \epsilon\, r\omega \sin\beta + \qquad (10)$$

$$+ \frac{c_f\, r \sin\beta}{b \cos\beta} \left[(1-\epsilon)\left(r\omega + W_j \sin\beta\right) C_j + \epsilon\left(r\omega + W_w \sin\beta\right) C_w\right] = 0$$

The continuity equations (1) and (2) are differentiated and (1) multiplied by $W_j \cos\beta$ and (2) by $W_w \cos\beta$ then (1) becomes:

$$- (1-\epsilon) W_j^2\, r \sin\beta \cos\beta \dot{\beta} + (1-\epsilon) W_j^2 \cos^2\beta + (1-\epsilon) W_j\, r \cos^2\beta \overset{\circ}{W}_j \qquad (11)$$

$$- r \cos^2\beta\, W_j^2 \overset{\circ}{\epsilon} + \frac{f W_j \cos\beta}{2\pi b} = 0$$

and (2)

$$- \epsilon W_w^2\, r \sin\beta \cos\beta \dot{\beta} + \epsilon W_w^2 \cos^2\beta + \epsilon W_w\, r \cos^2\beta \overset{\circ}{W}_w \qquad (12)$$

$$+ W_w^2 \cos^2\beta\, r \overset{\circ}{\epsilon} - \frac{f W_w \cos\beta}{2\pi b} = 0$$

Adding (11) and (12) to (10) the following form results:

$$(1-\epsilon)W_j^2 + W_j(1-\epsilon)r\dot{W}_j - \dot{\epsilon}\cos^2\beta\, r\left[W_j^2 - W_w^2\right] + \frac{P}{2\pi b}\cos\beta\left[W_j - W_w\right]$$

$$+ W_w^2\epsilon + W_w\epsilon r\dot{W}_w + 2r\omega\sin\beta\left[W_j(1-\epsilon) + W_w\epsilon\right] +$$

$$+ \frac{C_f r\sin\beta}{b\cos\beta}\left[(1-\epsilon)(r\omega + W_j\sin\beta)C_j + \epsilon(r\omega + W_w\sin\beta)C_w\right] = 0 \qquad (14)$$

Eliminating q from equations (4) and (6) another expression is obtained for the pressure.

$$\frac{1}{\rho}\frac{dp}{dr} = r\omega^2 - \frac{1}{2}\frac{dW_w^2}{dr} - \frac{C_f C_w}{b\cos\beta}\left(r\omega\sin\beta + W_w\right) +$$

$$+ \frac{\xi\,\mu\left(W_j - W_w\right)^2}{2\pi r\epsilon\cos^2\beta} \qquad (15)$$

Eliminating $\frac{dp}{dr}$ from (9) and (15) and multiplying by $\frac{\epsilon r}{2}$ one obtains:

$$r\epsilon W_j\dot{W}_j + W_w r\dot{W}_w\epsilon + \frac{\xi\,\mu\left(W_j - W_w\right)^2}{2\pi(1-\epsilon)\cos^2\beta}$$

$$+ \frac{C_f\epsilon r}{b\cos\beta}\left[\left(W_j + r\omega\sin\beta\right)C_j - \left(W_w + r\omega\sin\beta\right)C_w\right] = 0 \qquad (16)$$

By adding (16) to (14) one is able to eliminate $\dot{W}_w$ so equation (7) follows

$$(1-\epsilon)W_j^2 + W_j r\dot{W}_j - \dot{\epsilon}\cos^2\beta\, r\left[W_j^2 - W_w^2\right] + \frac{P}{2\pi b}\cos\beta\left[W_j - W_w\right] \qquad (7)$$

$$+ W_w^2\epsilon + 2r\omega\sin\beta\left[W_j(1-\epsilon) + W_w\epsilon\right] + \frac{\mu\xi\left(W_j - W_w\right)^2}{2\pi(1-\epsilon)\cos^2\beta} +$$

$$+ \frac{C_f r}{b\cos\beta}\left[\left(r\omega\sin\beta + W_j\sin^2\beta\right)C_j + \epsilon\cos^2\beta\left(W_j C_j - W_w C_w\right)\right] = 0$$

Eliminating $\frac{dp}{dr}$ from (9) and (15), multiplying by $(1-\epsilon)\frac{r}{2}$ one gets:

$$r(1-\epsilon)W_j\dot{W}_j - (1-\epsilon)W_w r\dot{W}_w + \frac{\mu\zeta(W_j-W_w)^2}{2\pi\epsilon\cos^2\beta} +$$

$$+\frac{C_f r(1-\epsilon)}{b\cos\beta}\left[(W_j + r\omega\sin\beta)C_j - C_w(W_w + r\omega\sin\beta)\right] = 0 \qquad (17)$$

Subtracting (17) from (14) we obtain an expression for W_j, W_w, ϵ which is equation 8 of the text.

$$(1-\epsilon)W_j^2 - \dot{\epsilon}\cos^2\beta\, r\left[W_j^2 - W_w^2\right] + \frac{f\cos\beta}{2\pi b}\left[W_j - W_w\right] + W_w^2\epsilon + W_w r\dot{W}_w -$$

$$-\frac{\mu\zeta\left[W_j - W_w\right]^2}{2\pi\epsilon\cos^2\beta} + 2r\omega\sin\beta\left[W_j(1-\epsilon) + W_w\epsilon\right] \qquad (8)$$

$$\frac{+C_f r}{b\cos\beta}\left[(W_w\sin^2\beta + r\omega\sin\beta)C_w - (1-\epsilon)\cos^2\beta(W_j C_j - W_w C_w)\right] = 0$$

Appendix II

BOUNDARY LAYER EFFECT ON SHEAR FORCE

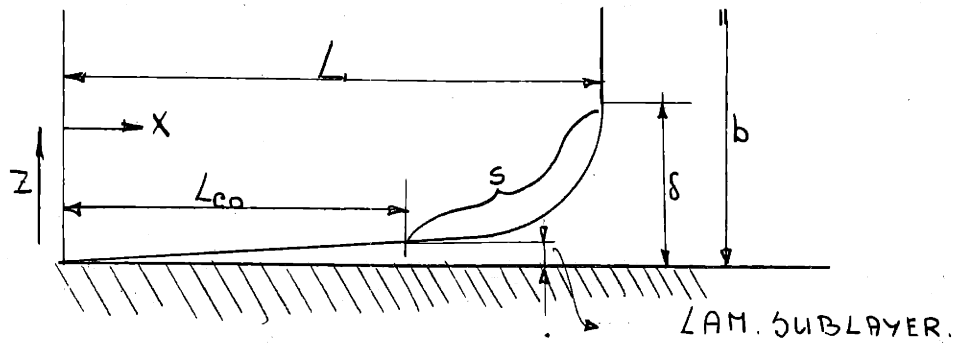

The surface on which the shear force is acting is $\frac{dr}{\cos\beta}\left[b - 2\delta + 2S\right]$

The form of the curve may be written as (see sketch)

$$\frac{X}{L} = \left[\frac{Z}{\delta}\right]^{1/10} \quad \text{FOR } 0 \leq Z \leq \delta \quad \text{AND} \quad L = \int_{r_i}^{r} \frac{dr}{\cos\beta}$$

Further

$$dS = \sqrt{(dZ)^2 + (dX)^2} = \sqrt{1 + \left(\frac{dZ}{dX}\right)^2}\, dX \approx \left[1 + \left(\frac{dZ}{dX}\right)^2 \frac{1}{2}\right] dX$$

$$\text{OR} \quad S = \int_{X=L_{co}}^{X=L} \left[1 + \left(\frac{dZ}{dX}\right)^2 \frac{1}{2}\right] dX = \int_{L_{co}}^{L} \left[1 + 50\, \frac{X^{18}\delta^2}{L^{20}}\right] dX$$

The value of δ should be estimated from boundary layer theory (ref. 3). The following values were obtained for a particular case where $C_i = 80\ ft/_{SEC}$ and $\alpha = 20^\circ$

R	1.02	1.06	1.1	1.18	1.26	1.34	1.42
inches δ	.1	.1869	.2629	.396	.5089	.626	.7073

The thickness of the laminar sublayer may be found from

$$\frac{zV^*}{\nu} = 50 \qquad V^* = \sqrt{\frac{\tau_o}{\rho}} = \sqrt{\frac{C_f}{2}U^2} = 16 \quad \text{OR} \quad z = 0.024 \text{ INCH.}$$

Now one is able to estimate the value of L_{co}

$$\text{AT} \quad R = 1.1 \quad \frac{L_{co}}{L} = \left[\frac{0.024}{0.2629}\right]^{1/10} = 0.79$$

With this information we are able to calculate the distance S. Figure 5 gives the final result for the area increase which is essentially the multiplier μ.

Nomenclature for Part One

A	area for heat transfer
b	diffuser depth
C	absolute velocity
C	friction coefficient
C	specific heat at constant pressure
f	area rate of flow crossing the wake border
F	wall friction force per unit area
g_o	conversion factor
$\bar{h}$	enthalpy
H	shape factor displacement thickness over momentum thickness
l	mixing length
L	length of path of flow particle
L_{co}	length up to cut-off point
M	mass
p	pressure
P_{Rt}	turbulent Prandtl number $\frac{C_p \epsilon_m}{\epsilon_h}$
q	pressure force
Φ	heat rate $BTU\|_{SEC}$
r	radius
R	dimensionless radius $\frac{r}{r_i}$; Rey = Reynold number
$\bar{R}$	gas constant
S	length

S	shear force per unit area
t	time
T	temperature
u	velocity in direction of main stream
v^*	friction velocity
v	velocity perpendicular to u
$\overline{u'v'}$	Reynold stress
V_1	velocity of mass crossing the wake boundary
V_θ	tangential velocity
W	relative velocity
x	direction of main stream
y	direction perpendicular to x and parallel to diffuser walls
z	direction perpendicular to x and y

Subscript

i	values at initial condition
j	value at free stream condition
w	value at wake stream
W', β', ε'	quantities differentiated with respect to r
o	values at stagnation condition
ϑ	with respect to momentum thickness
u^*	with respect to friction velocity

Greek letters

α	angle between absolute flow direction and radial direction
β	angle between relative flow direction and radial direction
Γ	coefficient for mass transfer
δ	boundary layer thickness
Δ	difference
ϵ	ratio of wake width and sum of free stream and wake width
ϵ_m	momentum diffusivity
ϵ_h	heat diffusivity
ϵ_Γ	mass diffusivity
ξ	turbulent shear force coefficient
μ	multiplier
ν	kinematic viscosity
ρ	density
τ	shear force
ω	angular velocity

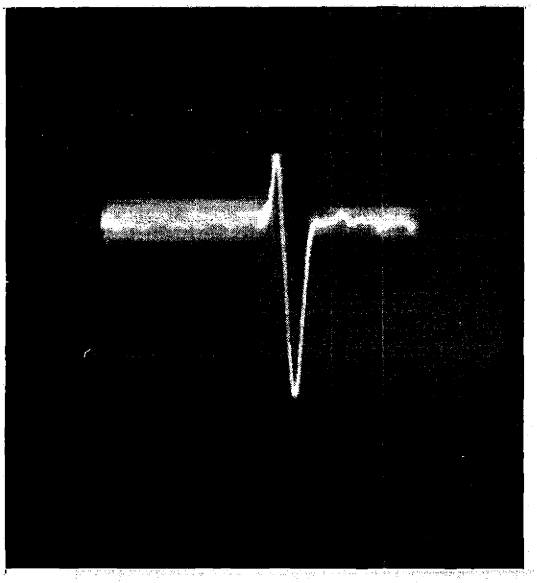

PICTURE A.

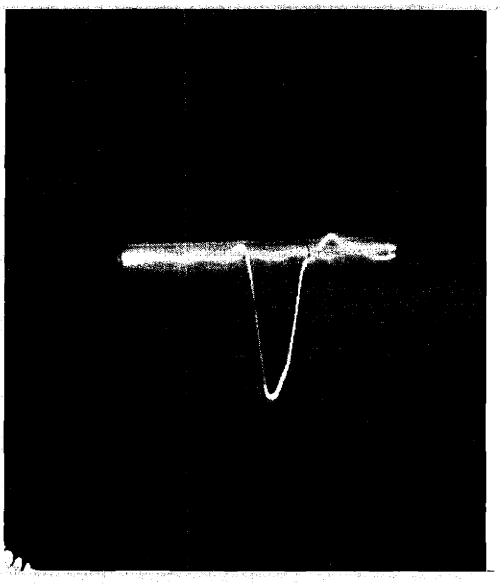

PICTURE B

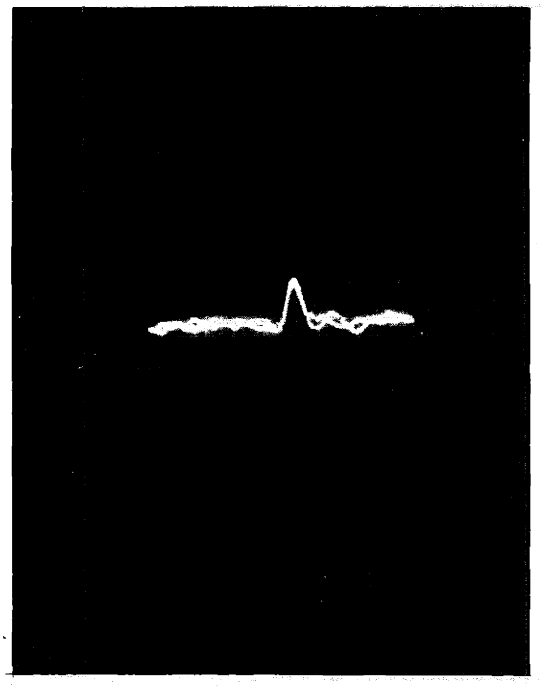

PICTURE C

FIG. 1. HOT-WIRE RESPONSES FOR LOW AND HIGH WAKE SPEEDS.

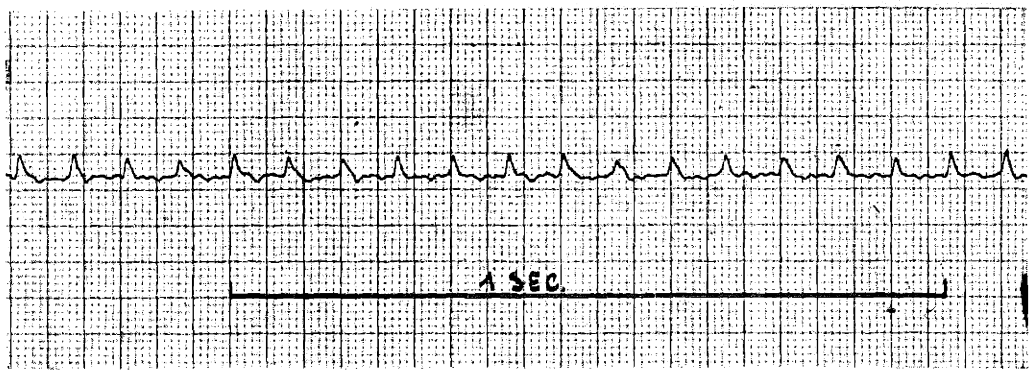

TRACE a R = 1.03.

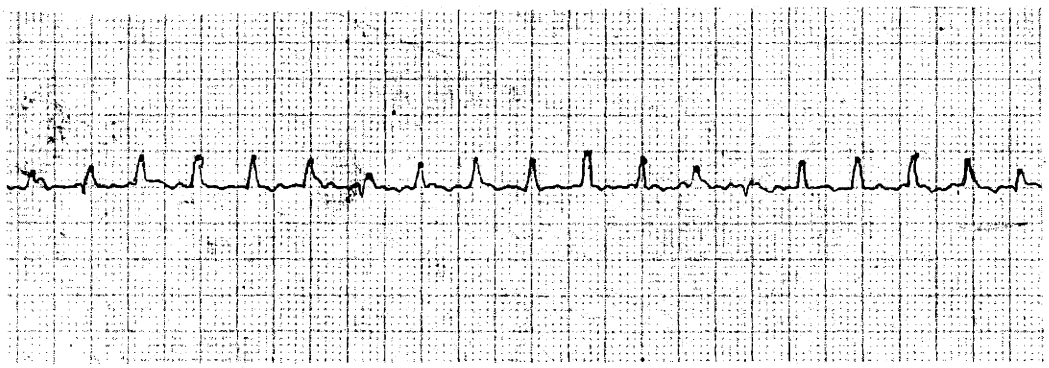

TRACE b R = 1.26

FIG. 2 WAKE AND FREE-STREAM VELOCITIES VERSUS TIME [HIGH WAKE SPEED]

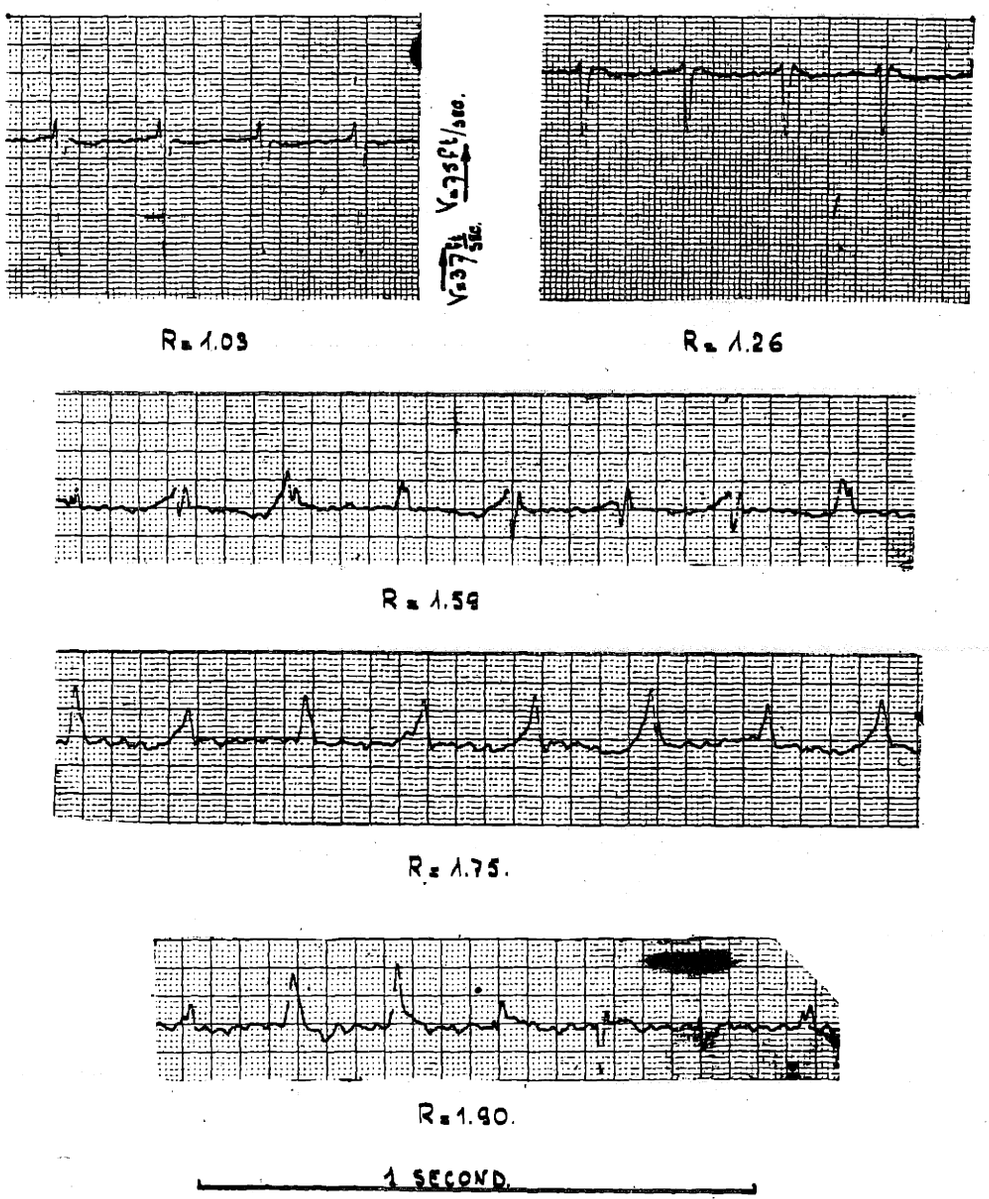

FIG. 3 WAKE AND FREE-STREAM VELOCITIES VERSUS TIME. [LOW WAKE SPEED]

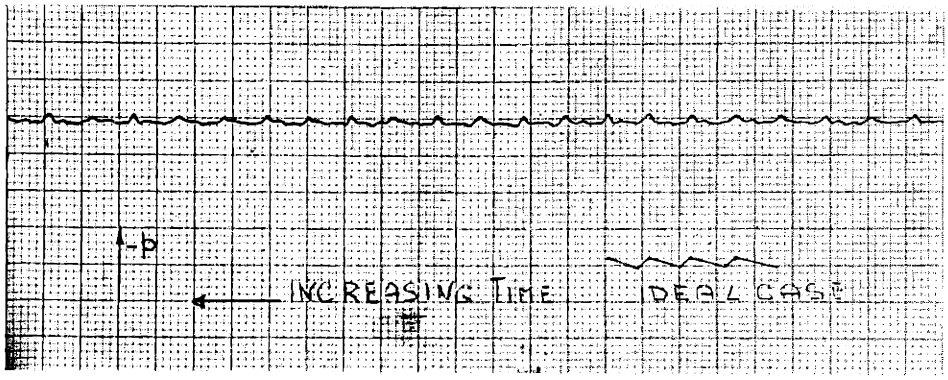

FOR HIGH WAKE SPEEDS

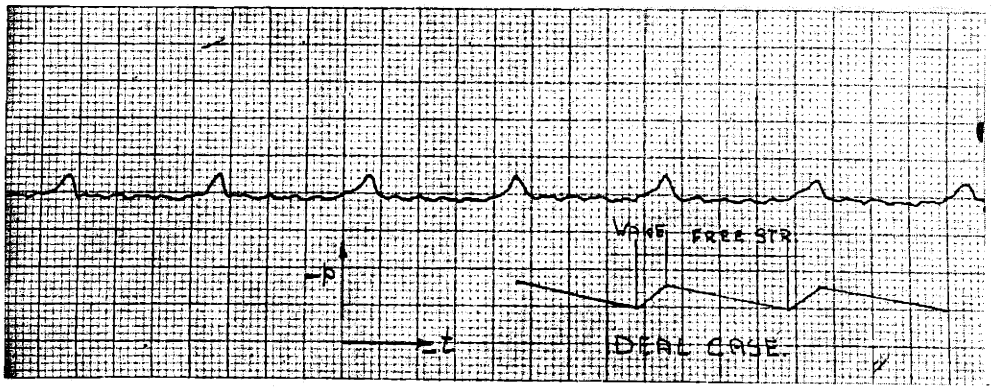

LOW WAKE SPEED.

FIG. 4 DYNAMIC PRESSURE RESPONSE. [1SEC = 97MM]

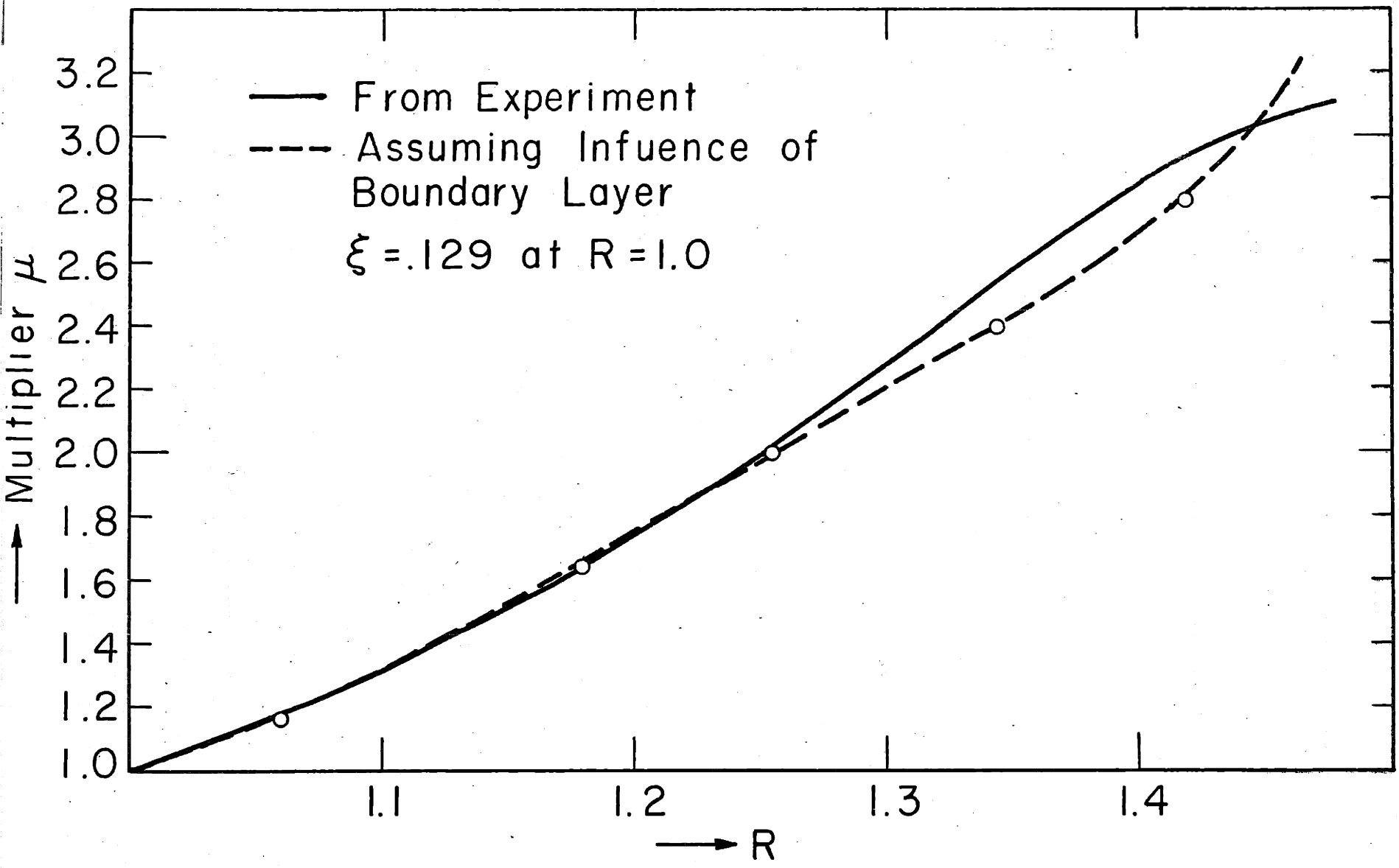

FIG. 5 COMPARISON OF BEHAVIOR OF MULTIPLIER FOR SHEAR STRESS AREA

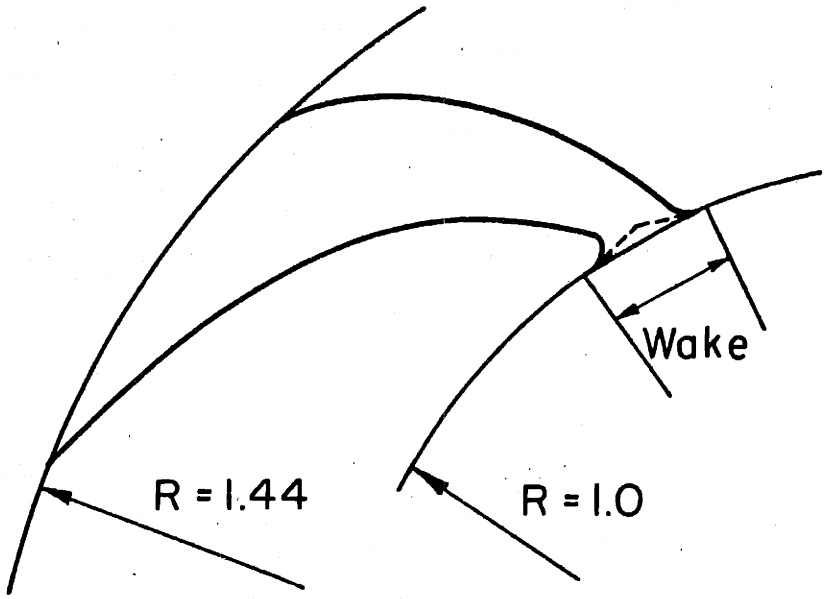

V_w = 90 ft/sec

—— Wake [Present Theory]

--- Senoo's Theory

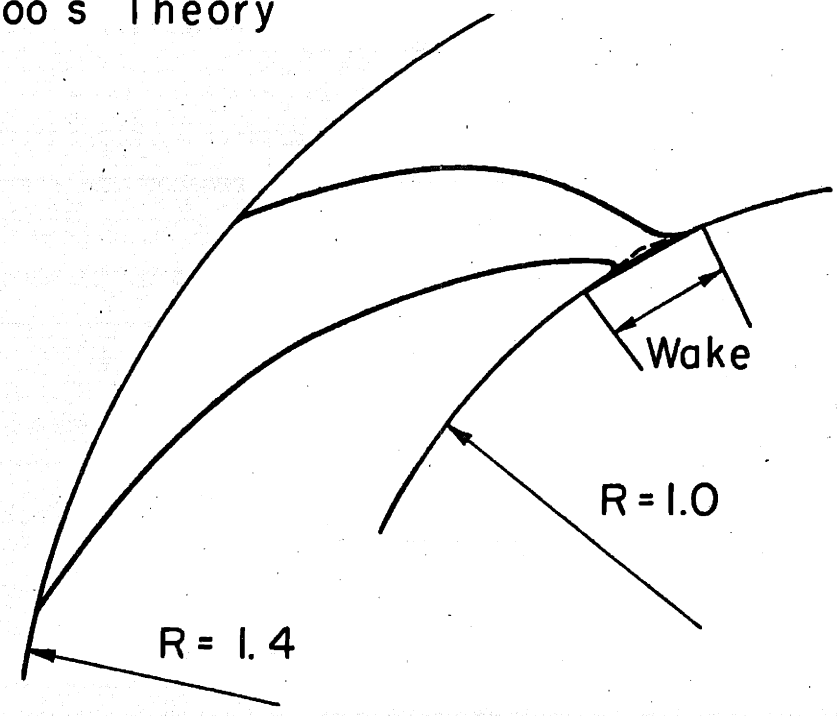

V_w = 110 ft/sec

FIG. 6 FORM OF WAKE AS OBSERVER IS ROTATING WITH THE WAKE

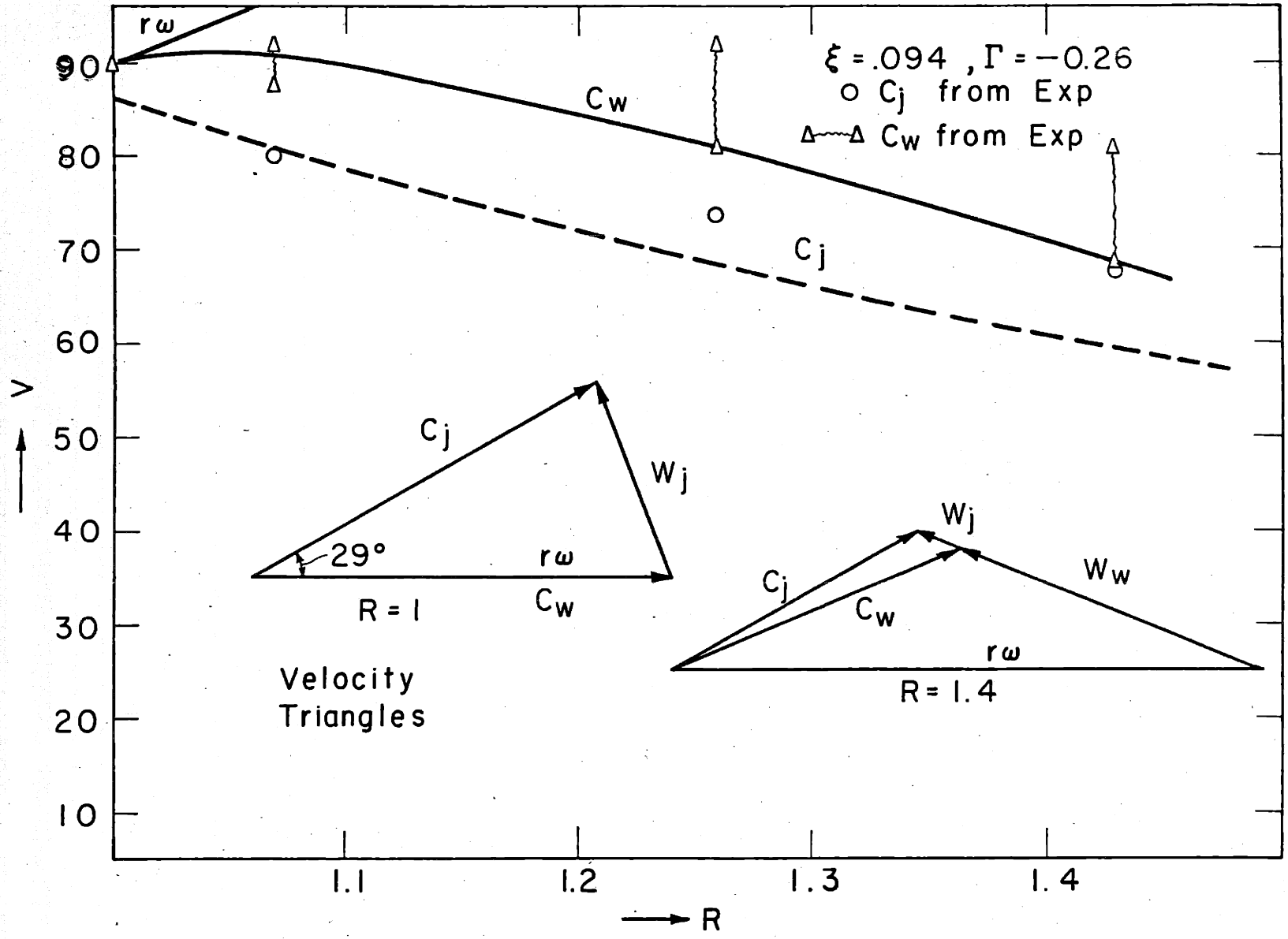

FIG. 7 WAKE AND FREE-STREAM VELOCITIES TEST VII

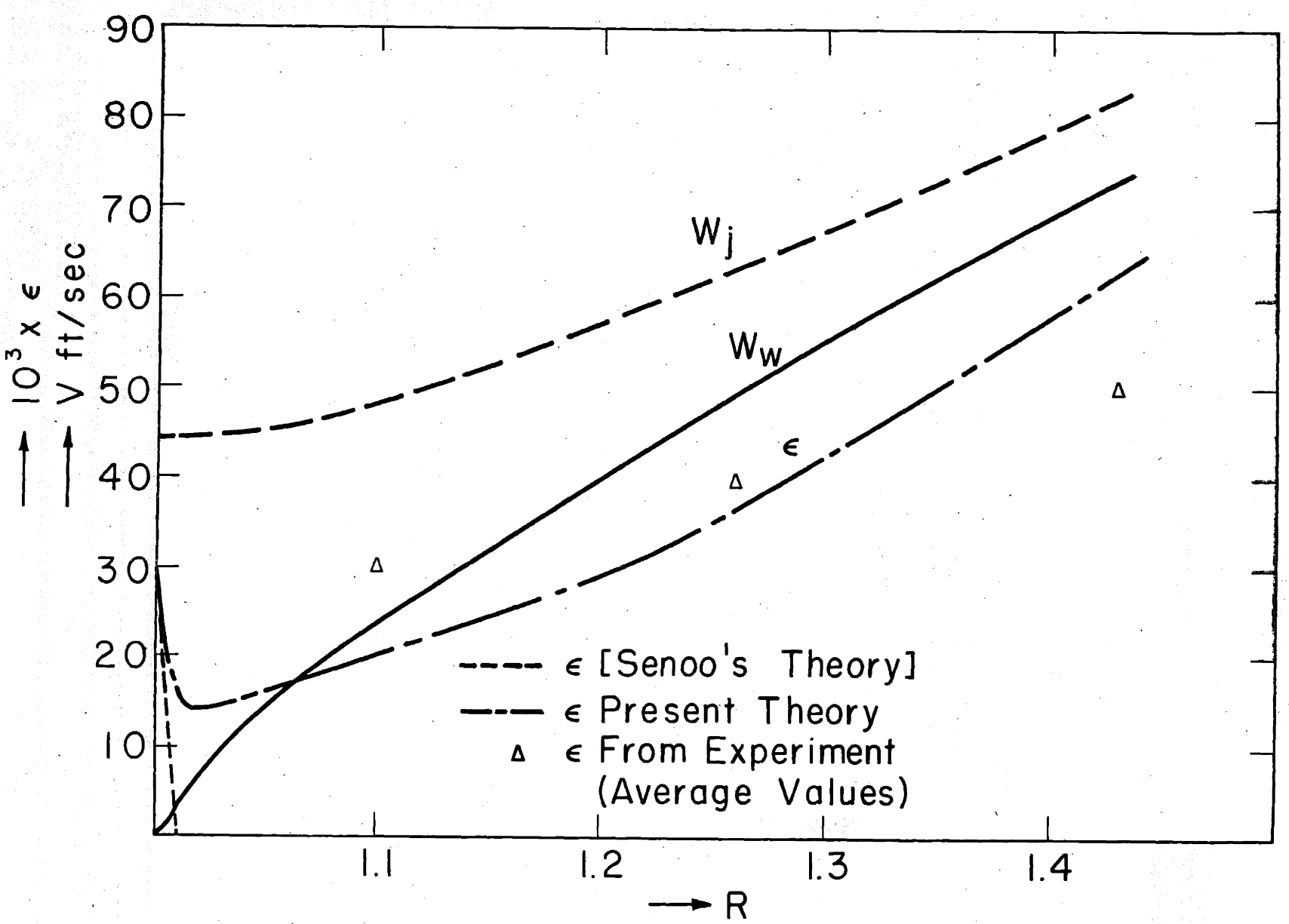

FIG. 8 RELATIVE VELOCITIES AND WAKE WIDTH (TEST VII)

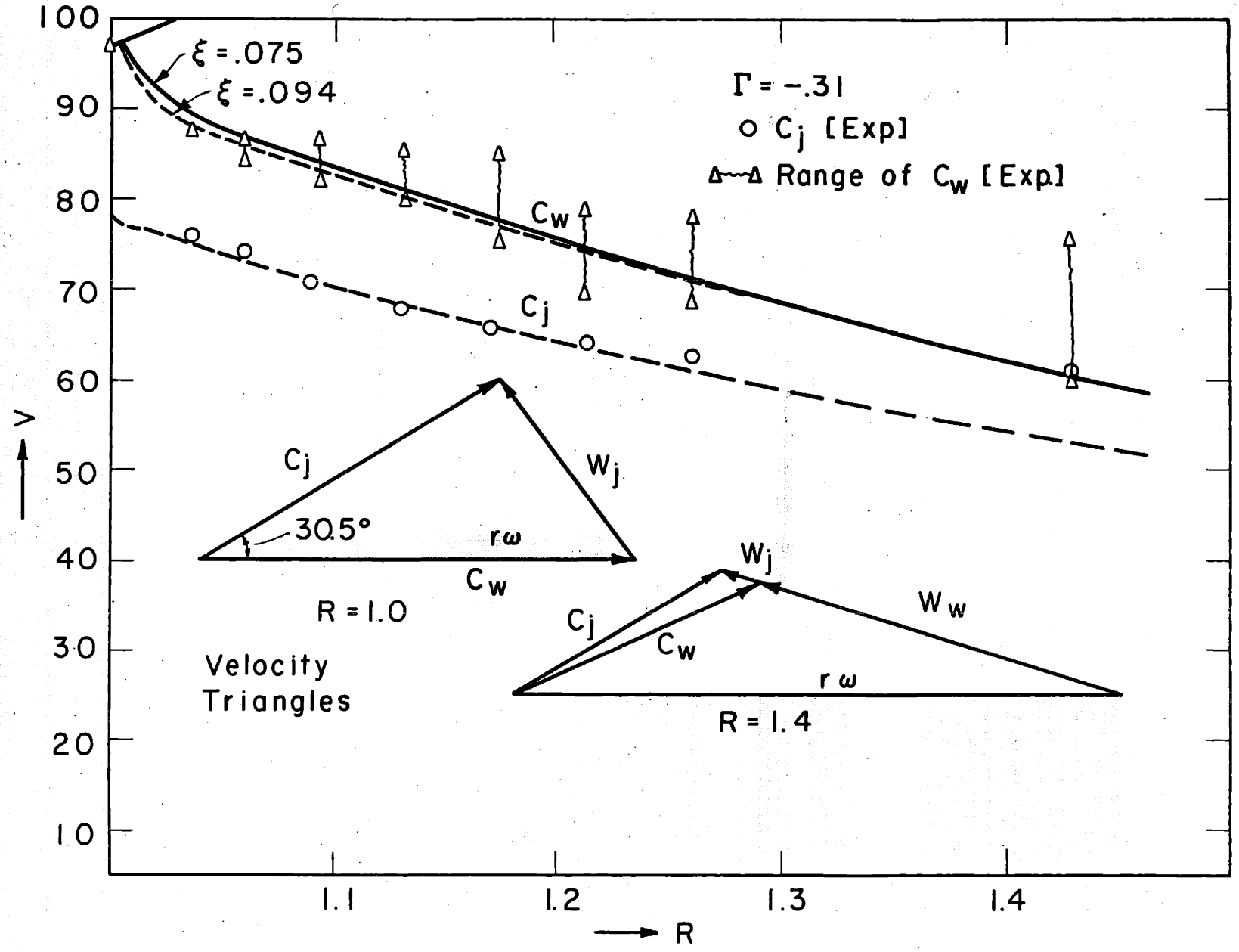

FIG. 9 WAKE AND FREE STREAM VELOCITIES TEST XI

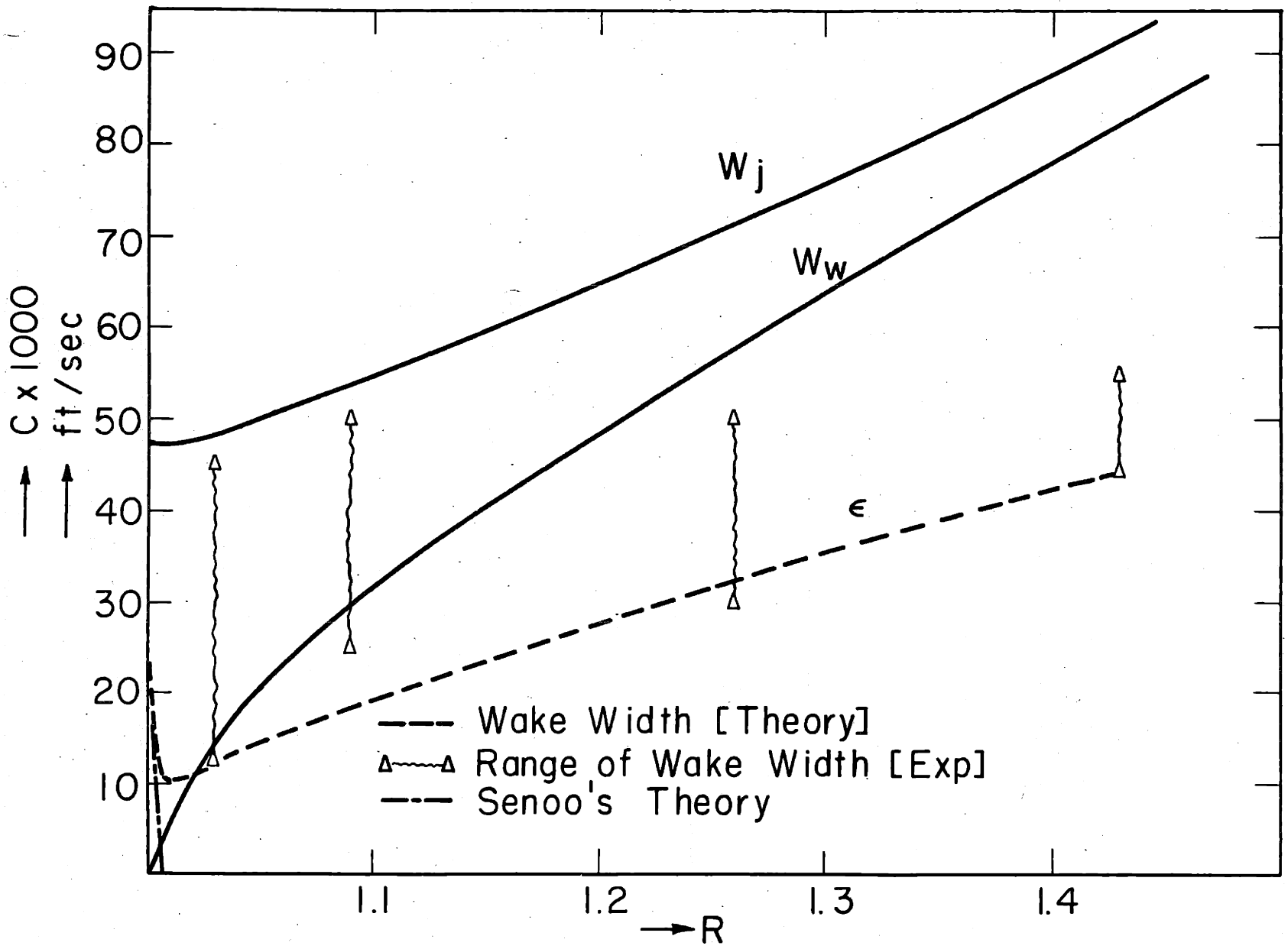

FIG. 10 RELATIVE VELOCITIES AND WAKE WIDTH TEST XI

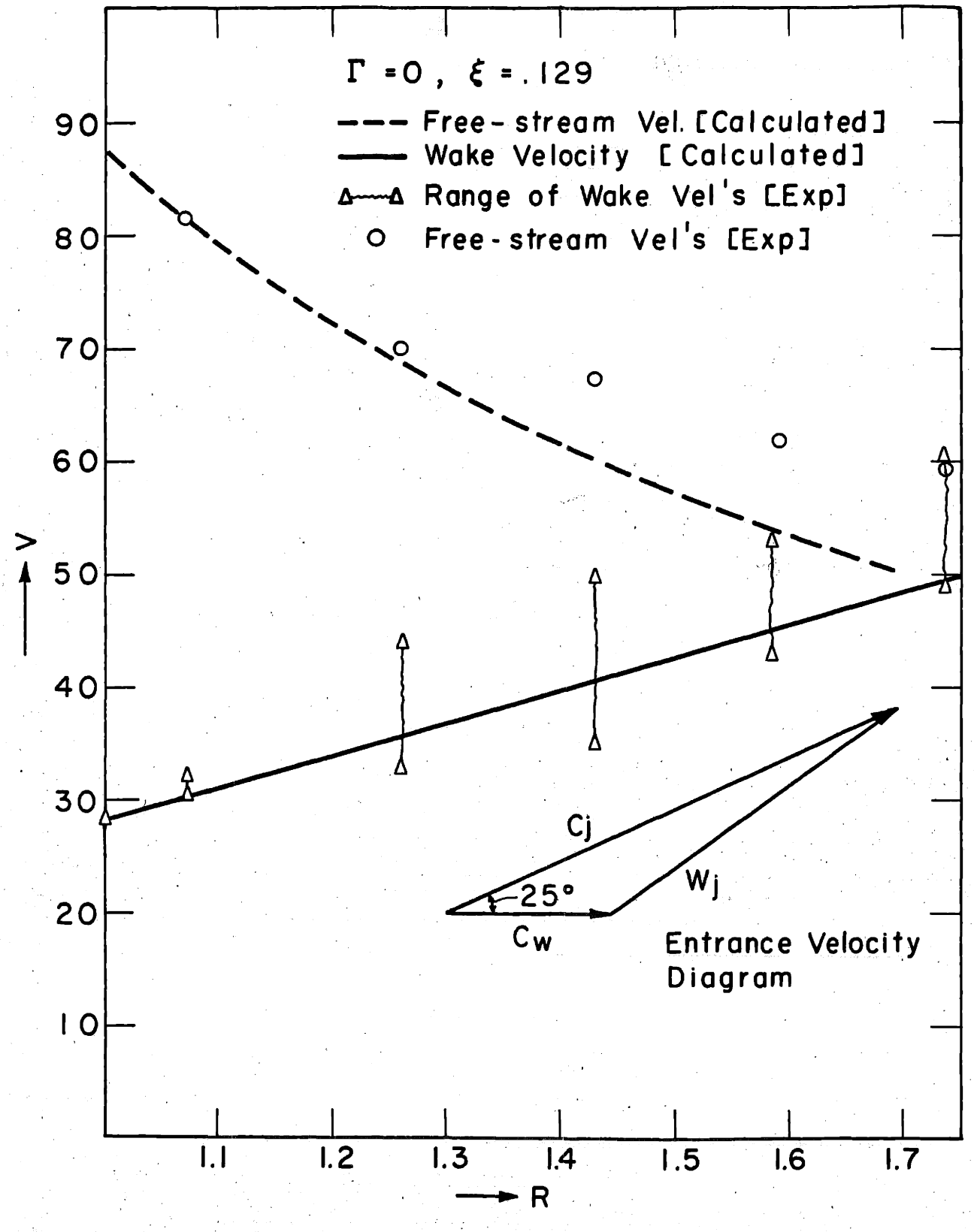

FIG. 11 WAKE AND FREE STREAM VELOCITIES
[V_W = 28.4 ft/sec] TEST 111

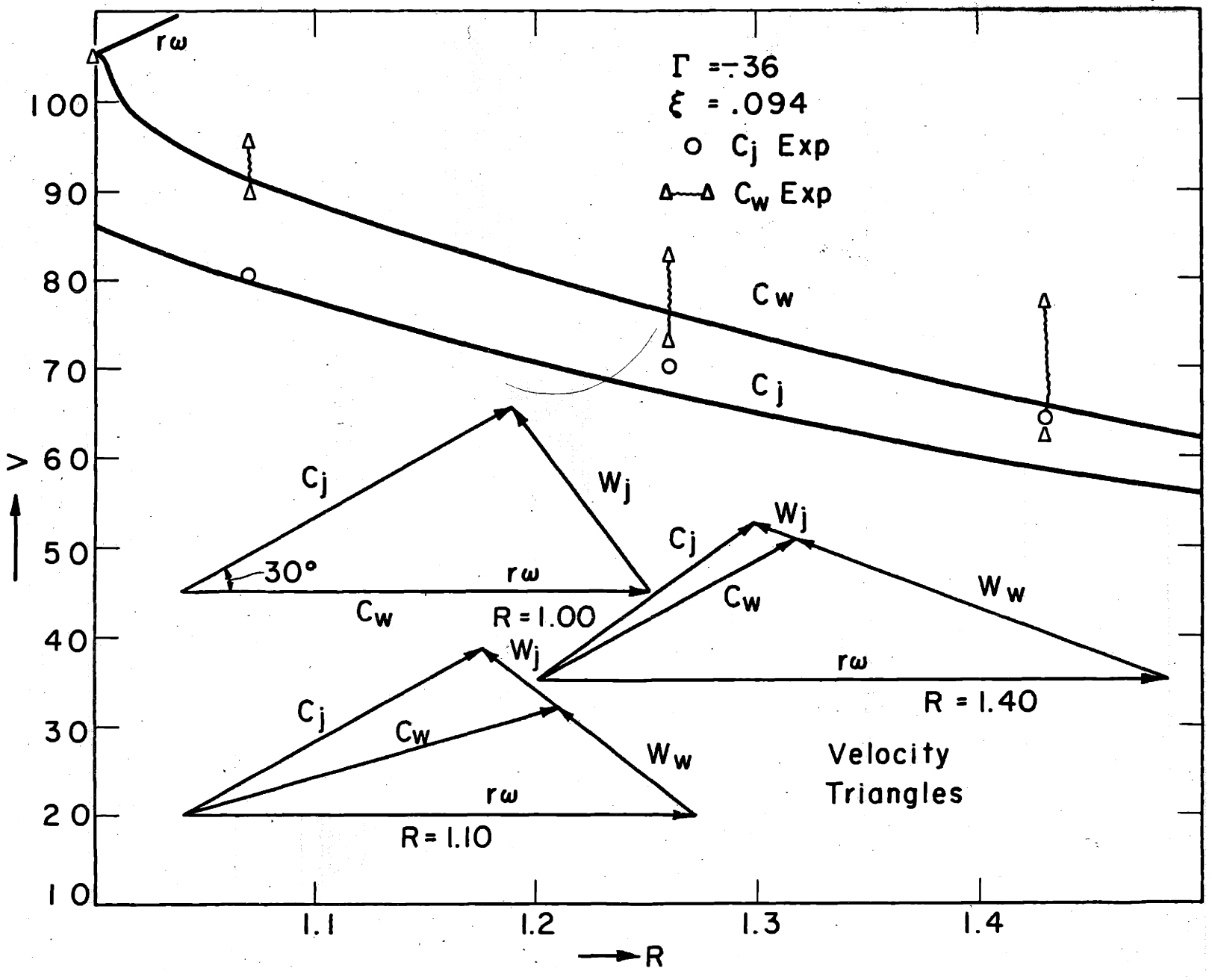

FIG. 12 WAKE AND FREE-STREAM VELOCITIES (TEST VIII)

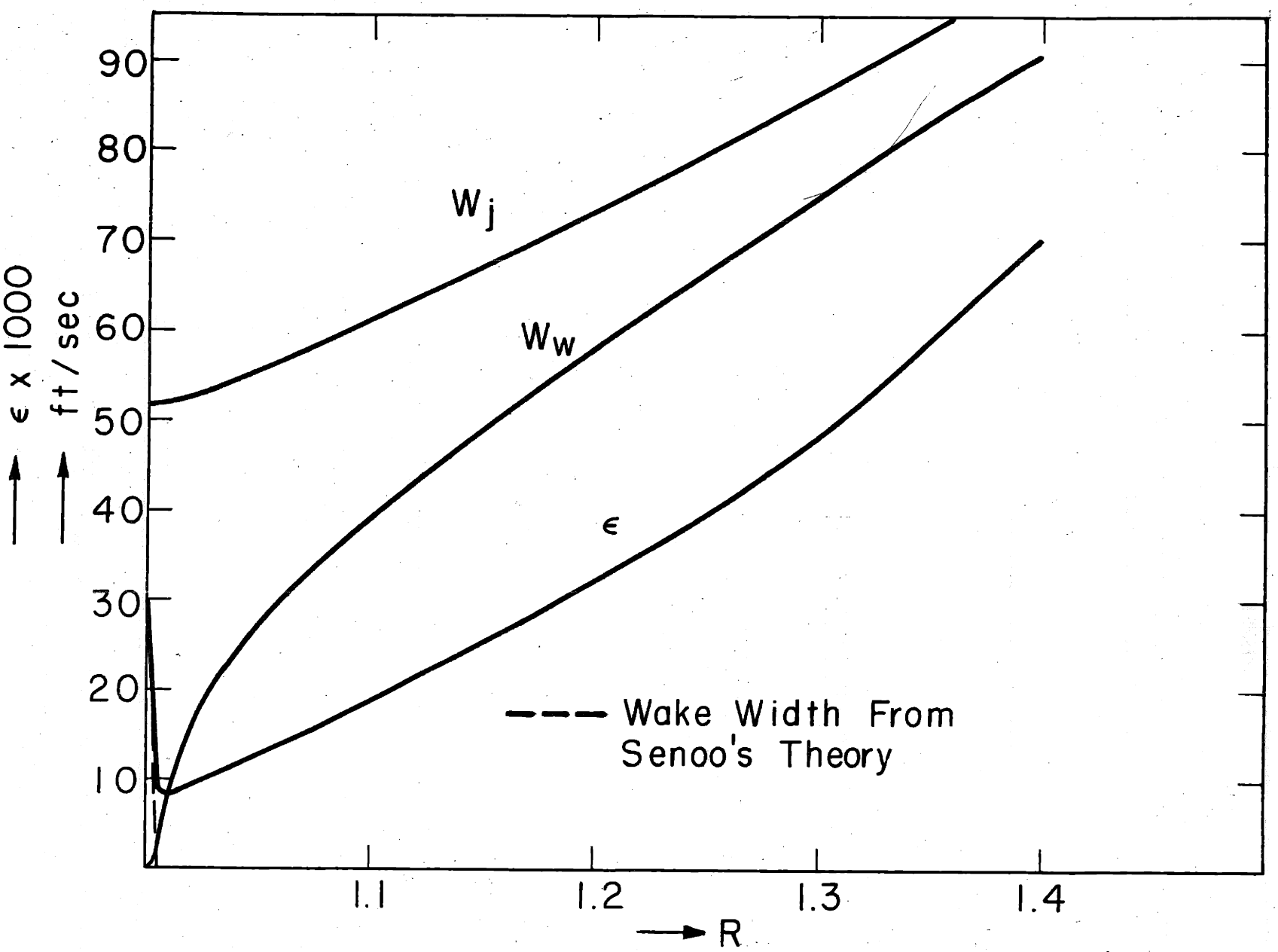

FIG. 13 RELATIVE VELOCITIES AND WAKE WIDTH FROM PRESENT THEORY (TEST VIII)

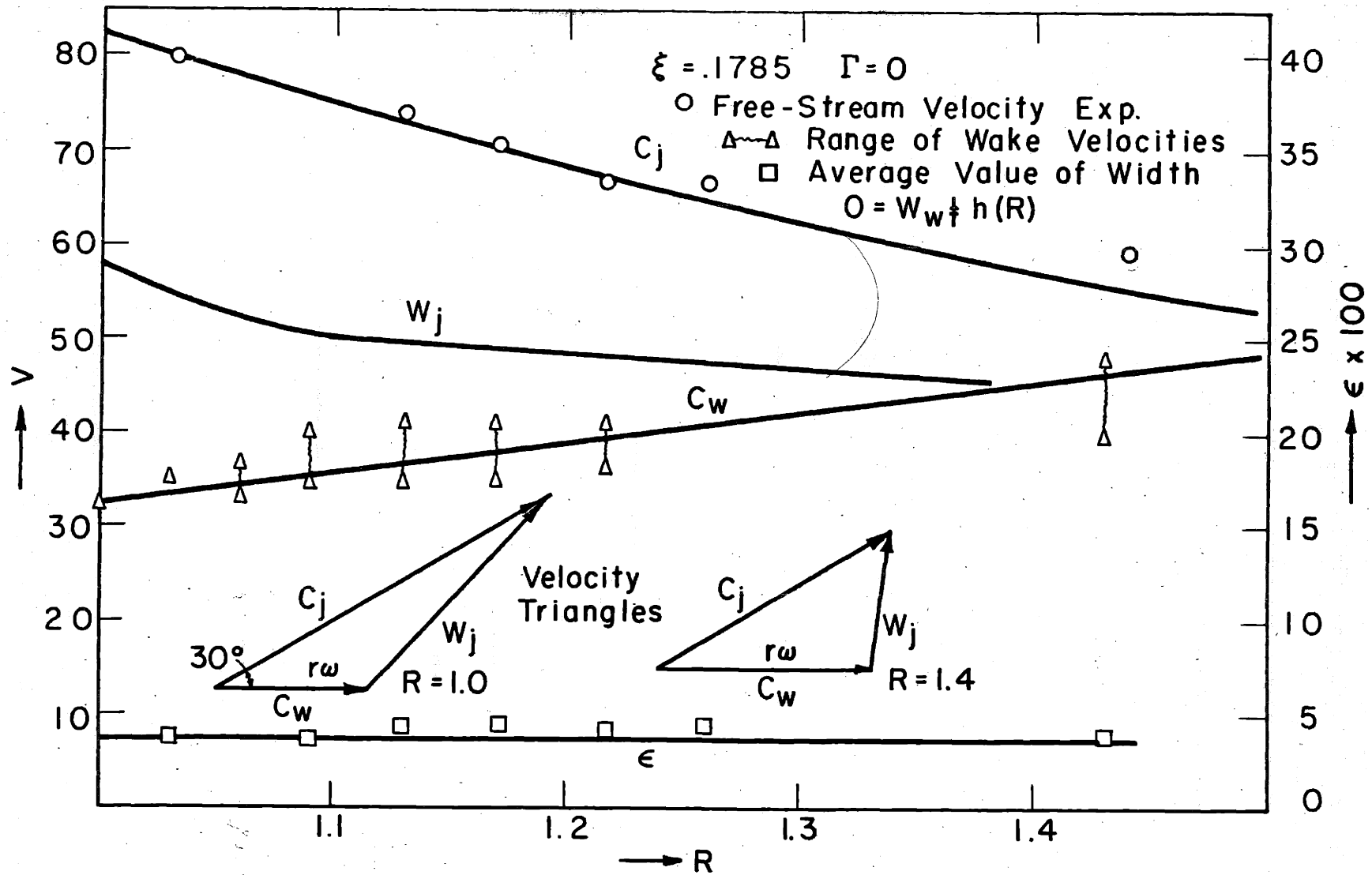

FIG. 14 ABSOLUTE VELOCITIES AND WAKE WIDTH (TEST X)

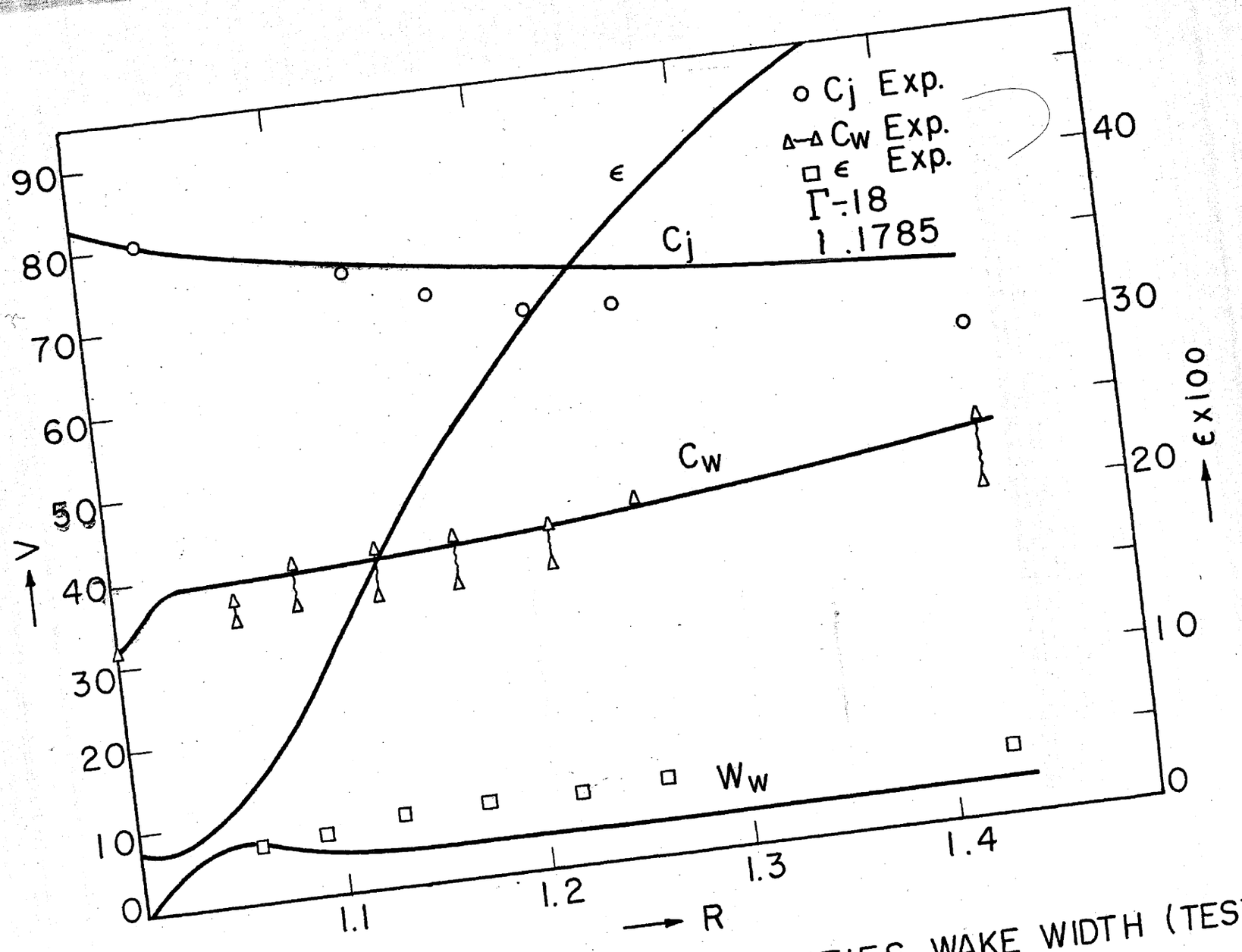

FIG. 15 FREE-STREAM AND WAKE VELOCITIES WAKE WIDTH (TEST X)

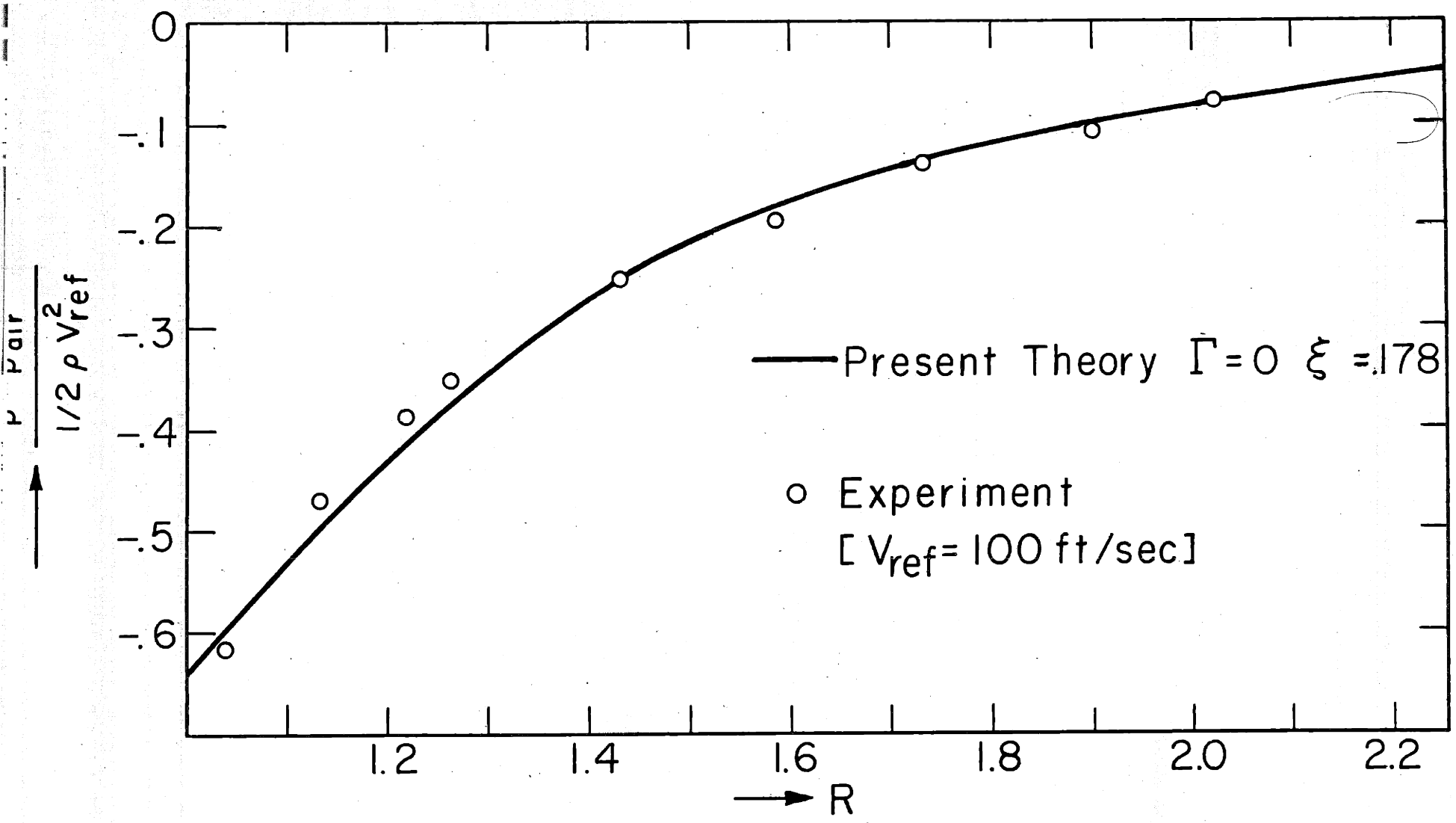

FIG. 16 STATIC PRESSURE RISE IN DIFFUSER (TEST X)

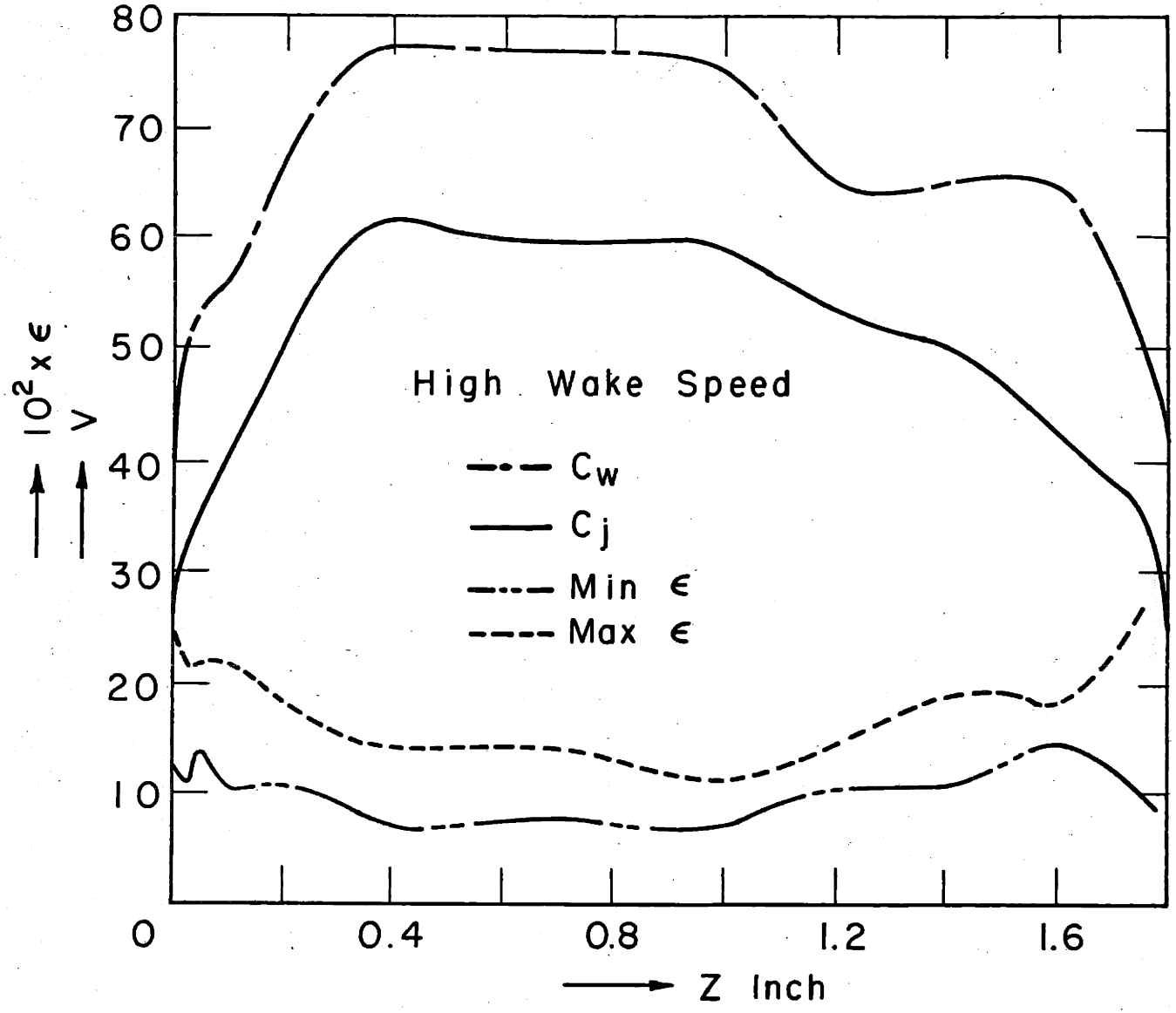

FIG. 17 VARIATION OF C_j, C_w AND ϵ VERSUS DIFFUSER DEPTH [EXP.]

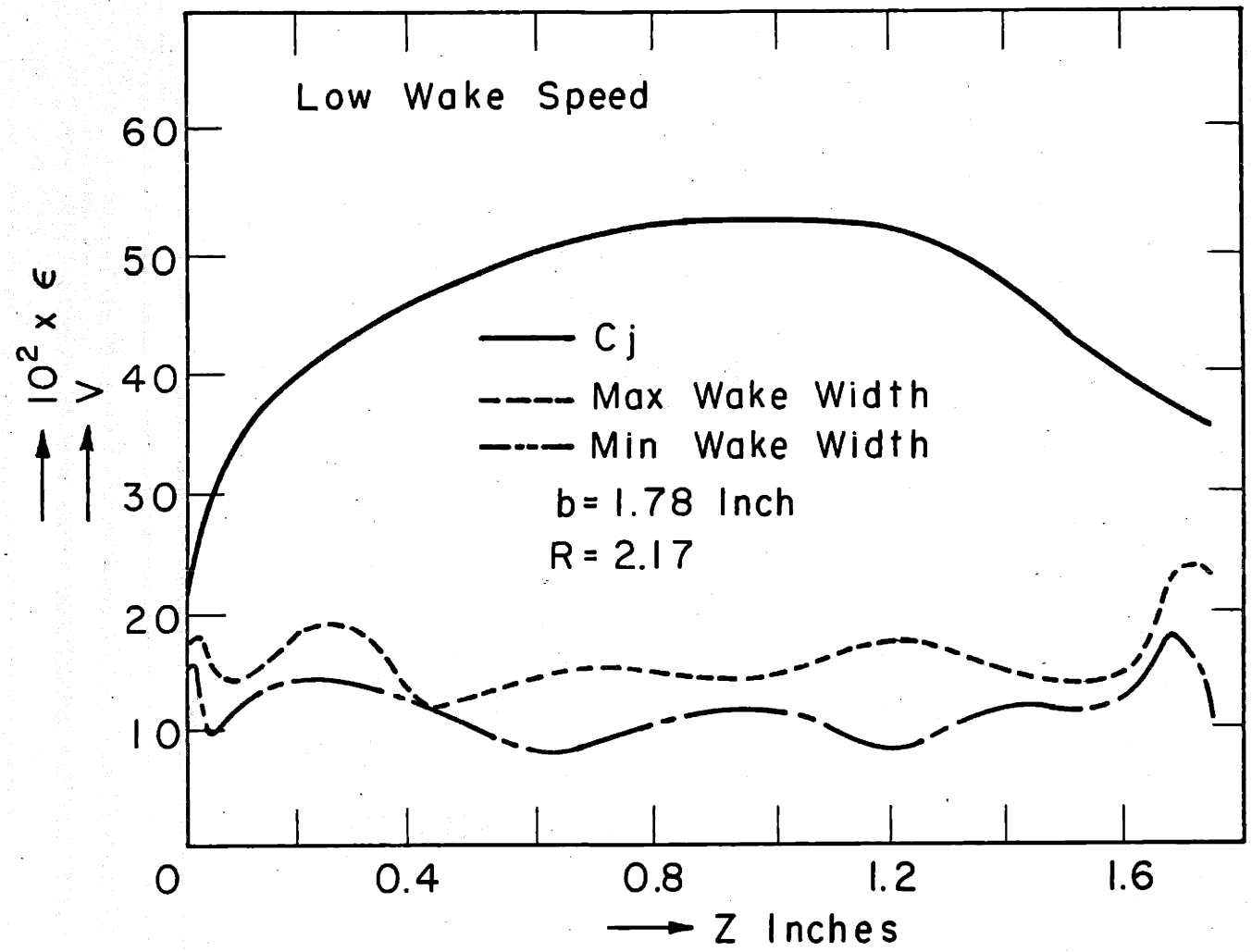

FIG. 18 VARIATION OF Cj AND ϵ VERSUS DIFFUSER DEPTH [EXPERIMENTAL]

I INTRODUCTION TO PART II

The problems concerning the motion of rotating masses has from ancient times attracted much attention. Since 1850, attention was focussed on the behavior of liquid on a rotating sphere, which was essentially an attempt to predict the tidal waves of the oceans on the rotating earth, under the influence of some attractive force (moon, sun, etc.). The numerous tables for tides now available show the success of these theoretical investigations of man like McLaurin, Jacobi, and Poincaré. Narrowing our attention, we note the first success of the theory of hydrodynamic stability applied to motion of rotating liquid, which was achieved by G. I. Taylor (12). His experiments were conducted with a liquid contained between two concentric cylinders, which could rotate with different velocities. Present investigations, following the outlined tradition, involve the motions under the influence of coriolis forces, gravitation and electro-magnetic fields. The first two are important in problems related to meteorology, while all three factors enter astrophysical problems.

In the following we will investigate the problem of a rotating fluid mass, when it passes through a radial vaneless diffuser, where the pressure increases and the velocity decreases. The problem manifested itself when there was an attempt to decrease the through flow, so that the angle of flow β would become bigger than $75°$. Observations showed that the flow became pulsating and periodic. The only other manifestation of this problem known to the author is

that of reference 13 (Maroti). On the other hand, it is known that a centrifugal impeller in combination with a radial diffuser will "surge" when the through flow is cut down well below the design value. Experiments in industry have indicated that if certain provisions are made in the diffuser, the "surge" may be delayed. It is therefore felt that an investigation of the problem encountered here would be very valuable for the understanding of the flow phenomena occurring in centrifugal pumps and compressors.

I-1 ANALYSIS OF THE UNSTEADY FLOW

The general case of a perturbed flow may be treated as a superposition of two flows: the steady flow and an unsteady flow. The steady flow in this case will be a free vortex flow and the assumption is made that the steady part is unaffected by the unsteady flow; accordingly the radial and tangential velocities are inversely proportional to the radius and the pressure is proportional to $1/r^2$. The unsteady part will be treated as an unknown function of time, angle and radius:

$$\hat{u} = f(\alpha, r, t) \; ; \; \hat{v} = g(\alpha, r, t) \; ; \; \hat{p} = h(\alpha, r, t)$$

The flow is assumed to be inviscid, two-dimensional and incompressible. The problem then reduces to the solution of the three unknowns $\hat{u}, \hat{v}, \hat{p}$ with the equations of continuity and momentum in the radial and tangential directions. If μ is the tangent of the angle between the steady streamline and the circumference, then the total velocities and pressure may be expressed as

$$u = \bar{w}\left(\frac{\mu}{r} + \hat{u}\right) \qquad (1)$$

$$V = \varpi\left(\frac{1}{r} + \hat{V}\right) \tag{2}$$

$$p = K + \tfrac{1}{2}\rho\varpi^2\left[-\frac{1}{r^2} - \frac{\mu^2}{r^2} + \hat{p}\right] \tag{3}$$

where ϖ = constant = $\Omega \bar{r}^2$

The momentum equation in radial direction

$$\frac{\partial u}{\partial t} + u\frac{\partial u}{\partial r} + \frac{v}{r}\frac{\partial u}{\partial \alpha} - \frac{v^2}{r} = -\frac{\partial p}{\partial r}\frac{1}{\rho} \tag{4}$$

and in tangential direction

$$\frac{\partial v}{\partial t} + u\frac{\partial v}{\partial r} + \frac{v}{r}\frac{\partial v}{\partial \alpha} + \frac{uv}{r} = -\frac{1}{r}\frac{\partial p}{\partial \alpha}\frac{1}{\rho} \tag{5}$$

with the continuity equation

$$\frac{1}{r}\frac{\partial (ru)}{\partial r} + \frac{1}{r}\frac{\partial v}{\partial \alpha} = 0$$

constitutes the formal statement of the problem. Inserting (1), (2) and (3) into (4) and (5), the following two equations result:

$$\varpi\frac{\partial \hat{u}}{\partial t} - \frac{\varpi^2}{r^2}\mu\hat{u} + 2\varpi^2\frac{\mu}{r}\frac{\partial \hat{u}}{\partial r} + \frac{\varpi^2}{r^2}\frac{\partial \hat{u}}{\partial \alpha} + \frac{\varpi^2}{r}\hat{V}\frac{\partial \hat{u}}{\partial \alpha} - 2\frac{\varpi^2}{r^2}\hat{V} - \frac{\varpi^2}{r}\hat{V}^2 = -\frac{1}{2}\varpi^2\frac{\partial \hat{p}}{\partial r} \tag{6}$$

$$\varpi\frac{\partial \hat{v}}{\partial t} + \varpi^2\frac{\mu}{r}\frac{\partial \hat{v}}{\partial r} + \varpi^2\hat{u}\frac{\partial \hat{v}}{\partial r} + \frac{\varpi^2}{r^2}\frac{\partial \hat{v}}{\partial \alpha} + \frac{\varpi^2}{r}\hat{V}\frac{\partial \hat{v}}{\partial \alpha} + \varpi^2\frac{\mu\hat{v}}{r^2} + \frac{\varpi^2}{r}\hat{u}\hat{v} = -\frac{1}{2}\frac{1}{r}\varpi^2\frac{\partial \hat{p}}{\partial \alpha} \tag{7}$$

The continuity equation becomes

$$\frac{\varpi}{r}\frac{\partial (\hat{u}r)}{\partial r} + \frac{\varpi}{r}\frac{\partial \hat{v}}{\partial \alpha} = 0$$

From this point, two procedures can be followed to find the final outcome of this set of equations. In the solution of the tidal wave propagation, usually the velocities are expressed in terms of the pressure, and a final form for the pressure is found (Lamb, Hydrodynamics)(19). This procedure when applied here involves extremely laborious algebra. On the other hand it may be observed that the continuity equation allows one to introduce a function $\underline{\phi}$ such that $\hat{u} = \frac{1}{r}\frac{\partial \underline{\phi}}{\partial \alpha}$ and $\hat{v} = -\frac{\partial \underline{\phi}}{\partial r}$

Substituting this in equations 6 and 7, and eliminating $\hat{p}$ by differentiating 6 with respect to α and 7 with respect to r, one equation in $\underline{\phi}$ results. After rearranging terms the result is as follows. (See Appendix I)

$$\frac{1}{\omega}\frac{\partial}{\partial t}\nabla^2\underline{\phi} + \frac{1}{r}\left[\underline{\phi}_\alpha + \mu\right]\frac{\partial}{\partial r}\nabla^2\underline{\phi} - \left[\frac{1}{r}\underline{\phi}_r - \frac{1}{r^2}\right]\frac{\partial}{\partial \alpha}\nabla^2\underline{\phi} = 0 \qquad (9)$$

where $\nabla^2\underline{\phi}$ denotes $\frac{\partial^2\underline{\phi}}{\partial r^2} + \frac{1}{r}\frac{\partial \underline{\phi}}{\partial r} + \frac{1}{r^2}\frac{\partial^2 \underline{\phi}}{\partial \alpha^2}$

Due to the appearance of the non-linear terms a solution for equation 9 in closed terms is not known. It is therefore essential to investigate what the influence of these non-linear terms is. It is assumed for the moment, to facilitate the problem, that $\mu \approx 0$ so that the term with μ may be neglected. Secondly, it is assumed that the time and angle dependence are exponential functions; therefore

$$\underline{\phi}(r, \alpha, t) = \psi(r)\, e^{i(\sigma t + \lambda \alpha)}$$

The nature of such an assumption will be elaborated on in a later chapter.

Equation (9) then changes to

$$\frac{i\sigma}{\omega}\nabla^2\dot{\psi} + \frac{1}{r}\psi_\alpha \frac{\partial}{\partial r}\nabla^2\dot{\psi} - \left[\frac{1}{r}\psi_r - \frac{1}{r^2}\right] i\lambda\nabla^2\psi = 0 \qquad (10)$$

In the following steps a method of successive approximations is adopted. Solutions of this type were used by Helmholtz to illustrate his theory of combination tones in music (ref. 19). The convergence of the series has been proved for fairly wide conditions. Assume thus a solution in the form of a series

$$\dot{\Phi} = \sum_{n=1}^{\infty} \psi_n(r) c^n e^{in(\sigma t + \lambda\alpha)}$$

After inserting this in (9) and equating coefficients of the different powers of c, one obtains the following set of equations:

$$\frac{i\sigma}{\omega}\nabla^2\dot{\psi}_1 + \frac{i\lambda}{r^2}\nabla^2\dot{\psi}_1 = 0$$

$$\frac{2i\sigma}{\omega}\nabla^2\psi_2 + \frac{i\lambda}{r}\psi_1\frac{\partial}{\partial r}\nabla^2\psi_1 - \frac{i\lambda}{r}\psi_{1r}\nabla^2\psi_1 + 2\frac{i\lambda}{r}\nabla^2\psi_2 = 0$$

ETC.

In this case it follows that

$$\nabla^2\psi_1 = \nabla^2\psi_2 = \nabla^2\psi_3 = \cdots\cdots = 0$$

so the total solution becomes

$$\dot{\Phi} = c\,e^{i(\sigma t + \lambda\alpha)}\left(C_1 r^{\lambda} + C_2 r^{-\lambda}\right) + c^2 e^{2i(\sigma t + \lambda\alpha)}\left(C_3 r^{2\lambda} + C_4 r^{-2\lambda}\right) \qquad (11)$$

The second term signifies a wave with twice the wave number of that of the first term, and the rotational motion of that wave is also twice as fast. The constants C_3 and C_4 can be expressed in terms of C_1 and C_2 by applying the appropriate boundary conditions.

Sketch 1 shows the behavior of such a solution for $\lambda = -2$. In the experiments it was always found that waves associated with the first term of (11) were prominent and only in some special cases the influence of these second term waves was felt. This was the case when

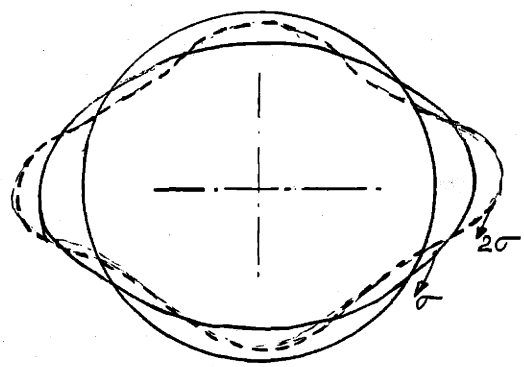

Perturbed Path of Fluid Particles ($\mu = 0$)
Sketch 1

waves associated with $\lambda = -2$ changed in waves with =-1. Accordingly it is felt that these additional terms due to the non-linearity of the problem determine the wave number. Formula (11) indicates that when the constants C^2C_3 and C^2C_4 which depend on CC_1 and CC_2 become bigger relative to CC_1 and CC_2, then waves of the second term will dominate in amplitude and take over the "first term" waves. This last statement is only qualitative because, in the first place, it was impossible analytically to determine C_1 as the boundary conditions render this constant undeterminable. (The equations for C_1 and C_2 are homogeneous.)

The non-linear terms then do not enter into the solution of the linear equation and only appear in waves which have different wave numbers and rotational speeds. In the following text the non-linear terms are left out, not because of the assumption that the perturbations are small but because they create other waves than those we will consider, and their effect upon the main motion is assumed to be small.

2-2 SOLUTIONS OF THE LINEARIZED EQUATIONS

The governing wave equation in linear form is

$$\frac{1}{\omega}\frac{\partial}{\partial t}\nabla^2\phi + \frac{1}{r}\mu\frac{\partial}{\partial r}\nabla^2\phi + \frac{1}{r^2}\frac{\partial}{\partial\alpha}\nabla^2\phi = 0 \tag{12}$$

From the theory of Fourier analysis it is known that a series in the form of $\phi = \sum_{p=1}^{\infty}\sum_{\lambda=1}^{\infty} \psi(r)e^{ip\sigma t}e^{i\lambda\alpha}$ is a solution. In this case only one mode exists, which is similar to the case of buckling where one mode (mostly the lowest) exists, $p=1$ λ REAL. Wave theory also indicates that negative values of λ denote forward moving waves while waves with positive values for λ indicate one which moves in the negative direction. Here it is assumed that λ is a whole real number and that σ is a complex number without any restrictions. The solution then may be written as

$$\phi = \psi(r)e^{i(\sigma t+\lambda\alpha)} \tag{13}$$

To show the significance of this solution we will again in an example assume that $\mu = 0$.

The radial velocity is

$$\hat{u} = \varpi \psi(r) i\lambda\left[\cos(\sigma t+\lambda\alpha) + i \sin(\sigma t+\lambda\alpha)\right]$$

and if one assumes consecutively $\lambda = 1, 2,$ and 3, then the sketch shows how $\hat{u}$ varies with angle.

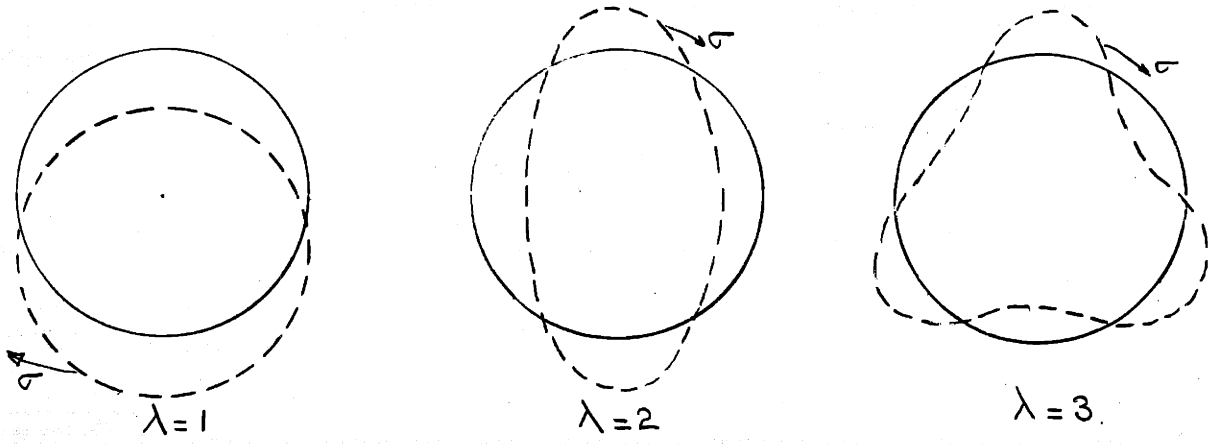

Perturbed Path of Fluid Particle for Different λ's

The amplitude of these perturbations changes with r according to $\psi(r)$ Further, σ is non-zero, so these patterns will rotate steadily for a stationary observer, σ_{re} being the angular velocity of the rotation of these patterns. These rotating patterns are actually the unsteady flows occurring in the vaneless diffuser and the frequency, meaning how many complete revolutions these patterns make per unit of time is equal to $\frac{\sigma_{re}}{2\pi}$.

In the sketch the wave patterns are sketched as being purely sinusoidal; in general a combination of sine and cosine will occur; however the waves will remain purely sinusoidal. Again:

$$\hat{u} = i\frac{\lambda}{r}\varpi\ \psi(r)\left[\cos(\sigma t+\lambda\alpha)+i\sin(\sigma t+\lambda\alpha)\right]$$

$$\hat{v} = -\varpi\ \frac{\partial\psi}{\partial r}\left[\cos(\sigma t+\lambda\alpha)+i\sin(\sigma t+\lambda\alpha)\right]$$

$\hat{u}$ and $\hat{v}$ are equal to the real part of the above expression, where $\psi(r)$ is in general not real but complex. Fig. 1 gives a comparison of a sine curve and a curve sine $\alpha - .37\cos\alpha$. The sine curve is shifted over 0.355 (ARCTG .37) radians. This property of $\hat{u}$ and $\hat{v}$, especially the shifting of the curve, introduces the possibility that the locus of points with maximum $\hat{u}$ or $\hat{v}$ is not along a radius but can be any curved line in the system. The calculations have to give the quantitative results.

Equation 12 may be written with the assumption 13 as

$$\frac{i\sigma}{\omega}\nabla^2\psi + \frac{\mu}{r}\frac{\partial}{\partial r}\nabla^2\psi + \frac{i}{r^2}\lambda\nabla^2\psi = 0 \qquad (14)$$

where

$$\nabla^2\psi = \psi_{rr} + \frac{1}{r}\psi_r - \frac{\lambda^2}{r^2}\psi$$

A particular solution of (14) is $\nabla^2\psi = 0$ which is the Laplacian in cylindrical coordinates. The solution for ψ is

$$\psi = c_1 r^{\lambda} + c_2 r^{-\lambda}$$

The rest of the solution from (14) is

$$\text{or} \qquad \frac{\partial}{\partial r}\nabla^2\psi = -\frac{i}{\mu}\left[\frac{\sigma r}{\omega} + \frac{\lambda}{r}\right]\nabla^2\psi$$

$$\nabla^2\psi = C\, e^{-i/\mu\left[\sigma/\omega\, \frac{r^2}{2} + \lambda \ln r\right]} \qquad (15)$$

For any value of μ the value of $\frac{\sigma}{\omega}\frac{r^2}{2}\Big/\lambda \ln r \ll 1$ this ratio

being around 1/40 for $\mu = 0.4$ Without losing much precision, the term $\frac{\sigma}{\omega}\frac{r^2}{2}$ may be neglected in formula (15), thus simplifying the calculations. Then (15) can be rewritten as

$$\nabla^2 \psi = C r^{-\frac{i\lambda}{\mu}}$$

or

$$\psi_{rr} + \frac{1}{r}\psi_r - \frac{\lambda^2}{r^2}\psi = C r^{-\frac{i\lambda}{\mu}}$$

The complete solution then is

$$\psi = c_1 r^{\lambda} + c_2 r^{-\lambda} + b r^{q} \tag{16}$$

where $q = -\frac{i\lambda}{\mu} + 2$ AND $b = \frac{C}{q^2 - \lambda^2}$

For very small values of μ, say $0 < \mu < 0.3$ the term r^q is a fluctuating function with very high frequency. This is very unlikely to happen in the real flow and in addition when $\mu \to 0$ then $b \to 0$. It is therefore assumed that for small values of μ the solution for ψ may be written as

$$\psi = c_1 r^{\lambda} + c_2 r^{-\lambda} \tag{17}$$

while for values of μ higher than $\mu = 0.4$ the solution for ψ remains as the complete solution (16).

2-3 BOUNDARY CONDITIONS

No information can be obtained from equation (14) when we do not specify the boundary condition to which (14) is subject.

Formula (14) is a boundary value problem and the characteristic

values σ together with the constants of integration are to be determined by the boundary conditions. The flow associated with the system is that of a vaneless diffuser, which starts at r = 1 and ends at $r = r_o$. At r = 1 a screen is rotating giving the flow a rotational velocity and the free atmosphere is at the outlet. The latter means that for $r = r_o$ or $\frac{\partial \hat{p}}{\partial \alpha} = 0$. Furthermore, just outside the diffuser $(r > r_o)$ the pressure change in radial direction is zero.*

Experiments showed that the disturbances at r = 1 depend very much on the value of μ . For $\mu = 0$ the maximum disturbances were at the entrance of the diffuser, while for $\mu = 0.4$ the disturbances had almost disappeared at the inner radius and were growing with the radius. Because of the changing character of both boundary conditions and solutions with changing μ it is felt that two solutions have to be used; one for small μ and one for large μ The two solutions will overlap and the answers for intermediate μ's are expected to lie between the two solutions.

2-4 SOLUTION FOR SMALL μ

As is seen from the previous chapters, the solution for ψ can be written as:

$$\psi = C_1 r^{\lambda} + C_2 r^{-\lambda} \quad \text{AND} \quad \hat{\phi} = \left[C_1 r^{\lambda} + C_2 r^{-\lambda}\right] e^{i(\sigma t + \lambda \alpha)}$$

subject to the boundary conditions

$$r = r_o \; ; \; \frac{\partial \hat{p}}{\partial \alpha} = 0 \; ; \; \frac{\partial \hat{p}}{\partial r} = 0$$

* One may argue that at $r = r_o$ there could be a discontinuity in $\partial \hat{p} / \partial r$ for this idealized two-dimensional flow, but for a real flow this will not hold true.

Formulae (6) and (7), when the values $\hat{u}$ and $\hat{v}$ are replaced by the appropriate values of ϕ, give the governing equations for the boundary conditions.

Thus, neglecting the non-linear terms

$$\frac{1}{\omega r}\bar{\phi}_{\alpha t} - 2\frac{\mu}{r^3}\bar{\phi}_{\alpha} + \frac{\mu}{r^2}\bar{\phi}_{\alpha r} + \frac{1}{r^3}\bar{\phi}_{\alpha\alpha} + \frac{2}{r^2}\bar{\phi}_{r} = -\frac{1}{2}\frac{\partial \hat{p}}{\partial r} \tag{18}$$

$$-\frac{1}{\omega}\bar{\phi}_{rt} - \frac{\mu}{r}\bar{\phi}_{rr} - \frac{1}{r^2}\bar{\phi}_{r\alpha} - \frac{\mu}{r^2}\bar{\phi}_{r} = -\frac{1}{2}\frac{1}{r}\frac{\partial \hat{p}}{\partial \alpha} \tag{19}$$

or

$$\frac{-\sigma\lambda}{\omega r}\left[C_1 r^{\lambda} + C_2 r^{-\lambda}\right] - 2\frac{i\lambda\mu}{r^3}\left[C_1 r^{\lambda} + C_2 r^{-\lambda}\right] + \frac{i\lambda^2\mu}{r^3}\left[C_1 r^{\lambda} - C_2 r^{-\lambda}\right]$$

$$-\frac{\lambda^2}{r^3}\left[C_1 r^{\lambda} + C_2 r^{-\lambda}\right] + \frac{2\lambda}{r^3}\left[C_1 r^{\lambda} - C_2 r^{-\lambda}\right] = 0 \Big|_{r=r_o} \tag{20}$$

and

$$\Big|_{r=r_o} -\frac{i\sigma\lambda}{\omega r}\left[C_1 r^{\lambda} - C_2 r^{-\lambda}\right] - \frac{\mu\lambda^2}{r^3}\left[C_1 r^{\lambda} + C_2 r^{-\lambda}\right] - \frac{i\lambda^2}{r^3}\left[C_1 r^{\lambda} - C_2 r^{-\lambda}\right] = 0 \tag{21}$$

Equations (20) and (21) have two unknowns, σ and $c_1|_{c_2}$, which can be solved by these equations. The solution is given in Appendix II and the procedure is as follows: eliminate σ from (20) and (21), thus obtaining a quadratic equation for $c_1|_{c_2}$ Assume $c_1|_{c_2} = a + bi$, a and b real, and solve for a and b versus μ . Substitute $c_1|_{c_2}$ back into 21 and an equation for σ is obtained. For $\lambda = -2$, a wave number mostly encountered in the diffuser, the real value for σ

$$\sigma_{re} = \left[1 - \frac{2\mu b}{(a-1)^2+b^2}\right] \frac{\omega 2}{r_o^2} \tag{22}$$

and the imaginery part

$$\sigma_{im} = \frac{\left[a^2+b^2-1\right]}{(a-1)^2+b^2} \mu \frac{\omega 2}{r_o^2} \tag{23}$$

Fig. 2 shows the behavior of the functions $a(\mu)$ and $b(\mu)$. The behavior of formulae 22 and 23 will be shown with the experimental results.

The velocity distribution follows, if $c_1|_{c_2}$ is known. For $\mu = o$; $c_1|_{c_2} = r_o^{-2\lambda}$

$$\hat{u} = \frac{1}{r}\frac{\partial \phi}{\partial \alpha} = i\frac{c_2}{r}\lambda\left[\frac{c_1}{c_2} r^{\lambda} + r^{-\lambda}\right] = i\frac{c_2}{r}\lambda\left[\frac{r^{\lambda}}{r_o^{2\lambda}} + r^{-\lambda}\right]$$

$$\hat{v} = -\frac{\partial \phi}{\partial r} = -\frac{\lambda c_2}{r}\left[\frac{c_1}{c_2} r^{\lambda} - r^{-\lambda}\right] = -c_2\frac{\lambda}{r}\left[\frac{r^{\lambda}}{r_o^{2\lambda}} - r^{-\lambda}\right]$$

2-5 SOLUTIONS FOR LARGE μ

The general equation for this case is equation 16.

$$\Phi = \left[C_1 r^{\lambda} + C_2 r^{-\lambda} + \frac{C\, r^{-\frac{i\lambda}{\mu}+2}}{-\left(\frac{i\lambda}{\mu}+2\right)^2 - \lambda^2} \right] e^{i(\sigma t + \lambda\alpha)}$$

subject to the boundary conditions:

$$r = 1 \quad \hat{u} = 0 \quad ; \quad r = r_o \quad \frac{\partial \hat{p}}{\partial \alpha} = 0$$
$$\hat{v} = 0$$

The boundary condition $\frac{\partial \hat{p}}{\partial r}$ will not be used here as one of the constants C_1, C_2 cannot be determined.

$$\hat{u} = \frac{i\lambda}{r}\Phi = \frac{i\lambda}{r}\left[C_1 r^{\lambda} + C_2 r^{-\lambda} + p r^{q} \right] e^{i(\sigma t + \lambda\alpha)}$$

$$\hat{v} = -\Phi_r = -\frac{1}{r}\left[C_1 \lambda r^{\lambda} - C_2 \lambda r^{-\lambda} + q\, p\, r^{q} \right] e^{i(\sigma t + \lambda\alpha)}$$

AT $r = 1$; $\hat{u} = 0$; $\hat{v} = 0$ AND ASSUME $\lambda = -2$

$$\hat{u} = 0 = 2C_1 + 2C_2 + 2p$$

$$\hat{v} = 0 = -2C_1 + 2C_2 + pq$$

Addition and subtraction result in

$$C_2 = -\frac{p}{4}\left[q + 2 \right] \quad ; \quad C_1 = -\frac{p}{4}\left[-q + 2 \right]$$

$$\hat{u} = -\frac{b}{r}\left[-\frac{r^{-2}}{\mu} - i\left(\frac{2i}{\mu}+4_1\right)\frac{r^2}{2} + 2i\, r^{(2i/\mu+2)}\right] e^{i(\sigma t+\lambda\alpha)} \qquad (24)$$

$$\hat{v} = -\frac{b}{r}\left[-\frac{i\,r^{-2}}{\mu} - \left(\frac{2i}{\mu}+4_1\right)\frac{r^2}{2} + \left(\frac{2i}{\mu}+2\right) r^{(2i/\mu+2)}\right] e^{i(\sigma t+\lambda\alpha)} \qquad (25)$$

The perturbation velocities $\hat{u}$ and $\hat{v}$ are only the real parts of (24) and (25) respectively.

For convenience one may write

$$\hat{u} = k\left[W + iX\right] e^{i(\sigma t+\lambda\alpha)} \quad \text{AND} \quad \hat{v} = k\left[Y + iZ\right] e^{i(\sigma t+\lambda\alpha)}$$

or

$$\hat{u} = \left(W\cos 2\alpha + X \sin 2\alpha\right) k\, e^{i\sigma t}$$

$$\hat{v} = \left(Y\cos 2\alpha + Z \sin 2\alpha\right) k\, e^{i\sigma t}$$

As was pointed out in paragraph 2-1, the combination of a sine and a cosine results in another periodic function which is shifted along α dependent on W and X or Y and Z. The term $e^{i\sigma t}$ denotes the rotation of this flow pattern around the center. In the case of λ =-2 the forms for W, X, Y and Z are from 24 and 25.

$$W = \frac{2}{r^2\mu^2} - \frac{2r^2}{\mu^2} + \frac{4r^2}{\mu}\sin\left(\frac{2}{\mu}\ln r\right) - 8r^2 + 8r^2\cos\left(\frac{2}{\mu}\ln r\right)$$

$$X = \frac{4}{r^2\mu} + 8r^2\sin\left(\frac{2}{\mu}\ln r\right) - \frac{4r^2}{\mu}\cos\left(\frac{2}{\mu}\ln r\right)$$

$$Y = \frac{4r^2}{\mu^2}\sin\left(\frac{2}{\mu}\ln r\right) + \frac{4r^2}{\mu}\cos\left(\frac{2}{\mu}\ln r\right) + 8r^2\sin\left(\frac{2}{\mu}\ln r\right) - \frac{4}{r^2\mu}$$

$$Z = 8r^2 + \frac{2}{r^2\mu^2} + \frac{2r^2}{\mu^2} - \left(8r^2 + \frac{4r^2}{\mu^2}\right)\cos\left(\frac{2}{\mu}\ln r\right) + \frac{4r^2}{\mu}\sin\left(\frac{2}{\mu}\ln r\right)$$

$$K = \frac{2C\mu}{\left(1/\mu^2+1\right)} \qquad (25a)$$

The unknown characteristic value σ will be estimated with the boundary condition $r = r_o \; ; \; \frac{\partial \hat{p}}{\partial \alpha} = 0$

From 19 it follows that

$$\left[-\frac{i\sigma}{\omega r} - \frac{\lambda i}{r^3}\right]\frac{r^3}{\mu} = \frac{\frac{\partial}{\partial r}\Phi_r r}{\Phi_r} = \frac{c_1\lambda^2 r^\lambda + c_2\lambda^2 r^{-\lambda} + q^2 p r^q}{c_1\lambda\, r^\lambda - c_2\lambda r^{-\lambda} + q\, p\, r^q}\Bigg|_{r=r_o} \qquad (26)$$

where

$$q = -\frac{\lambda i}{\mu} + 2 \; ; \; c_1 = -\frac{p}{4}\left[-q+2\right] \; ; \; c_2 = -\frac{p}{4}\left[q+2\right]$$

then with $\lambda = -2$

$$\left[\frac{-i\sigma}{\omega r} - \frac{i\lambda}{r^3}\right]\frac{r^3}{\mu} = -\frac{p(-q+2)r^{-2} - p(q+2)r^2 + q^2 p r^q}{p/2(-q+2)r^{-2} - p/2(q+2)r^2 + q\,p\,r^q}\Bigg|_{r=r_o}$$

or after collecting real and imaginary terms

$$\left[\frac{-i\sigma}{\omega r} - \frac{i\lambda}{r^3}\right]\frac{r^3}{\mu} =$$

$$= \frac{\left[-4 + \left(-\frac{4}{\mu^2}+4\right)\cos\left(\frac{2}{\mu}\ln r\right) - \frac{8}{\mu}\sin\left(\frac{2}{\mu}\ln r\right)\right] + i\left[-\frac{2}{\mu} + 2r^{-4}/\mu + \left(4 - \frac{4}{\mu^2}\right)\sin\frac{2}{\mu}\ln r + \frac{8}{\mu}\cos\frac{2}{\mu}\ln r\right]}{\left[-2 + 2\cos\left(\frac{2}{\mu}\ln r\right) - \frac{2}{\mu}\sin\left(\frac{2}{\mu}\ln r\right)\right] + i\left[-\frac{1}{\mu}\left(1 + r^{-4}\right) + \frac{2}{\mu}\cos\left(\frac{2}{\mu}\ln r\right) + 2\sin\frac{2}{\mu}\ln r\right]}$$

or in symbols

$$\left[\frac{-i\sigma}{\omega r} - \frac{i\lambda}{r^3}\right]\frac{r^3}{\mu} = \frac{A+iB}{C+iD} = \frac{AC+BD}{C^2+D^2} + i\,\frac{(BC-DA)}{C^2+D^2}\,.\quad A,B,C,D \text{ REAL.}$$

$$\sigma_{re} = \frac{2\omega}{r_o^2}\left[1 - \frac{\mu}{2}\frac{BC-DA}{C^2+D^2}\right] \text{ AND } \sigma_{im} = \left[\frac{AC+BD}{C^2+D^2}\right]\frac{\mu\omega}{r_o^2} \qquad (28)$$

Fig. 4 gives account of the functions A, B, C and D. Their behavior for small μ is as expected, due to the great influence of the terms containing $1/\mu \sin(\frac{2}{\mu}\ln r)$ and $1/\mu \cos(\frac{2}{\mu}\ln r)$ and therefore only a reasonable answer is expected for values of μ bigger than $\mu = 0.4$. Besides this, as was already said for values lower than $\mu = 0.4$ the boundary conditions $\hat{u} = 0$; $\hat{v} = 0$ AT $r = 1$ do not hold any longer, as was seen in the experiments.

3 STABILITY CRITERIA

In all the theory treated thus far, nothing has been said about the unsteadiness of the perturbations. More specifically with the introduction of the term $\sigma^{i\sigma t}$ with σ complex, it was possible in the analysis that the imaginary part of σ would cause the perturbation to be non-periodic. Dependent on the sign of σ_{im} the perturbations would grow for $\sigma_{im} < 0$; decay for $\sigma_{im} > 0$ and stay constant for $\sigma_{im} = 0$

Fig. 3 shows the behavior of σ_{im} for the solution of small μ from formula (23). The value of σ_{im} changes sign when $\mu = 0$ and the motion becomes unstable (i.e. the perturbations amplify). According to the theory, the motion is stable for all positive values of μ. Calculations for large μ showed that in that case σ_{im} was always positive (see formula 28) for values of μ $-0.2 > \mu > 0.2$.

The indications from the experiments are that the theory for large holds very well for $\mu \geqslant 0.4$. This indicates that for positive values of μ the flow is always stable. However, for negative values of μ the flow is unstable if one uses the theory of small μ , but it is stable if one uses the analysis for large μ . This indicates that a free vortex flow is unstable for values of μ between -0.2 and zero and that a free vortex flow with radial inflow with stream angles bigger than 110° is again stable. One should keep in mind that such a flow must satisfy the boundary conditions which were applied in this analysis. A confirmation of this stability criterion for the case of a net radial inflow was not found in the experiments, as only a radial outflow could be obtained.

The experiments indicate that the motion is purely periodic for fixed conditions and no unsteadiness could be observed. This means then that the periodic motion superposed on the steady motion was in complete equilibrium; moreover, the real part of it was clearly adjusted by the flow, with the overall result that the non-periodical term $e^{i\sigma_m t}$ reduced to 1.

It is known from previous investigations that the flow is not at all two-dimensional, as was assumed here (refs. 4 and 5). The streamlines near the wall curve more inwards than the streamlines in the middle of the passage. In other words the wall streamlines in certain instances have a flow direction with $\mu < 0$ while the mid-streamlines flow in a direction with $\mu > 0$. This then, according to the analysis, indicates that the perturbations at the

wall are being amplified and that the perturbations in the mid-stream are decaying. As the resultant motion of the overall flow in the diffuser is a steady periodic motion, the following hypothesis may be stated: there is a process involved, whereby the production of the amplified distrubances in the wall-flow region and the decay of the disturbances in the mid-stream region are in balance. If the value for μ is made smaller, then the production process delivers a greater quantity of disturbances and the decaying process is somewhat less strong than before. The resultant disturbances will therefore have a greater amplitude and the flow adjusts itself so that the non-periodical term $e^{i\sigma_m t}$ becomes 1 again. Figs. 5 and 6 illustrate this. In Fig. 5 the perturbed velocities are plotted while the steady velocity is drawn according to $V_{st} \sim \frac{1}{r}$. In fig. 5 where $\mu = .425$ the amplitude is much less than that of fig. 6, where $\mu = 0.4$. In the analysis for both small and large μ the form of the perturbations could be determined, but the constant governing the amplitude could <u>not</u> be determined. G. I. Taylor, in his famous analysis of the stability of the fluid contained between two coaxial cylinders, used $\sigma_m = 0$ as a boundary condition. The same could be done here; let C in 25a and C_2 in 23a and 23b be determined so that $\sigma_m = 0$ and only purely periodical motions exist. The analysis of such a process is beyond the scope of this work and involves an accurate inspection of the three-dimensional equations for steady flow and knowledge of the form of the three-dimensional boundary layers.

One thing the theory seems to indicate is that finite periodic motions can only occur when the wall streamlines are

curved over an angle for which $\mu < 0$, for then and only then the amplification of the perturbation can in fact happen.*

One may recall that the stability criterion for laminor boundary layers is expressed in similar ways. Calculations show that for certain Reynolds numbers, the disturbances with certain wave-numbers are stable or unstable. The statement there is that the laminar boundary layer is unstable for disturbances with wave number α if and only if the Reynolds number is greater than a certain value. If this Reynolds number is exceeded, the disturbances will amplify, but not indefinitely. It will grow to a certain amplitude and stay there in equilibrium.

3-2 ON THE STABILITY OF A THREE-DIMENSIONAL BOUNDARY LAYER

In the previous paragraph we have treated the flow as two-dimensional and frictionless. The stability criterion found there was stated as a hypothesis. It is known that the flow of a hurricane and the drainage of sinks, etc. are examples of free vortex flows and in these cases no instabilities have been observed. This may be because the flow in a hurricane and a sink possesses an axial velocity. On the other hand it could be that some other mechanism in the diffuser excites these wave lengths, so that they become finite.

Therefore it may be useful to focus attention on the shear layer in the diffuser and to investigate its stability. The steady flow in the diffuser is not two dimensional, but due to the friction on both walls a boundary layer grows. This boundary layer

* A quantitative development was made for the value of μ for which $\sigma_m = 0$ when wall friction in the form of the coefficient $C_f = \frac{2\tau_w r^2}{\rho\omega^2}$ was applied. However, the final result showed that μ changed from 0 to 0.005 for $C_f = 0.01$.

is three dimensional in character and its thickness increases with increased radius. Besides the stability criterion found in the previous chapters we will now investigate the stability of the flow due to the three-dimensional boundary layer. The stability of boundary layers has been treated very extensively in the literature, and almost all the efforts were purely on the problem of transition of a laminar boundary layer to a turbulent boundary layer. For a two-dimensional boundary layer in incompressible flow one has been able to predict transition Reynolds numbers quite accurately, although the methods of solving the problem were elaborate. With the use of the Navier Stokes equations in two-dimensions, the continuity equations, and introducing small perturbations u' and v' the Orr-Sommerfeld equation is obtained:

$$(\bar{U}-c)\left[\bar{\phi}''-\alpha\bar{\phi}\right]-\bar{U}''\bar{\phi}=-\frac{i\nu}{\alpha}\left[\bar{\phi}^{IV}-2\alpha^2\bar{\phi}''+\alpha^4\bar{\phi}\right]$$

where $\bar{\phi}$ is defined by $u'=\frac{\partial\bar{\psi}}{\partial y}$; $v'=-\frac{\partial\bar{\psi}}{\partial x}$ and $\psi=\bar{\phi}\,e^{i(\alpha x-\beta t)}$

$$\beta=\beta_r+i\beta_i \quad ; \quad \beta/\alpha=c=c_r+ic_i$$

This equation was first formulated in 1907. Lord Rayleigh (15) investigated the inviscid case. A much simpler equation follows:

$$\frac{\partial^2\bar{\phi}}{\partial y^2}-\alpha^2\bar{\phi}-\frac{\partial^2\bar{U}/\partial y^2}{(\bar{U}-c)}\bar{\phi}=0 \qquad (36)$$

This equation allows us to state a theorem.

The existence of a point of inflexion in the velocity profile of the mean flow $\partial^2\bar{U}/\partial y^2=0$ is a necessary condition for

the amplification of disturbances $(c_i > 0)$. The proof is indirect. From (36) we may state the differential expression

$$L(\phi) = \phi'' - \alpha^2 \phi - \frac{U''}{U-c}\phi$$

and $$\bar{L}(\bar{\phi}) = \bar{\phi}'' - \alpha^2 \bar{\phi} - \frac{U''}{U-\bar{c}}\bar{\phi}$$

The boundary conditions were $\phi = \bar{\phi} = 0$ AT $y = 0$; $y = \infty$

The dashed quantities are complex conjugates. Forming the expression $\bar{\phi} L(\phi) - \phi \bar{L}(\bar{\phi})$ and integrating between the boundaries y = 0 and y = ∞ we obtain

$$J = \int_{y=0}^{\infty} \left[\bar{\phi} L(\phi) - \phi \bar{L}(\bar{\phi}) \right] dy = 0$$

$$J = \int_{0}^{\infty} \left\{ \bar{\phi}\phi'' - \phi\bar{\phi}'' - \phi\bar{\phi}\left[\frac{U''}{U-c} - \frac{\bar{U}''}{\bar{U}-\bar{c}} \right] \right\} dy = 0$$

$$J = \left[-\bar{\phi}'\phi + \phi\bar{\phi}' \right]_{0}^{\infty} - 2ic_i \int_{0}^{\infty} \frac{U''}{|U-c|^2} \phi\bar{\phi}\, dy = 0$$

The first term vanishes in view of the boundary conditions. $\phi\bar{\phi}$ AND $|U-c|^2$ are positive quantities. This means that U'' must change sign somewhere in the boundary layer to make it possible for this integral to disappear. This shows that the velocity profile must have a point of inflexion causing the disturbances to be amplified.

Tolmien (16) proved that the existence of a point of inflexion is not only necessary but also a sufficient condition for

the existence of amplified disturbances. To summarize this we may state that velocity profiles with a point of inflexion are unstable.

It may be noted that this statement does not differentiate between a laminar or turbulent boundary layer. The laminar boundary layer which shows a point of inflexion will become turbulent. The turbulent boundary layer is much thicker due to the increased shear stress accompanying the turbulence and only points of inflexion occur in some cases when the flow starts to separate. Various experiments (Townsend, Schubauer) have shown that a turbulent separation is accompanied by unsteadiness, which proves the unstable character. One should bear in mind that a velocity profile can be unstable without a point of inflexion and that for the most part this instability (viscous instability) causes the transitions. Various authors have extended these ideas and applied them to three-dimensional boundary layers. Consider the motion with perturbation $u_i = \overline{u_i} + u_i' \quad (i=1,2,3)$ which are functions of the geometrical coordinates $x_i \; (i=1,2,3)$ It may be shown by careful examination of all the terms in the first order distrubance equations (which are sufficient to determine stability) of continuity and momentum that the basic flow may be treated as essentially two dimensional (Dunn 1953) (17). The equations then are simplified and may be written in the symbolic form.

$$\frac{Du_i}{Dt} + u_2' \frac{\partial u_i}{\partial x_2} = -\frac{\partial p'}{\partial x_i} + \text{FRICTION}$$

and $$\frac{\partial u_i}{\partial x_i} = 0 \quad \text{WHERE} \quad \frac{D}{Dt} = \frac{\partial}{\partial t} + \overline{u}_1 \frac{\partial}{\partial x_i} + \overline{u}_3 \frac{\partial}{\partial x_3}$$

In general, the solutions will be periodic and appear in the form

$$q' = \hat{q}(x_2) \exp\left(i[\alpha_1 x_1 + \alpha_3 x_3] - \sigma_i t\right)$$

In particular consider now the case where $x_3 = 0$. The result is that all the terms involving the u_3 and x_3 derivatives drop out of the system of equations. The following statement can now be made: By choosing the x_1 axis in the direction of wave propagation only the component of the basic flow in that direction needs to be considered (Lin).

This result is also obtained by Stuart (18) who treated the problem mathematically and afterwards made some important conclusions, which will be used here. The geometry of the diffuser flow is sketched below.

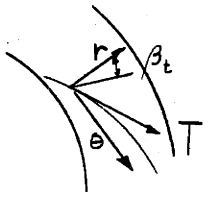

The direction T is tangent to the potential flow stream r and θ in the radial and tangential direction. We are only interested in the direction for the disturbances to be propagated for which β is $0 \leq \beta \leq 90°$ All other directions give wave propagations in $-\theta$ and $-r$ directions and in those directions the amplifying disturbances would enter regions where the conditions for amplification is absent.

Recalling the fact that for the existence of amplifying disturbances in one direction the velocity profile in that direction should have a point of inflexion (inflexional instability). One should examine the velocity profiles in the direction for which β is $0 \leq \beta \leq 90°$ Fig. 7 gives a comparison of some experimental profiles of the velocity in the r- direction at different angles for β_t (in the sketch the angle

between potential line and radius). The profiles are from Gas Turbine Laboratory Report No. 52. For the determination of a point of inflexion, the radial velocity profiles seem to be the most important ones. It can be seen that the possibilities for a point of inflexion increase at higher angles β_t. At 74.5° the velocity profile starts showing such a point, and for a flow of 75° the flow becomes unstable, as was found previously. At this point we have arrived at two hypotheses for the reasons for the excitement of the waves. Experimental data indicate that a point of inflexion in the shear layer starts to occur when the flow against the wall just starts to flow backwards. This was the reason why it was impossible to arrive at a definite answer as to which hypothesis was correct, because both predict the possibility of finite waves at the same point.

4-1 EXPERIMENTAL PROCEDURE

The experimental apparatus was the same as the one described in part one. Instead of a wake generator at the start of the diffuser, another screen was inserted. This screen was driven by an electro-motor, and a variable transmission gear was placed between driving motor and screen so that any desired rotational speed could be obtained. The through flow, which controls the radial velocity and the parameter μ, could be adjusted by means of a moving slot at the part where the air enters (far left in sketch). The phenomenon as explained was the occurrence of perturbations which seem to be fixed for the conditions under which one runs the apparatus. Thus, the angular variations of the perturbated velocities $\hat{u}$ and $\hat{v}$ rotate around

the center with a constant speed for one condition. The amplitudes of the perturbations were dependent on the conditions μ, λ and ϖ but were fixed and could be repeated when the flow was adjusted for these same values of μ and ϖ. It appeared from the experiments that the wave number λ denoting the number of maxima around the circumference 2π was very much dependent on ϖ and μ. In normal circumstances a wave number equal to two was dominant. Only in the case when μ was close to zero and when ϖ was high did the wave number λ change to one.

The velocities were measured with a hot-wire probe, and the output was amplified by a Sanborn amplifier and recorder. The sensitive hot wire was used with a constant current system and consisted of a 20% Pt 80% Ir wire 0.0005 inches in diameter and 3/32 inch long. The accuracy of the measurements was around 2%, hereby taking into account the errors in calibration and actual measurements. The wire itself was placed perpendicular to the direction of the motions so that the influence of different angles at different instants of time was eliminated.

The figures 5, 6, 8 and 9 show how the perturbed velocities change with the radius for one particular condition.

In figure 5 where $\mu = 0.42$ and figure 6 where $\mu = 0.4$ it can be seen that at $r = 1$ the amplitude of the perturbations is a minimum. The only apparent change is the amplitude of the disturbances, but the general shape is preserved with a minimum disturbance again at the entrance of the diffuser $r = 1$. In figure 8 the value of μ is decreased to 0.2 and a change in form of the perturbation amplitude with radius is observed. Finally in figure 9 for $\mu = 0$ (tangential flow),

the perturbation amplitude behaves quite differently with respect to the radius. Instead of an increasing amplitude, here one may observe a decreasing amplitude of the perturbations. Figure 8 already showed that the condition $\hat{u} = 0$ and $\hat{v} = 0$ at $r = 1$ cannot be maintained any longer. This is in accordance with the analysis of chapter 2 where for big μ the boundary condition $\hat{u} = \hat{v} = 0$ when $r = 1$ is used, while for small μ this condition was removed. Figure 10 shows a sequence of the traces of the hot wire response for the case of figure 6.

The variation of the amplitude of the oscillations along the steady flow with varying flow angle is pictured in figure 11. The traces are all taken at a radius of $r = 1.07$. For angles over $\mu = 0.38$ the perturbations are very small at this radius, but increase as μ decreases. Another feature which appears here is the frequency of the waves. With decreasing μ the frequency increases.

4-2 COMPARISON OF EXPERIMENT WITH ANALYSIS

a WAVE SPEEDS

Measurements of the wave frequencies were extremely simple to take but their interpretation was not easy because of the fact that they were dependent on ω and μ ; ω is the circulation and is a constant for steady free vortex motion. μ is the tangent of the angle between steady flow streamline and circumferential direction. If $\mu = 0$ then σ, the wave speed, is solely dependent on ω when $\lambda = -2$. $\sigma = \frac{2\omega}{r_o^2}$

(From form 23) The outer radius r_o was in this case $r_o = 2.92$ so that σ was proportional to ω Figure 12 shows

this plot for $\lambda = -1$, $\lambda = -2$ and $\lambda = -3$. The quantity $\sigma/2\pi$ is plotted in y-direction and signifies the number of rotations of one wave per second. The experimental data were taken when no air was supplied at the front end of the diffuser. For $\lambda = -2$ the experimental values check the theory quite well for a wide range of velocities. However, for $\lambda = -1$, the analysis predicts up to 33% lower values. The reason for this could be the very strong influence of the secondary waves which parasitize on the primary waves with $\lambda = -1$. The existence of these secondary waves was found by the occasionally irregular responses of the hot wire. In the case investigated here, waves with a wave number of 3 were never observed. For the case where μ was zero some experimental data of the same phenomenon are available in ref. (13). These experiments were conducted with an apparatus which consisted of two stationary walls, between which a disk was rotating. The object was to study the condensation on the rotating disk. Instead of a steady flow the investigators found a pulsating flow. They measured the wave speed against the speed of the disk and found that for a fixed λ all the experimental points lay on a line which could be extended to the origin. As a matter of fact, a similar plot was constructed with the experimental data as the one of figure 12 here.

The variation of the wave speed with the parameter μ was found for small μ by formula (22) and for large μ formula (27) was used. Figure 13 shows the behavior of these functions.

The experimental values are lower for the case of small μ The behavior of the solution when μ is big should clearly not be interpreted for $\mu < 0.4$

It should be understood that by comparing the experiments with the solution in figure 13 a double error will occur. First one has to estimate ϖ from the experiment, and afterwards μ . This kind of a procedure introduces a loss in exactness so far as the experimental data are concerned. In view of these facts it may be concluded that the analysis gives satisfying agreement with the experiments.

b PERTURBATION AMPLITUDES

In the case of small μ the velocities are represented by the functions for $\hat{u}$ and $\hat{v}$ at the end of paragraph 2-4. In the case of $\lambda = -1$ then

$$\hat{u} = i C_2 \left[\frac{8.5}{r^2} + 1\right] \quad ; \quad \hat{v} = - C_2 \left[\frac{8.5}{r^2} - 1\right]$$

The maxima of $\hat{u}$ and $\hat{v}$ are separated over $\pi/4$ radians. The maximum total velocity is plotted in figures 14 and 15. In figure 14 two curves appear, each one for different C_2. There is only fair agreement between theory and experiment, especially in the region of small radius. Figure 15 shows the same plot for an experiment with somewhat lower ϖ . Agreement appears to be much better here. The reason why agreement in figure 14 is fair and in figure 15 is good is unknown. Note, however, that the wave speed for the data of figure 14 agrees much less with respect to the theoretical value than in the case of figure 15.

In the case of large μ only the experiments for which $\mu \geq 0.4$ were compared with the analysis. The functions $\hat{u}$ and $\hat{v}$ are represented by the formulas 24 and 25. As the term which controls the amplitude is complex, we have here the case that the maxima of $\hat{u}$ and $\hat{v}$ will not necessarily stay at the same angle α while they are passing through the diffuser. The behavior of $\hat{u}$ and $\hat{v}$ are calculated for one case $\mu = 0.4$. Figure 16 indicates how the maxima of $\hat{u}$ and $\hat{v}$ change with angle α. The steady flow streamline and the locus of maxima lie in the same direction. Evidence of such a curved region of high flow was observed in a motion picture taken of a similar flow phenomenon and the experimental study of Maroti (ref. 13)

The two velocities $\hat{u}_{max}$ and $\hat{v}_{max}$ were combined to obtain the total velocity perturbation. Figure 17 shows this function. If the constant c is known, the form of this function represents the experimental values well. In figure 17, two sets of experimental data have been drawn, representing the figures 5 and 6. The value of c for the data of figure 5 was 2/3 times the value of c for the data of figure 6.

5 SOME REMARKS ABOUT THE MOTION PICTURE OF THE PERTURBED FLOW

Accompanying this report is a motion picture of the perturbed flow. The colored part shows the apparatus as described before. Through a window the fluctuating flow is made visible by tufts, and some shots of the Sanborn recorder follow indicating the response of the hot wire in the pulsating flow.

The black and white part shows a diffuser which is horizontal, and the impeller which is fed by a vertical pipe, through which a bi-refringient liquid flows upwards. The diffuser and impeller are made of plastic and a light source under the diffuser shines light upwards. The light is polarized by two polarizing plates and these light rays are affected by the bi-refringient liquid, which flows through the diffuser. The result is a visible flow pattern which consists of fringes (many fringes = high shear stress).

Figure 18 shows a picture of the impeller with the diffuser surrounding it. This apparatus was constructed by Ingersoll-Rand Co. and through their courtesy these pictures were taken. As the flow in the impeller was not the purpose of our study, the impeller is blacked out.

The pictures indicate clearly the steady motion with no perturbations. The flow is subsequently cut down and the perturbations appear. However, they are only visible at the outer part of the diffuser. By cutting the flow down more and more the perturbations grow inward, and at the same time one may observe that the waves move faster along the circumference. Also one may note the curved character of the region of maximum flow. When the radial flow is reduced to zero, one may observe the secondary waves due to the non-linearity of the problem. These secondary waves have twice the speed of the primary waves.

Appendix I

DERIVATION OF FORMULA (9)

Substituting $\hat{u} = \frac{1}{r}\frac{\partial \bar{\phi}}{\partial \alpha}$ and $\hat{v} = -\frac{\partial \bar{\phi}}{\partial r}$ into (6) and (7)

(6) becomes

$$\frac{1}{\omega r}\bar{\phi}_{\alpha t} - 2\frac{\mu}{r^3}\bar{\phi}_{\alpha} + \frac{\mu}{r^2}\bar{\phi}_{\alpha r} + \frac{1}{r^2}\bar{\phi}_{\alpha}\bar{\phi}_{\alpha r} - \frac{1}{r^3}\bar{\phi}_{\alpha}^2 + \frac{1}{r^3}\bar{\phi}_{\alpha\alpha} - \tag{I-a}$$

$$-\frac{1}{r^2}\bar{\phi}_r\bar{\phi}_{\alpha\alpha} + \frac{2}{r^2}\bar{\phi}_r - \frac{1}{r}\bar{\phi}_r^2 = -\frac{1}{2}\frac{\partial \hat{b}}{\partial r}$$

and

$$-\frac{1}{\omega}\bar{\phi}_{rt} - \frac{\mu}{r}\bar{\phi}_{rr} - \frac{1}{r}\bar{\phi}_{\alpha}\bar{\phi}_{rr} - \frac{1}{r^2}\bar{\phi}_{r\alpha} + \frac{1}{r}\bar{\phi}_r\bar{\phi}_{r\alpha} - \frac{\mu}{r^2}\bar{\phi}_r - \frac{1}{r^2}\bar{\phi}_{\alpha}\bar{\phi}_r = -\frac{1}{2}\frac{1}{r}\frac{\partial \hat{b}}{\partial \alpha} \tag{I-b}$$

Differentiating I-a to α

$$\frac{1}{\omega r}\bar{\phi}_{\alpha\alpha t} - 2\frac{\mu}{r^3}\bar{\phi}_{\alpha\alpha} + \frac{\mu}{r^2}\bar{\phi}_{\alpha\alpha r} + \frac{1}{r^2}\bar{\phi}_{\alpha\alpha}\bar{\phi}_{\alpha r} + \frac{1}{r^2}\bar{\phi}_{\alpha}\bar{\phi}_{\alpha\alpha r} - \frac{2}{r^3}\bar{\phi}_{\alpha}\bar{\phi}_{\alpha\alpha} +$$

$$+\frac{1}{r^3}\bar{\phi}_{\alpha\alpha\alpha} - \frac{1}{r^2}\bar{\phi}_{r\alpha}\bar{\phi}_{\alpha\alpha} - \frac{1}{r^2}\bar{\phi}_r\bar{\phi}_{\alpha\alpha\alpha} + \frac{2}{r^2}\bar{\phi}_{\alpha r} - \frac{2}{r}\bar{\phi}_r\bar{\phi}_{\alpha r} = -\frac{1}{2}\frac{\partial^2 \hat{b}}{\partial r\,\partial \alpha} \tag{I-c}$$

Differentiating the right-hand side of I-b to r results in:

$$\frac{1}{2}\frac{1}{r^2}\frac{\partial \hat{b}}{\partial \alpha} - \frac{1}{2}\frac{1}{r}\frac{\partial^2 \hat{b}}{\partial r\,\partial \alpha}$$

If for $\frac{\partial^2 \hat{b}}{\partial r\,\partial \alpha}$ the left-hand side of (I-c) is substituted and for $\frac{\partial \hat{b}}{\partial \alpha}$ the left-hand side of I-b, then the following form results:

$$-\frac{1}{\omega}\bar{\Phi}_{rrt} - \frac{\mu}{r}\bar{\Phi}_{rrr} + \frac{\mu}{r^2}\bar{\Phi}_{rr} - \frac{1}{r}\bar{\Phi}_{\alpha}\bar{\Phi}_{rrr} - \frac{1}{r}\bar{\Phi}_{\alpha r}\bar{\Phi}_{rr} + \frac{1}{r^2}\bar{\Phi}_{\alpha}\bar{\Phi}_{rr} +$$

$$+\frac{2}{r^3}\bar{\Phi}_{r\alpha} - \frac{1}{r^2}\bar{\Phi}_{rr\alpha} + \frac{1}{r}\bar{\Phi}_{r}\bar{\Phi}_{rr\alpha} + \frac{1}{r}\bar{\Phi}_{rr}\bar{\Phi}_{r\alpha} - \frac{1}{r^2}\bar{\Phi}_{r}\bar{\Phi}_{r\alpha} - \frac{\mu}{r^2}\bar{\Phi}_{rr} +$$

$$+\frac{2\mu}{r^3}\bar{\Phi}_{r} - \frac{1}{r^2}\bar{\Phi}_{\alpha}\bar{\Phi}_{rr} - \frac{1}{r^2}\bar{\Phi}_{\alpha r}\bar{\Phi}_{r} + \frac{2}{r^3}\bar{\Phi}_{\alpha}\bar{\Phi}_{r} + \frac{1}{\omega r}\bar{\Phi}_{rt} - \frac{\mu}{r^2}\bar{\Phi}_{rr} -$$

$$-\frac{1}{r^2}\bar{\Phi}_{\alpha}\bar{\Phi}_{rr} - \frac{1}{r^3}\bar{\Phi}_{r\alpha} + \frac{1}{r^2}\bar{\Phi}_{r}\bar{\Phi}_{\alpha r} - \frac{\mu}{r^3}\bar{\Phi}_{r} - \frac{1}{r^3}\bar{\Phi}_{\alpha}\bar{\Phi}_{r} - \frac{1}{\omega r^2}\bar{\Phi}_{\alpha\alpha t} +$$

$$+\frac{2\mu}{r^4}\bar{\Phi}_{\alpha\alpha} - \frac{\mu}{r^3}\bar{\Phi}_{\alpha\alpha r} - \frac{1}{r^3}\bar{\Phi}_{\alpha\alpha}\bar{\Phi}_{\alpha r} - \frac{1}{r^3}\bar{\Phi}_{\alpha}\bar{\Phi}_{\alpha\alpha r} + \frac{2}{r^4}\bar{\Phi}_{\alpha}\bar{\Phi}_{\alpha\alpha}$$

$$-\frac{1}{r^4}\bar{\Phi}_{\alpha\alpha\alpha} + \frac{1}{r^3}\bar{\Phi}_{r\alpha}\bar{\Phi}_{\alpha\alpha} + \frac{1}{r^3}\bar{\Phi}_{r}\bar{\Phi}_{\alpha\alpha\alpha} - \frac{2}{r^3}\bar{\Phi}_{\alpha r} + \frac{2}{r^2}\bar{\Phi}_{r}\bar{\Phi}_{\alpha r} = 0$$

Rearranging and collecting terms results in

$$\frac{1}{\omega}\frac{\partial}{\partial t}\nabla^2\bar{\Phi} + \frac{1}{r}\left[\bar{\Phi}_{\alpha} + \mu\right]\frac{\partial}{\partial r}\nabla^2\bar{\Phi} - \left[\frac{1}{r}\bar{\Phi}_{r} - \frac{1}{r^2}\right]\frac{\partial}{\partial\alpha}\nabla^2\bar{\Phi} = 0 \qquad (10)$$

where $\nabla^2\bar{\Phi} = \bar{\Phi}_{rr} + \frac{1}{r}\bar{\Phi}_{r} + \frac{1}{r^2}\bar{\Phi}_{\alpha\alpha}$

Appendix II

CALCULATION OF WAVESPEED AND CONSTANT OF INTEGRATION FOR LOW μ

Multiplying form 20 of the text by $i\left[c_1 r_o^{\lambda} - c_2 r_o^{-\lambda}\right]$ and formula (21) by $\left[c_1 r_o^{\lambda} + c_2 r_o^{-\lambda}\right]$ and denoting $\frac{c_1}{c_2} r_o^{2\lambda} = \mathcal{H}$ the following set of equations result.

$$-\frac{i\sigma\lambda}{\omega r}(\mathcal{H}+1)(\mathcal{H}-1) + \frac{2\lambda\mu}{r^3}(\mathcal{H}+1)(\mathcal{H}-1) - \frac{\lambda^2\mu}{r^3}\left[\mathcal{H}-1\right]^2 - \frac{i\lambda^2}{r^3}(\mathcal{H}+1)(\mathcal{H}-1) + \text{II-a}$$

$$+\frac{2i\lambda}{r^3}(\mathcal{H}-1)^2 = 0$$

$$-\frac{i\sigma\lambda}{\omega r}(\mathcal{H}+1)(\mathcal{H}-1) - \frac{\mu\lambda^2}{r^3}(\mathcal{H}+1)^2 - \frac{i\lambda^2}{r^3}(\mathcal{H}-1)(\mathcal{H}+1) = 0 \qquad \text{II-b}$$

Subtracting IIb from IIa an equation in $\mathcal{H}$ results:

$$\frac{2\lambda\mu}{r^3}(\mathcal{H}+1)(\mathcal{H}-1) - \frac{\lambda^2\mu}{r^3}\left[(\mathcal{H}-1)^2 - (\mathcal{H}+1)^2\right] + \frac{2i\lambda}{r^3}(\mathcal{H}-1)^2 = 0 \qquad \text{II-c}$$

or rearranged and divided by λ/r^3

$$2\mu(\mathcal{H}^2-1) + 4\lambda\mu\mathcal{H} + 2i\mathcal{H}^2 - 4i\mathcal{H} + 2i = 0$$

As $\mathcal{H}$ is a complex quantity two equations follow, setting the imaginary and real part of $\mathcal{H}$ equal to zero; so if $\mathcal{H} = a + bi$ where a and b are real quantities, then

$$i\left[4\mu ab + 4\mu\lambda b - 2b^2 + 2a^2 - 4a + 2\right] = 0 \qquad \text{II-d}$$

AND

$$\left[2\mu a^2 - 2\mu b^2 - 2\mu + 4\lambda\mu a - 4ab + 4b\right] = 0 \qquad \text{II-e}$$

Solving for a in II-d

$$a^2 + a(2\mu b - 2) + (1 - 4\mu b - b^2) = 0 \qquad \text{II-f}$$

OR

$$a = 1 - \mu b \pm \sqrt{\mu^2 b^2 + 2\mu b + b^2}$$

Substituting II-f in II-e one obtains

$$\mu(\mu^2 b^2 + 2\mu b + b^2) - 2\mu \mp (\mu + b + \mu^2 b)\sqrt{\mu^2 b^2 + 2\mu b + b^2} = 0 \qquad \text{II-g}$$

b can be solved as a function of μ by a trial and error method. Figure 2 gives the result where only the real solution of b is considered. Substituting b back into II-f, the functional relationship between μ and a is obtained. (See figure 2)

NOMENCLATURE FOR PART II

A	real number in complex quantity
a	" " " " "
q	quantity defined in text
B	real number in complex quantity
b	" " " " "
p	quantity defined in text
c	constant of integration
C_f	wall friction coefficient
C	real number in complex quantity
D	" " " " "
$f()$	functional relationships
$g()$	" "
$h()$	" "
i	$\sqrt{-1}$
k	constant
m	whole number
r	radius
p	pressure
t	time
u	velocity
v	"
W	real number in complex quantity
X	" " " " "
Y	" " " " "
Z	" " " " "

Greek letters

α	circumferential angle
β	angle between steady streamline and radius
∇^2	operator
λ	wave number
μ	tangent of angle enclosed between steady streamline and circumferential direction
Φ	stream function
Ψ	" "
σ	radian frequency
$\mathscr{H}$	complex quantity
ρ	density
τ	shear stress
ϖ	dimensionless circulation
Ω	angular velocity

Subscripts

$_{im}$	imaginary part of that quantity
$_{re}$	real " " " "
$_{,t}$	quantity differentiated with respect to subscript

Superscript

$^{\wedge}$	perturbed quantity

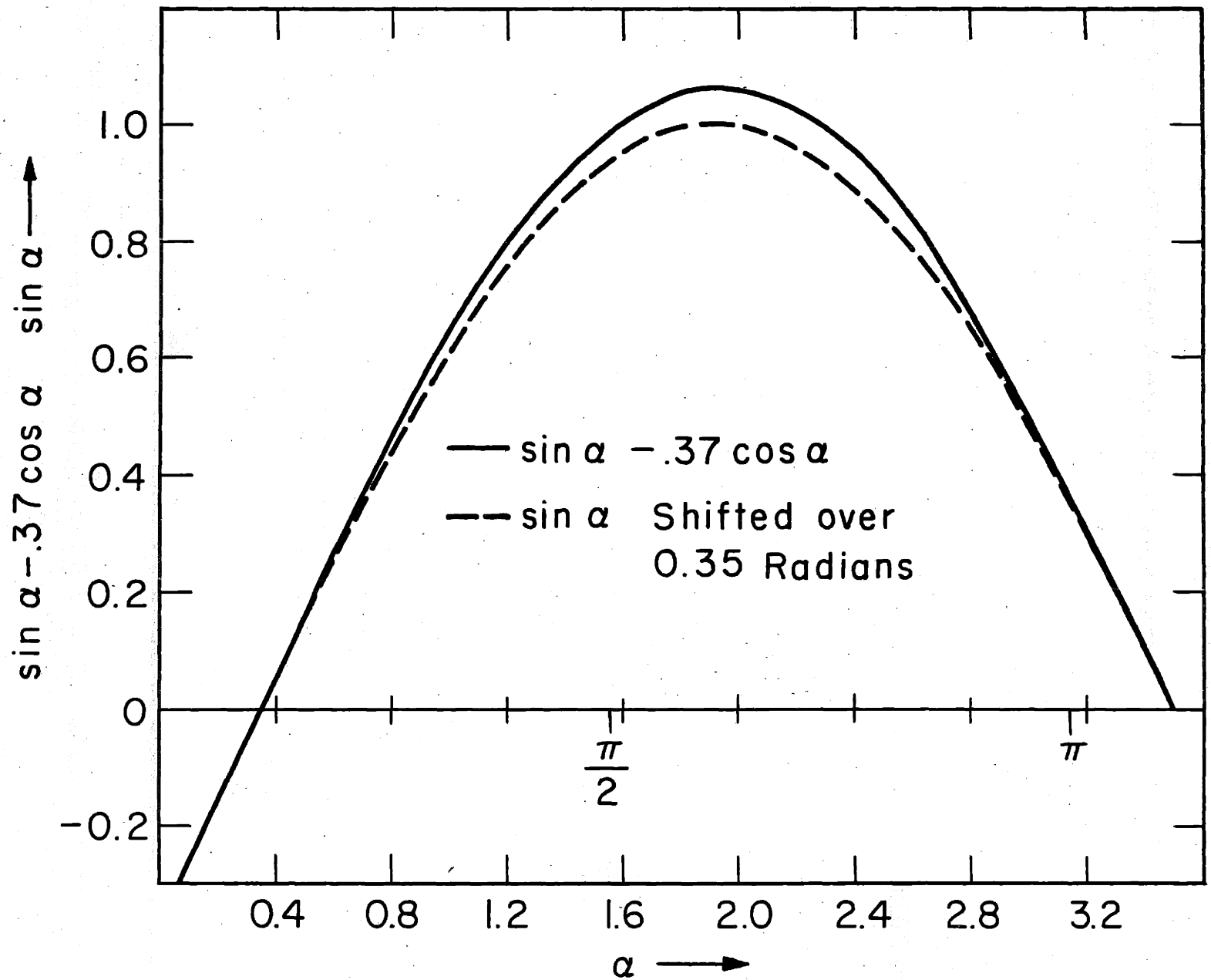

FIG.1 CURVE OF $\sin\alpha - \phi\cos\alpha$

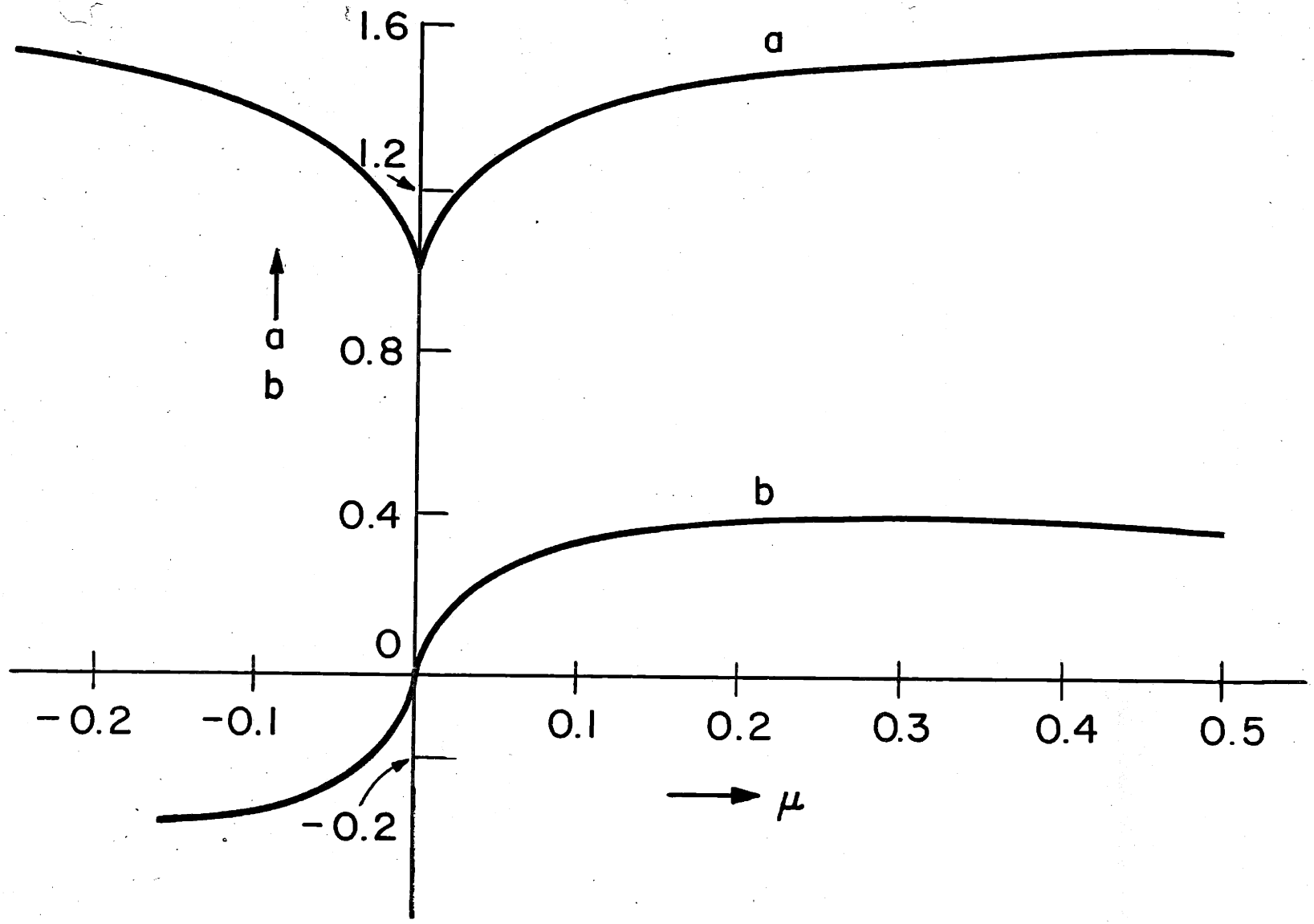

FIG. 2 CURVES FOR $a(\mu)$ AND $b(\mu)$

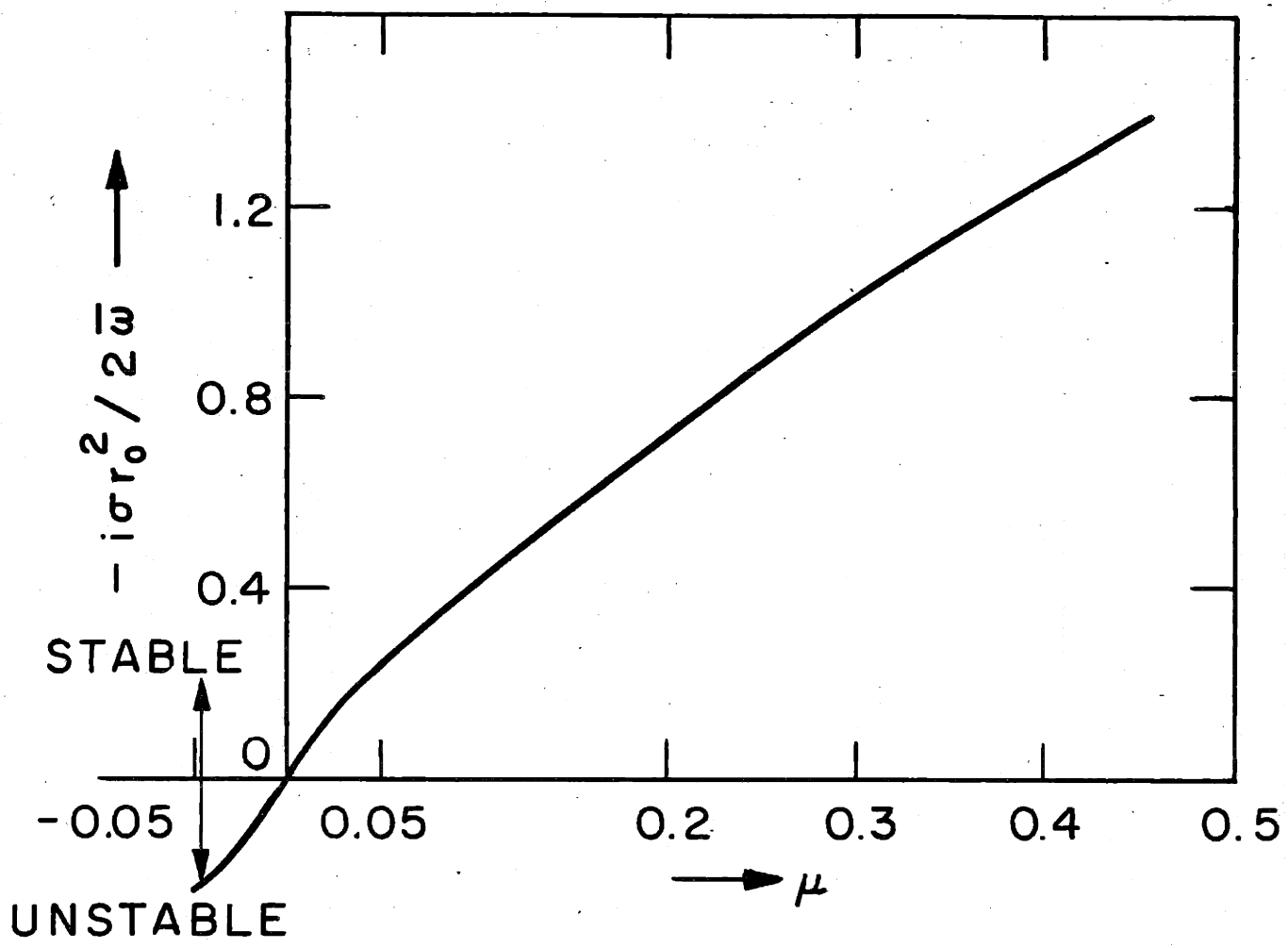

FIG. 3 REAL PART OF $i\sigma$ vs μ FOR SMALL(μ)

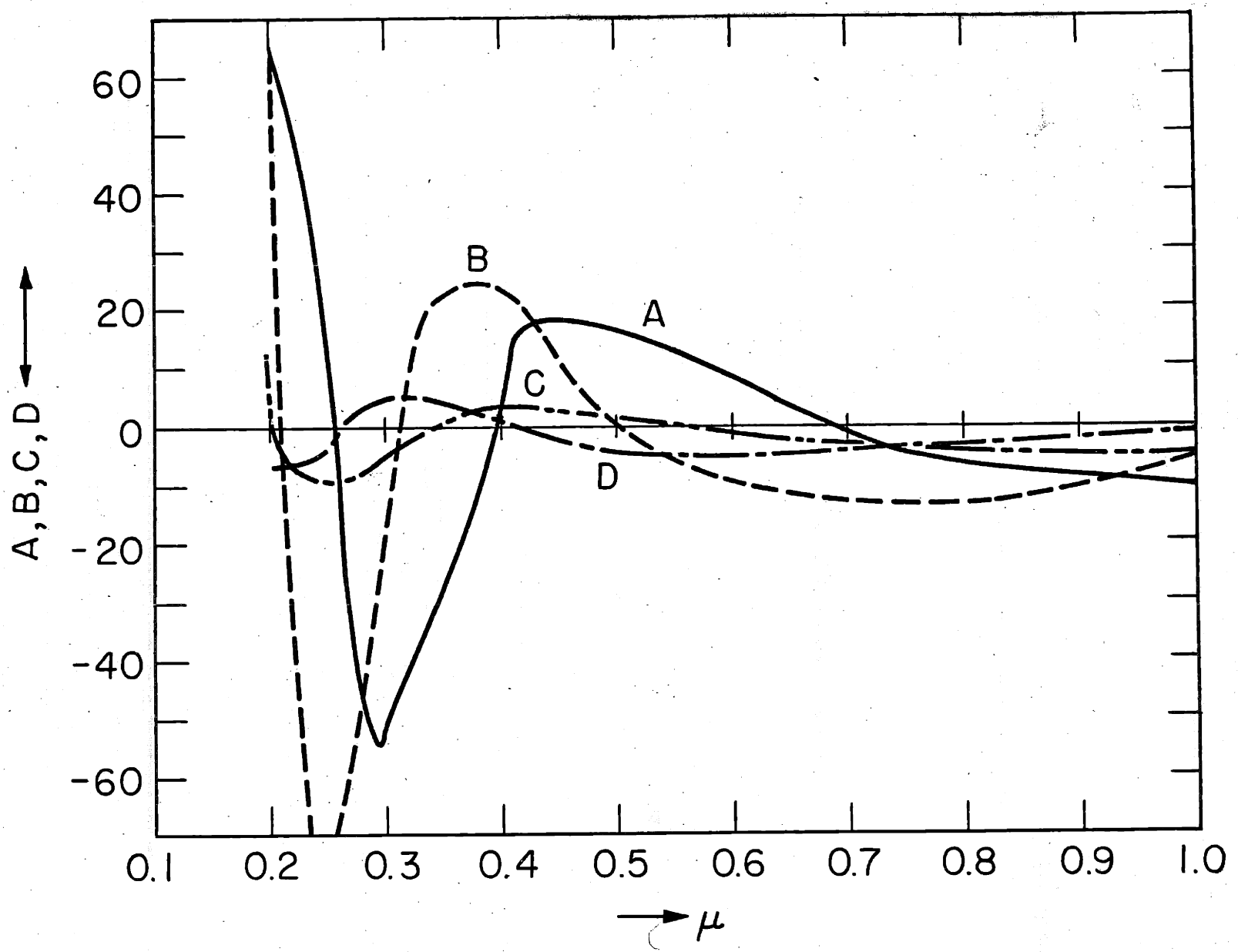

FIG. 4 THE BEHAVIOR OF THE TERMS A,B,C AND D WITH μ

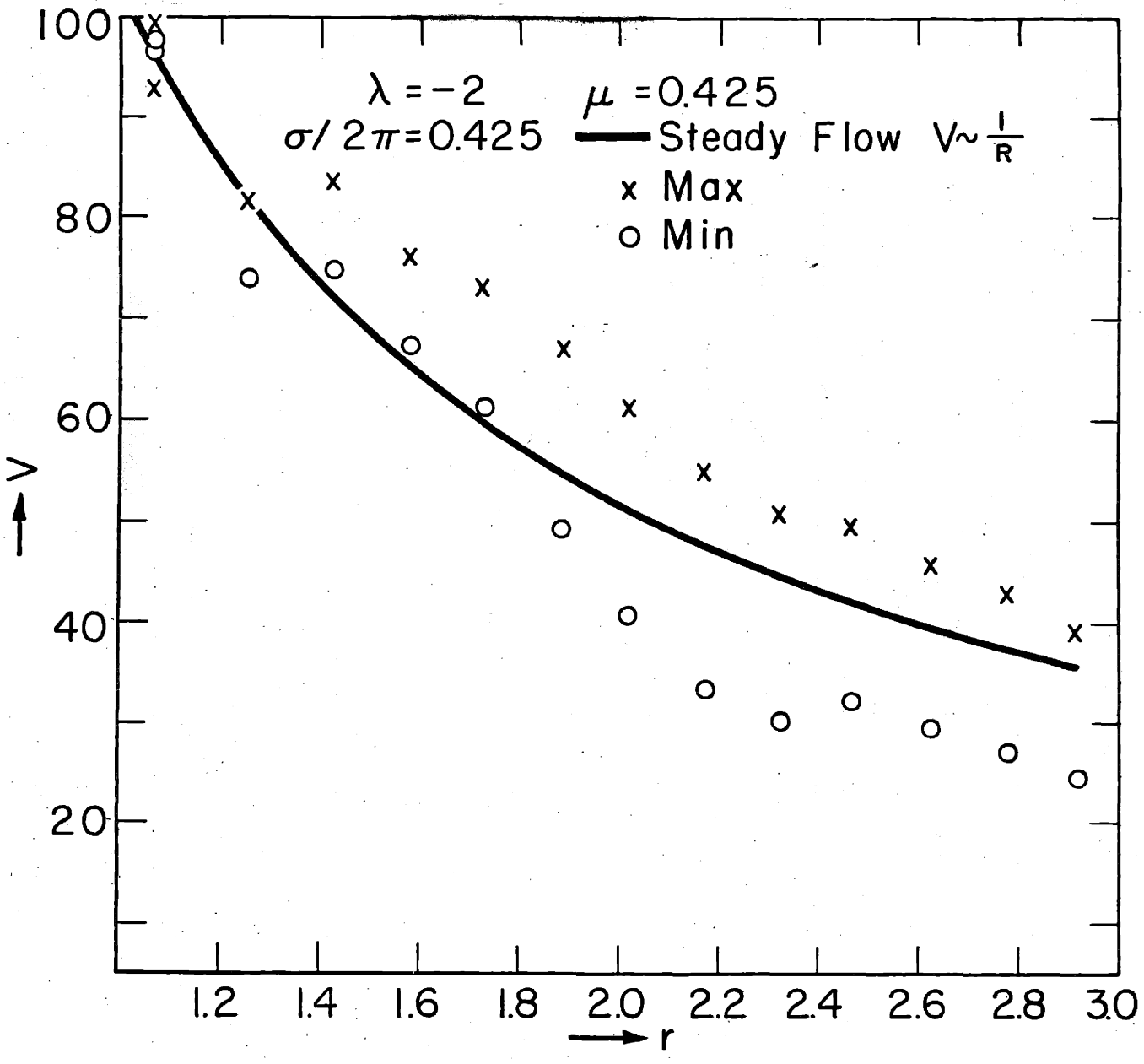

FIG. 5 PERTURBED TOTAL VELOCITIES VERSUS RADIUS

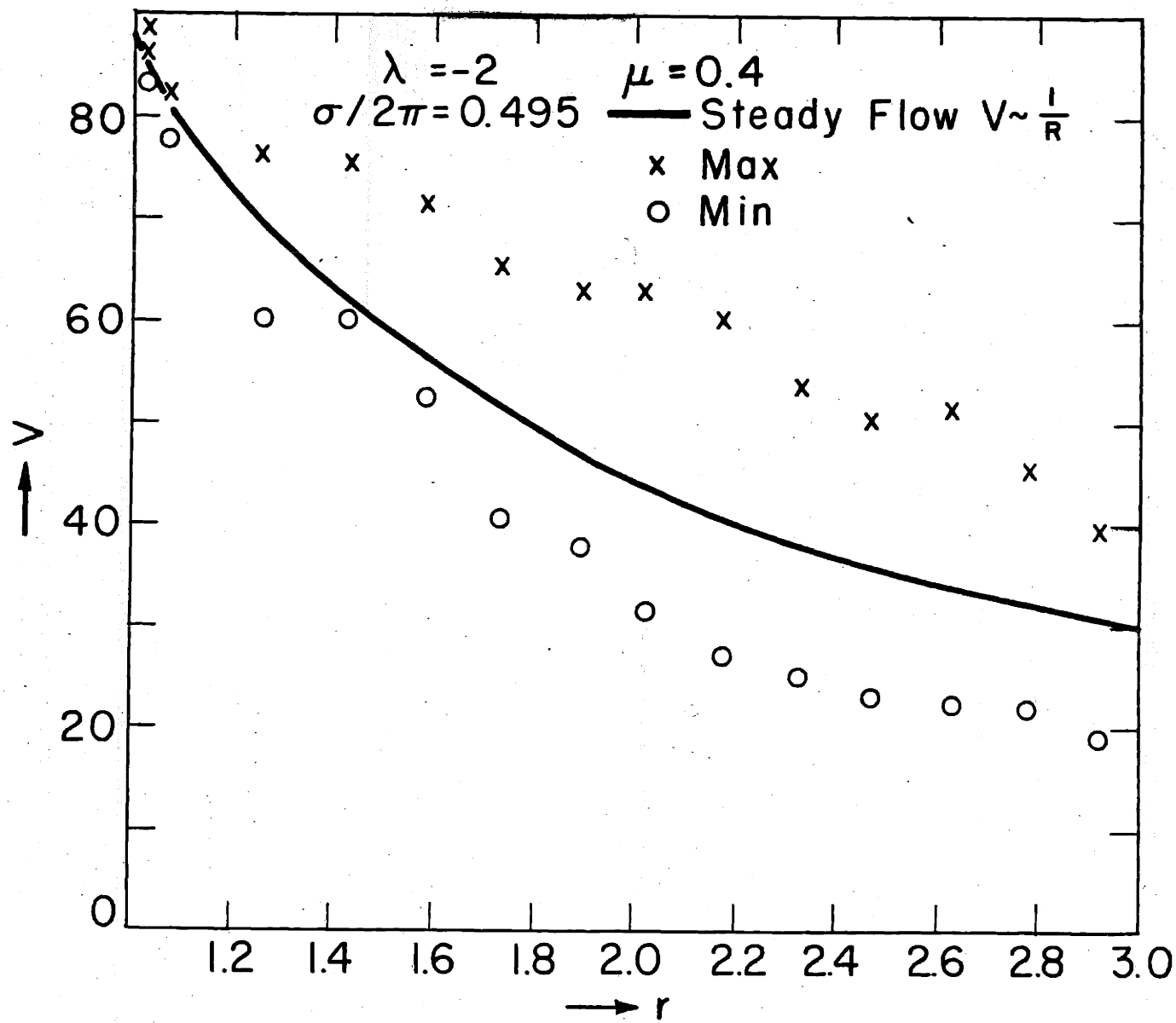

FIG. 6 PERTURBED TOTAL VELOCITIES VERSUS RADIUS

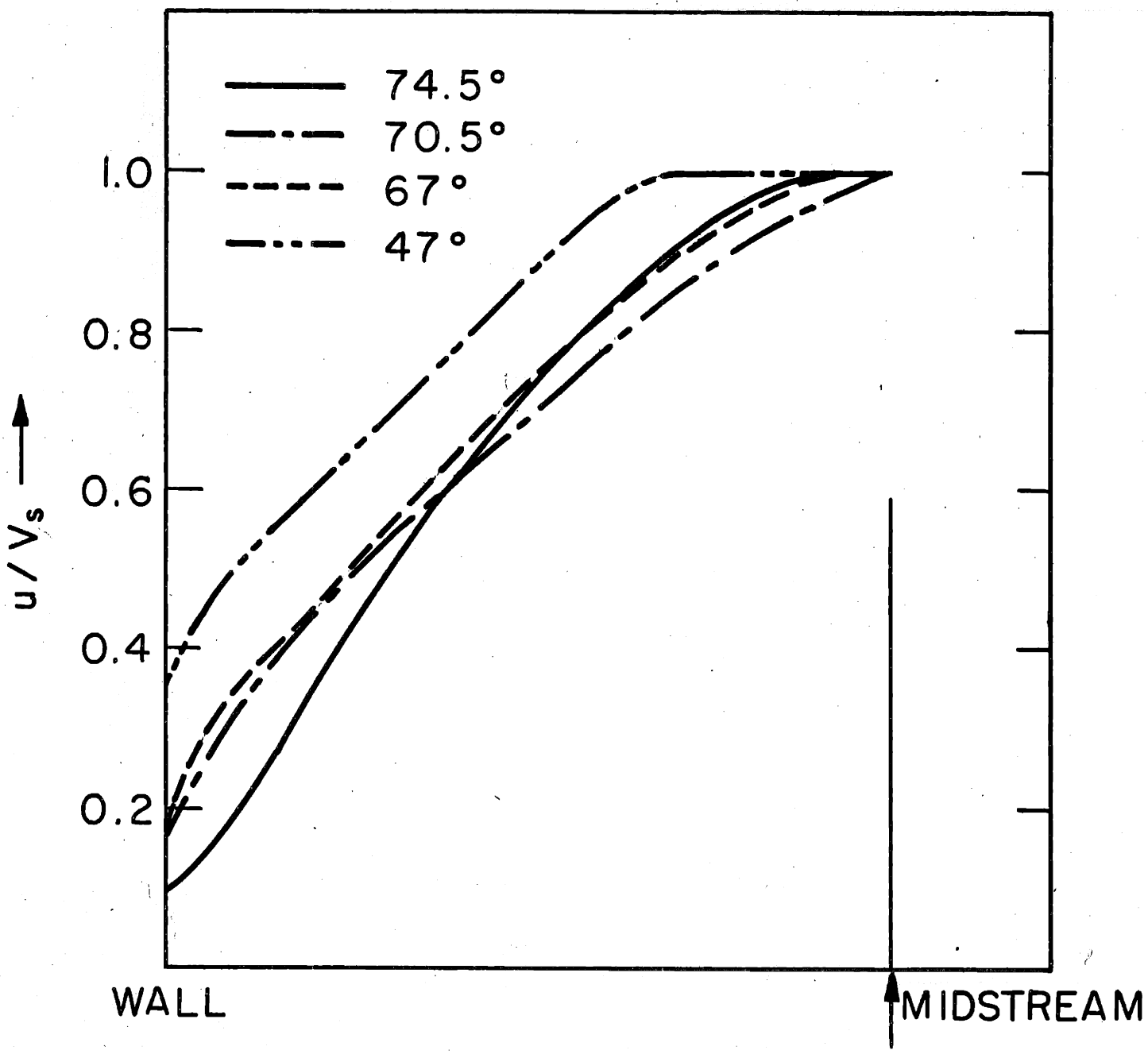

FIG. 7 STEADY FLOW RADIAL VELOCITY PROFILE FOR DIFFERENT STREAM ANGLES

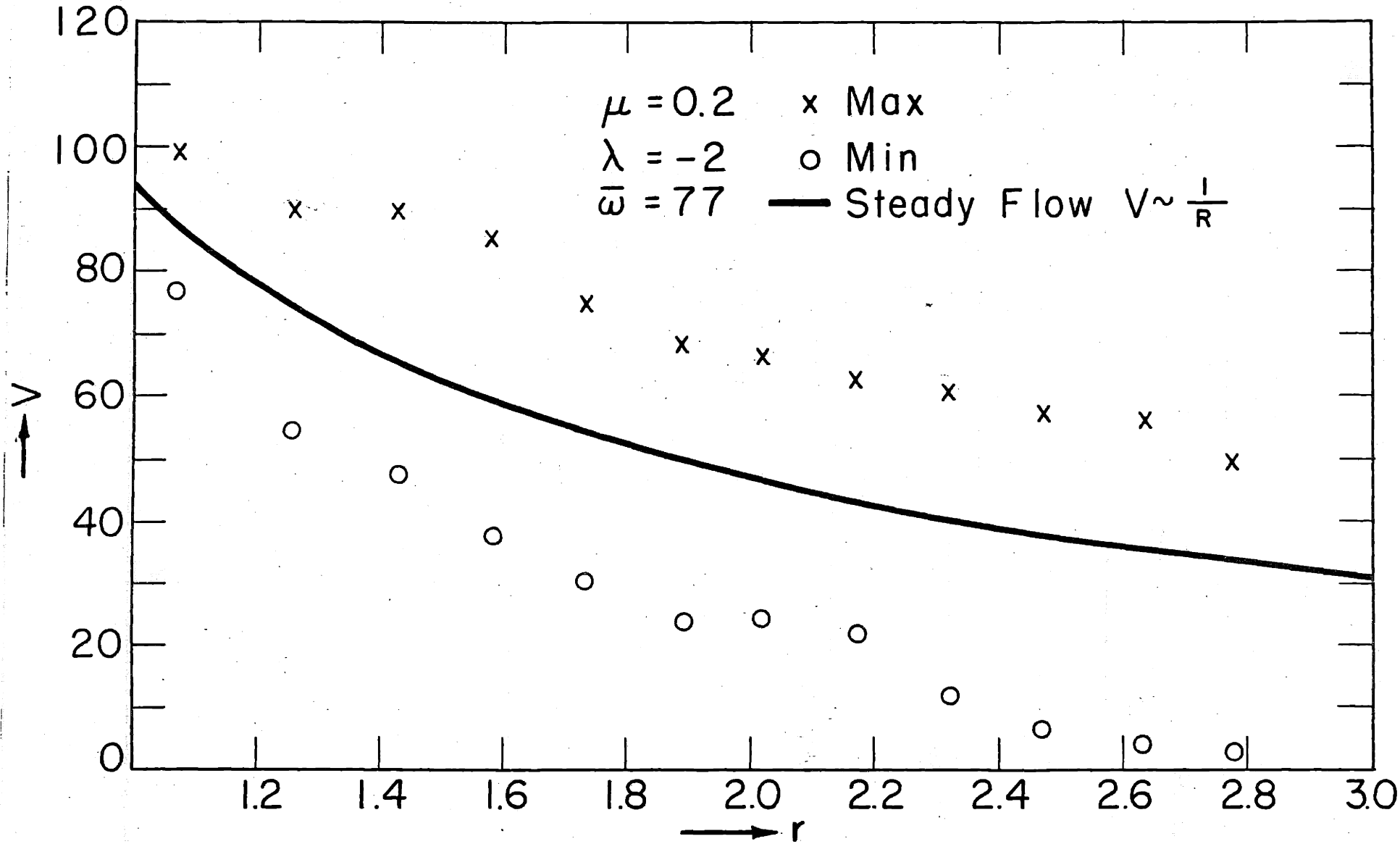

FIG. 8 MIN. AND MAX. PERTUBATION VELOCITIES. $\mu = 0.2$, $\lambda = -2$

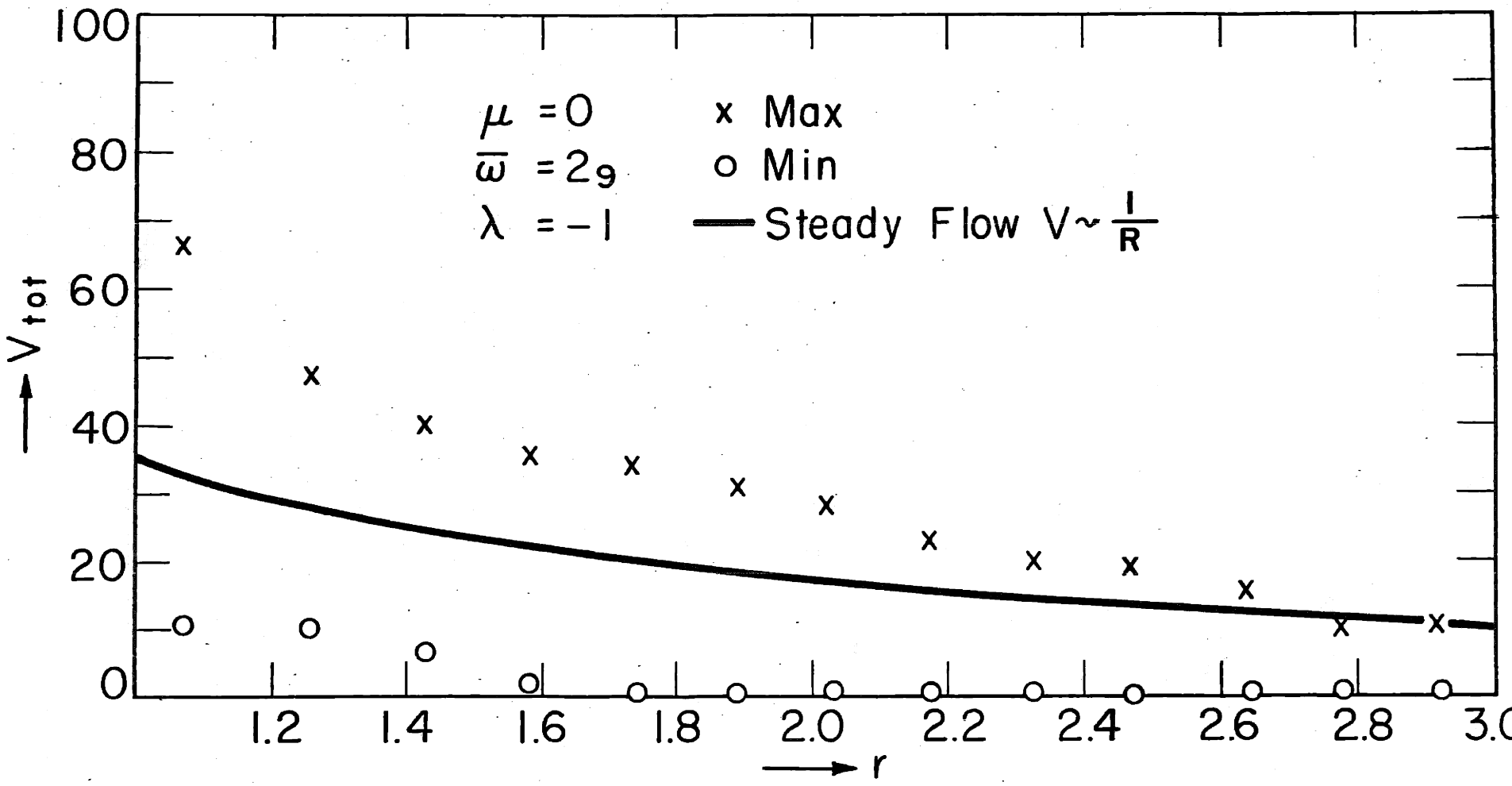

FIG. 9 MIN. AND MAX. VELOC. FOR $\mu = 0$, $\lambda = -1$

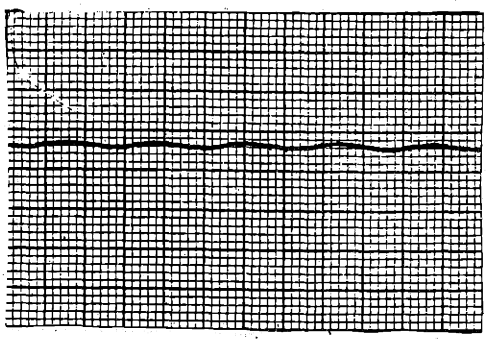

R = 1.07

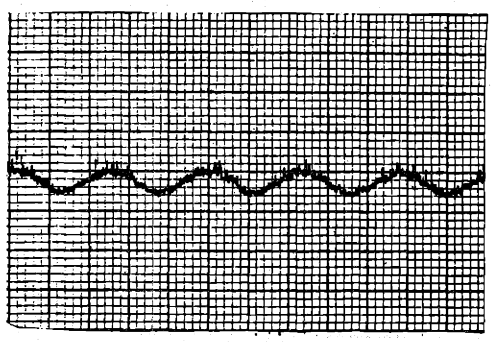

R = 1.43

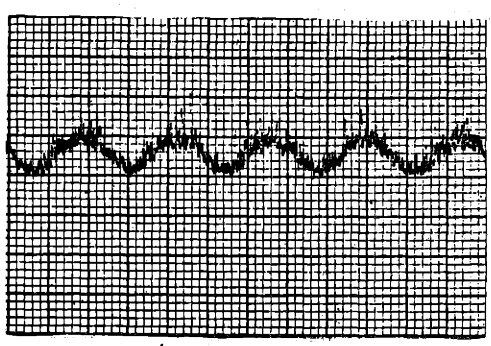

R = 1.89

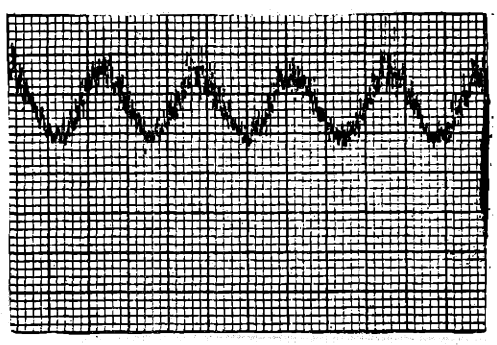

R = 2.17

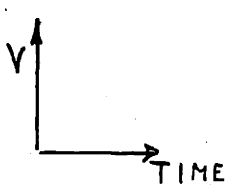

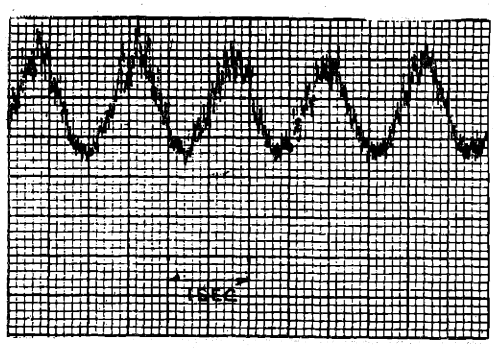

R = 2.32

FIG 10. HOTWIRE RESPONSES FOR $\mu = 0.4$.

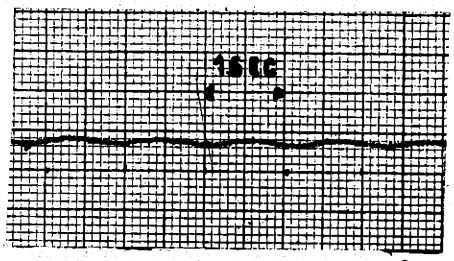

μ = 0.42 V_{MAX} = 92 ft/sec
V_{MIN} = 90 .

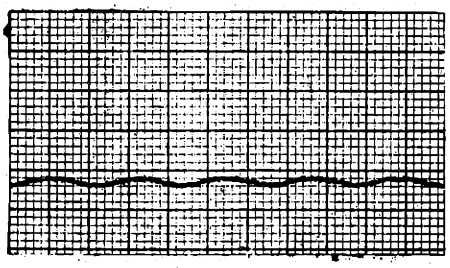

μ = 0.40 V_{MAX} = 89
V_{MIN} = 86

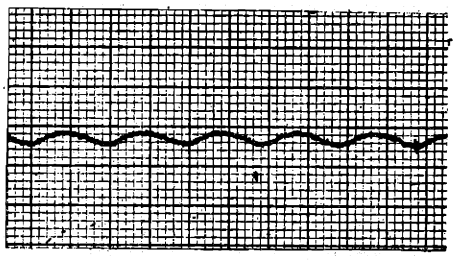

μ = 0.38 V_{MAX} = 86
V_{MIN} = 81.

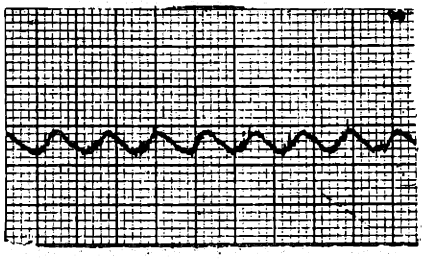

μ = 0.345 V_{MAX} = 84
V_{MIN} = 76

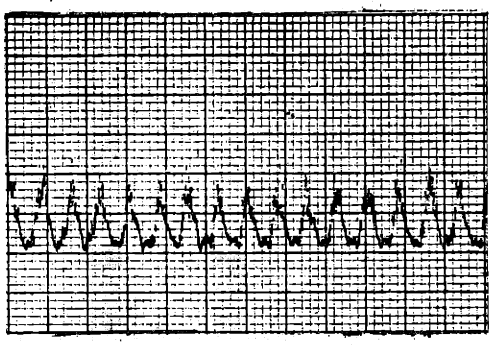

μ = 0.225 V_{MAX} = 87
V_{MIN} = 64

FIG 11. PERTURBED VELOCITIES AT DIFFUSER ENTRANCE FOR DIFFERENT FLOW ANGLES. [$tg\beta = \mu$]

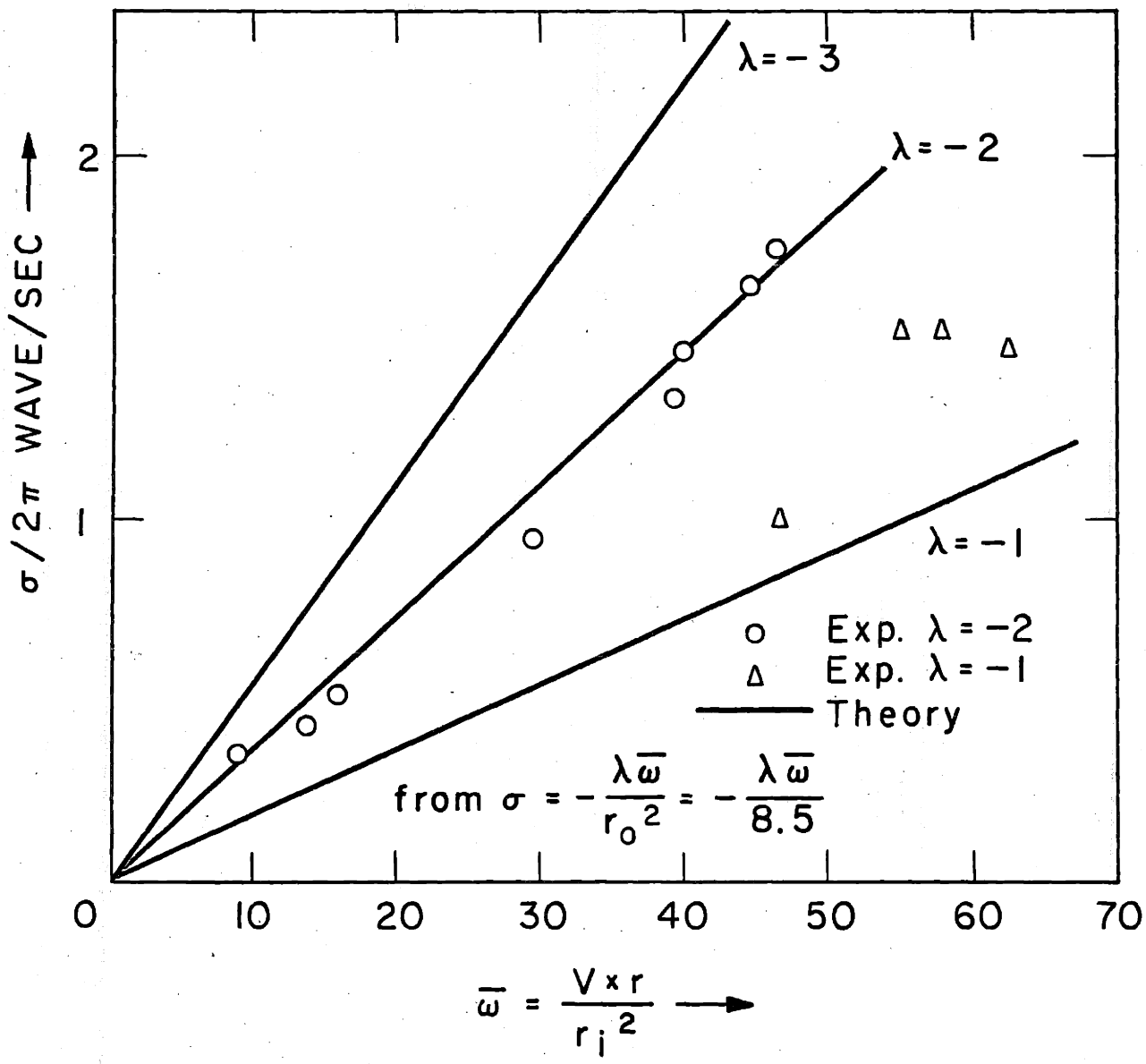

FIG. 12 DEPENDENCE OF σ ON $\bar{\omega}$ AND λ FOR $\mu = 0$

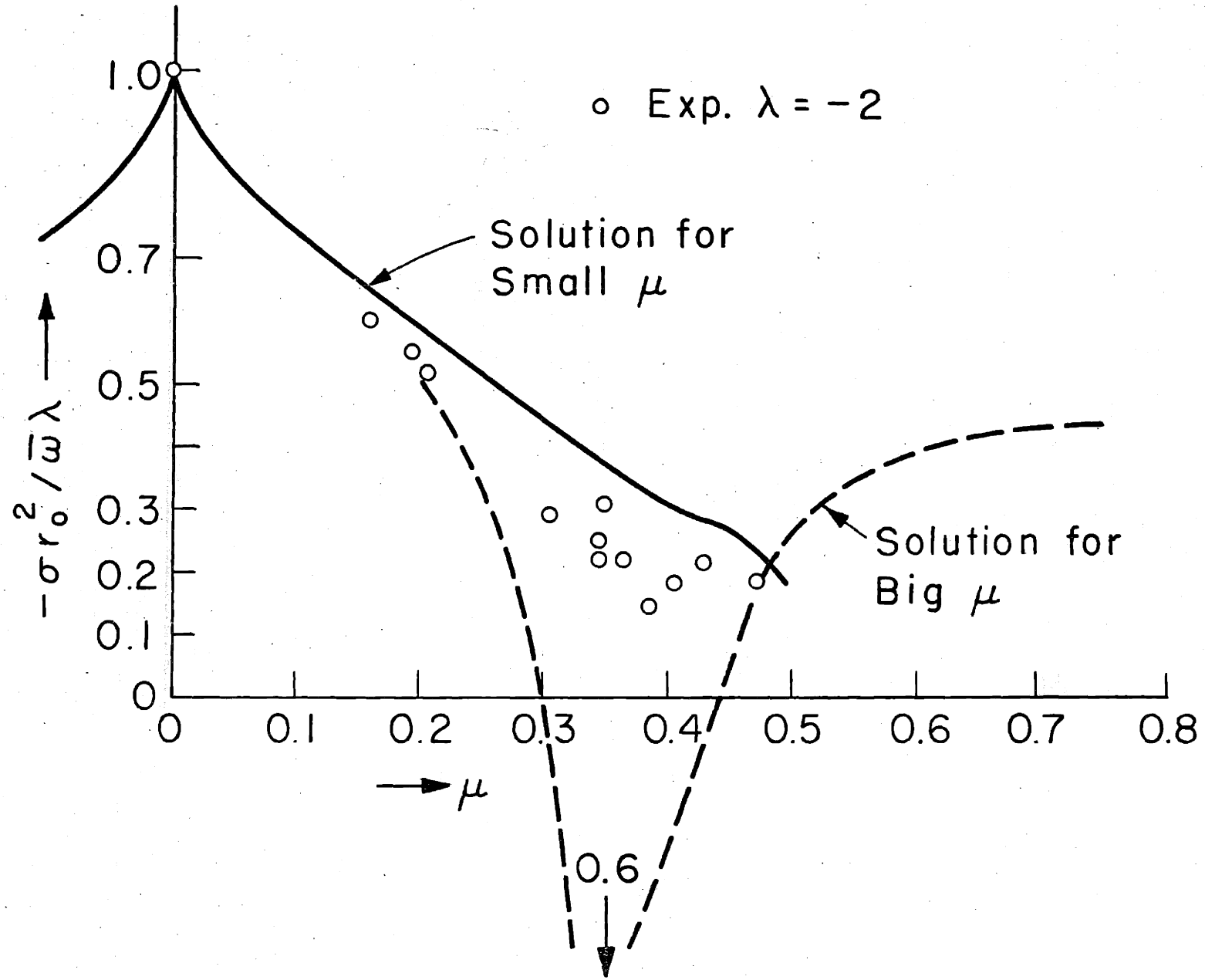

FIG. 13 WAVESPEED VERSUS μ

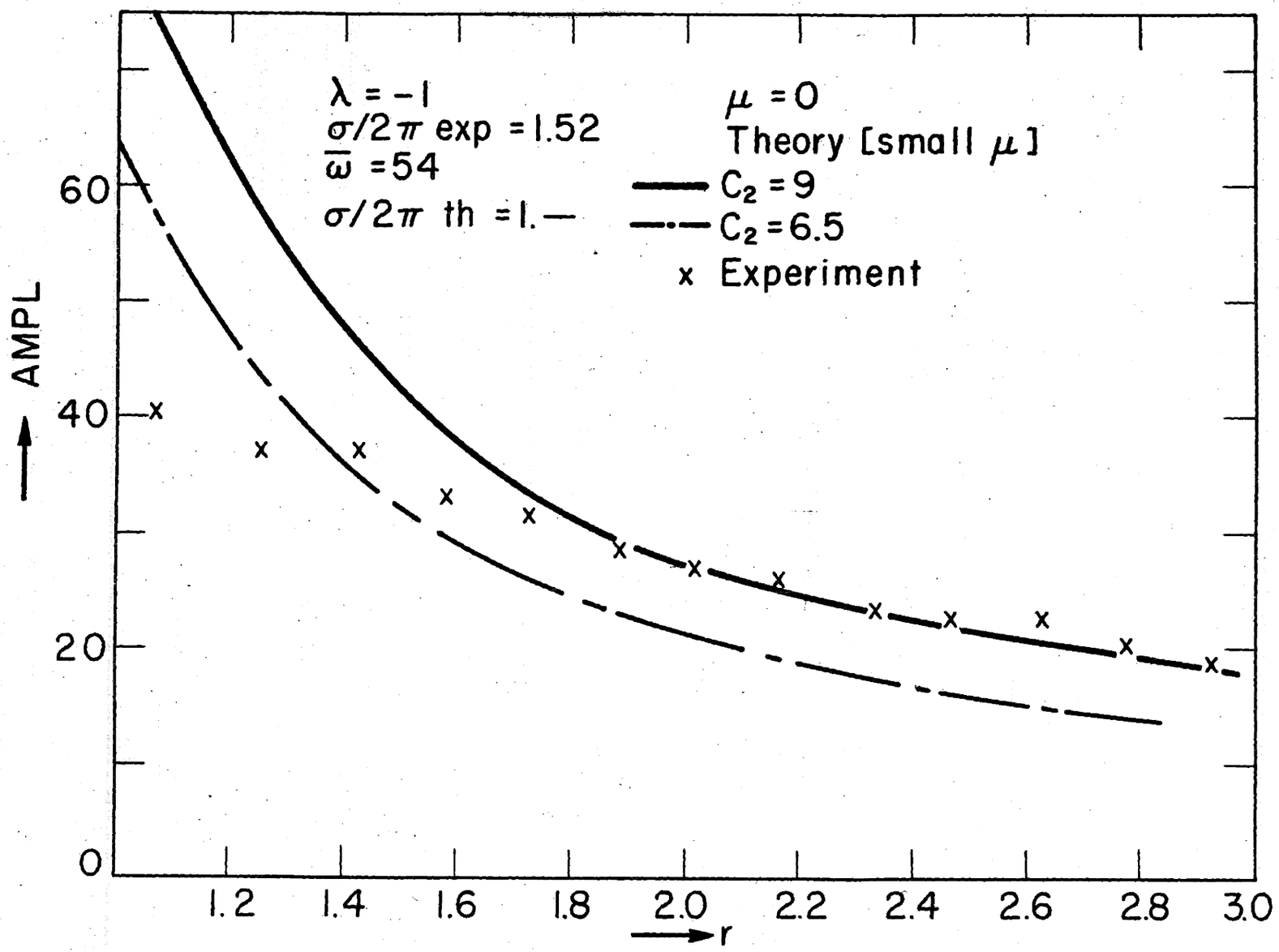

FIG. 14 AMPLITUDE OF PERTURBED VELOCITIES

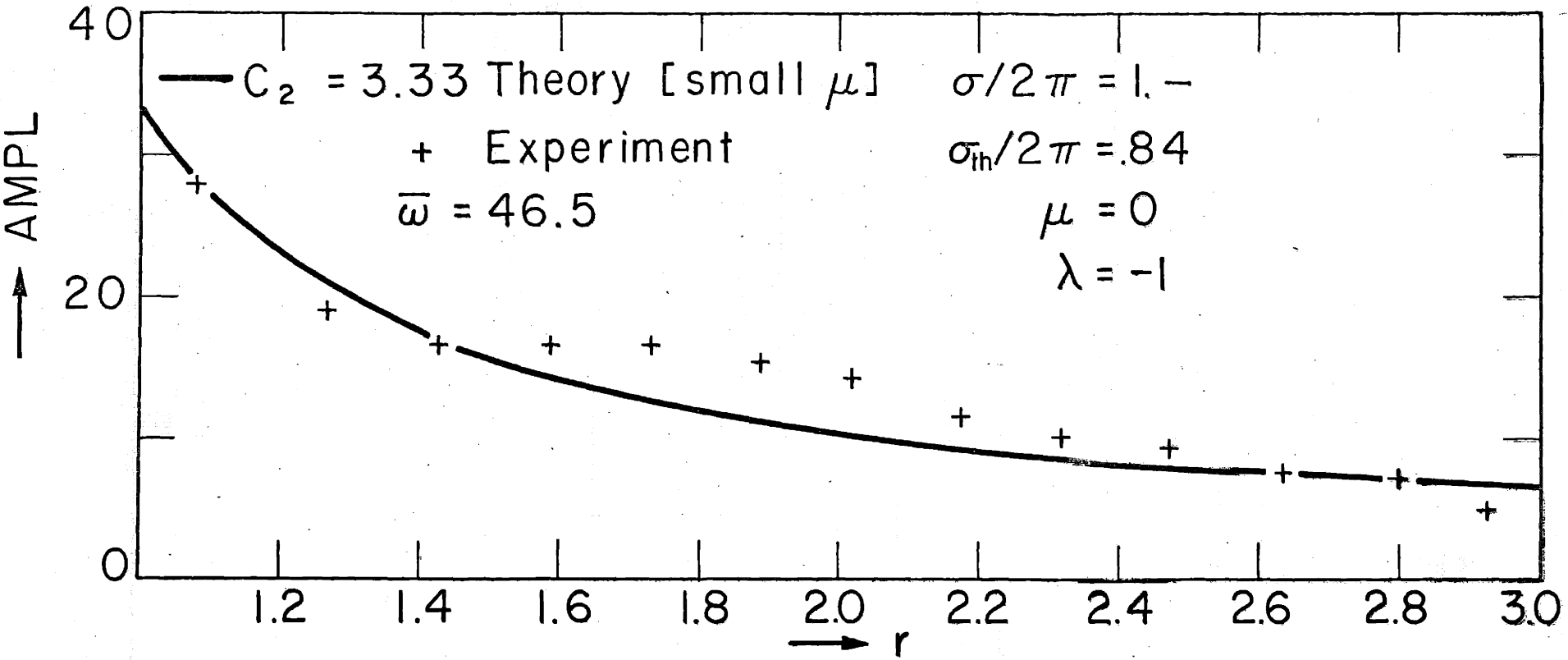

FIG. 15 AMPLITUDE OF PERTUBATIONS

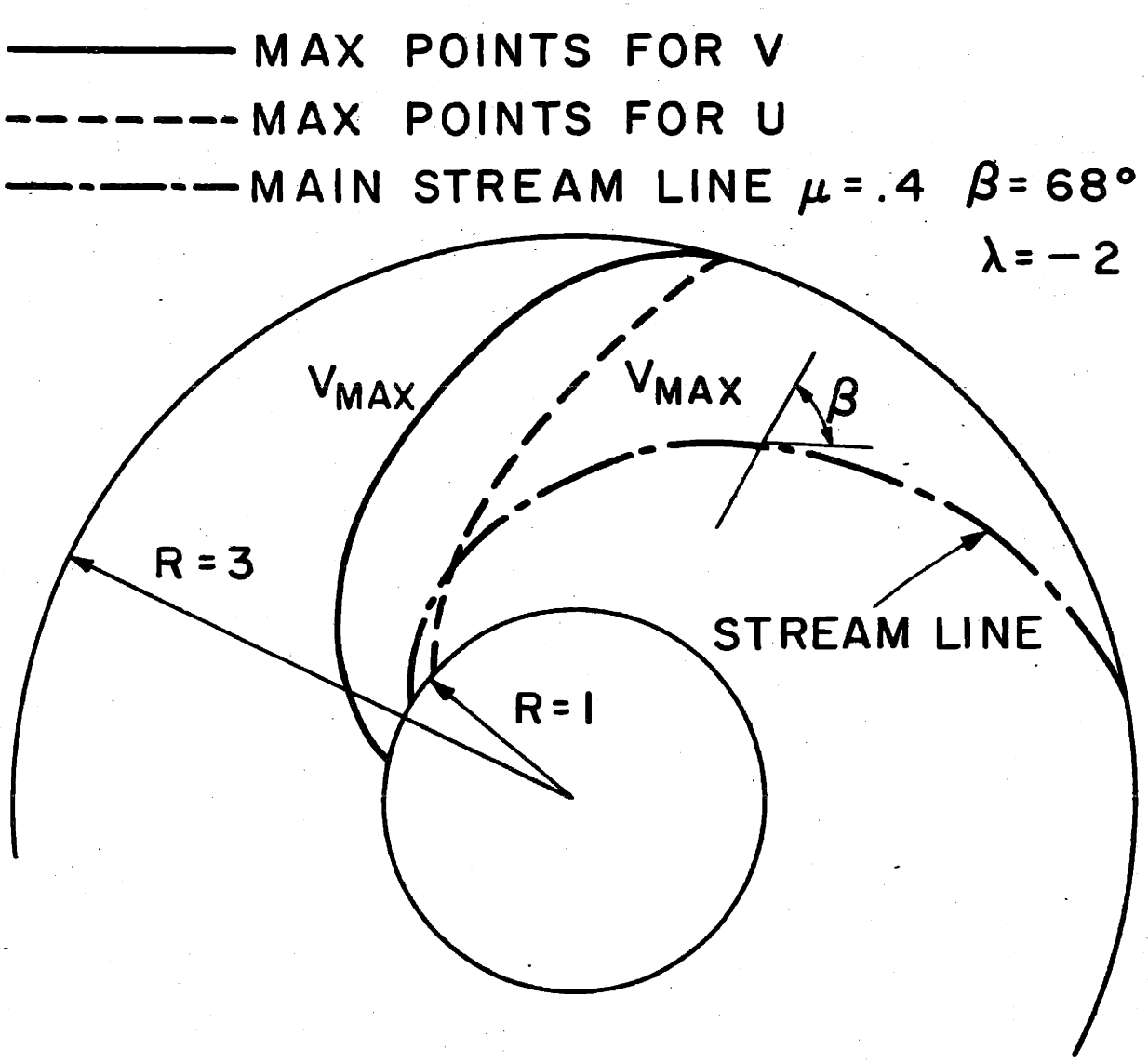

FIG. 16 LOCUS OF POINTS WHERE $\hat{U}$ AND $\hat{V}$ ARE MAX

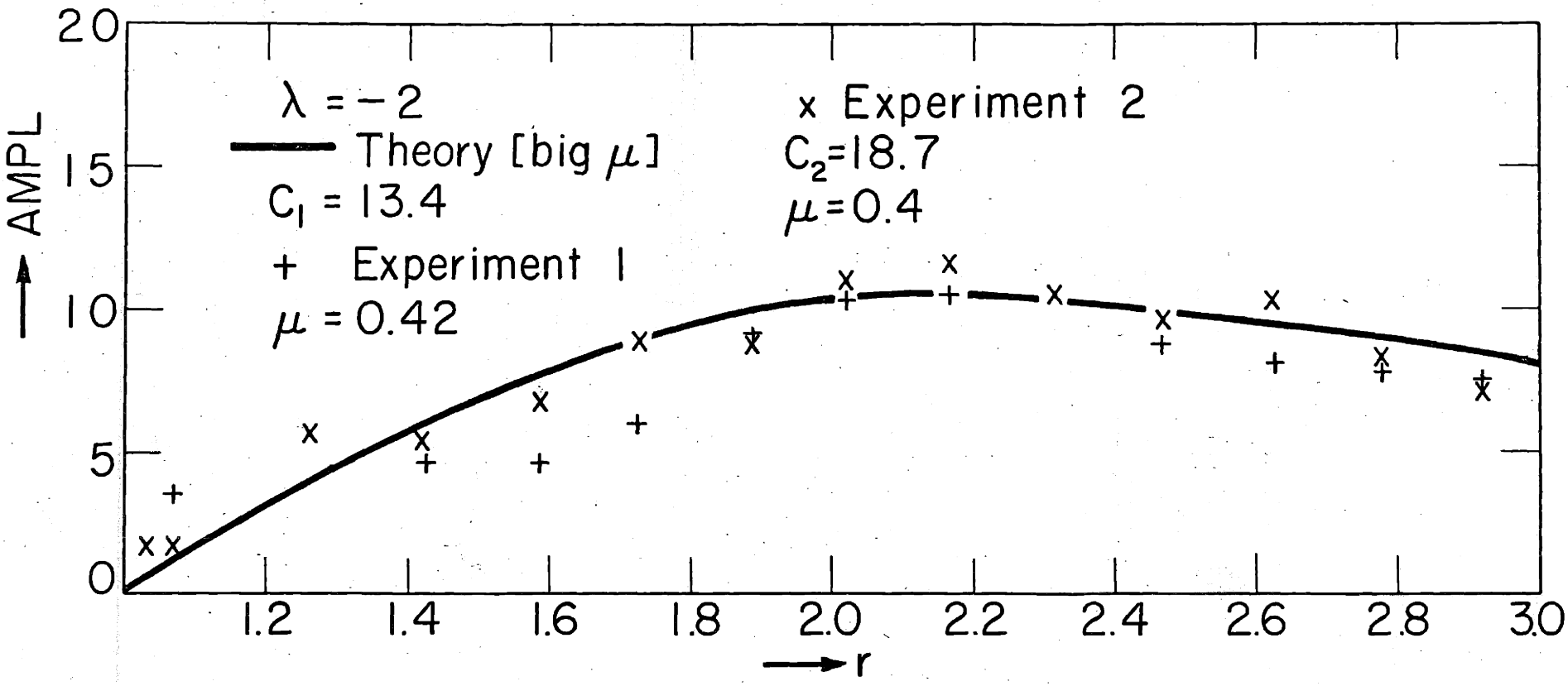

FIG. 17 AMPLITUDE OF VELOCITY PERTUBATION

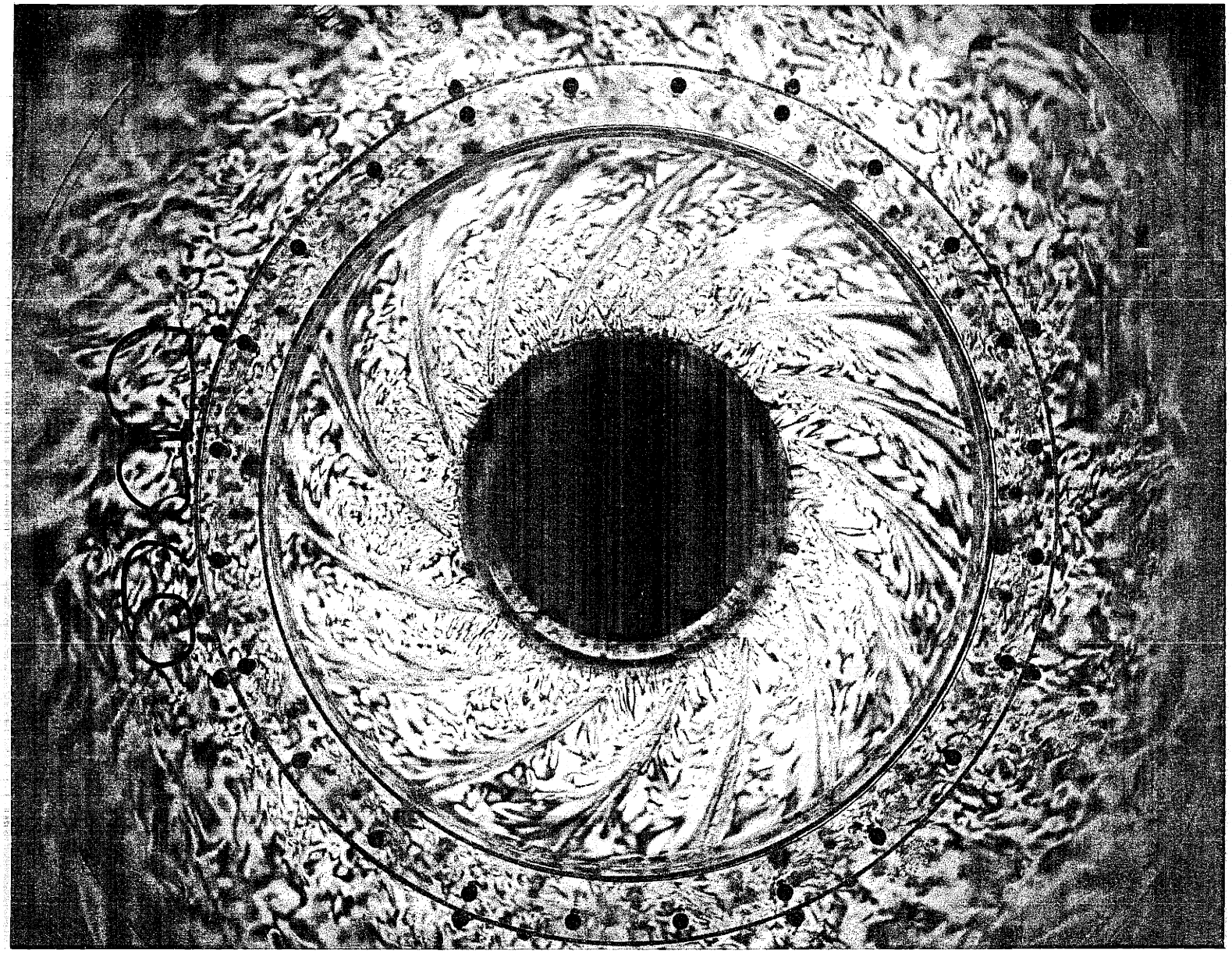

Fig. 18